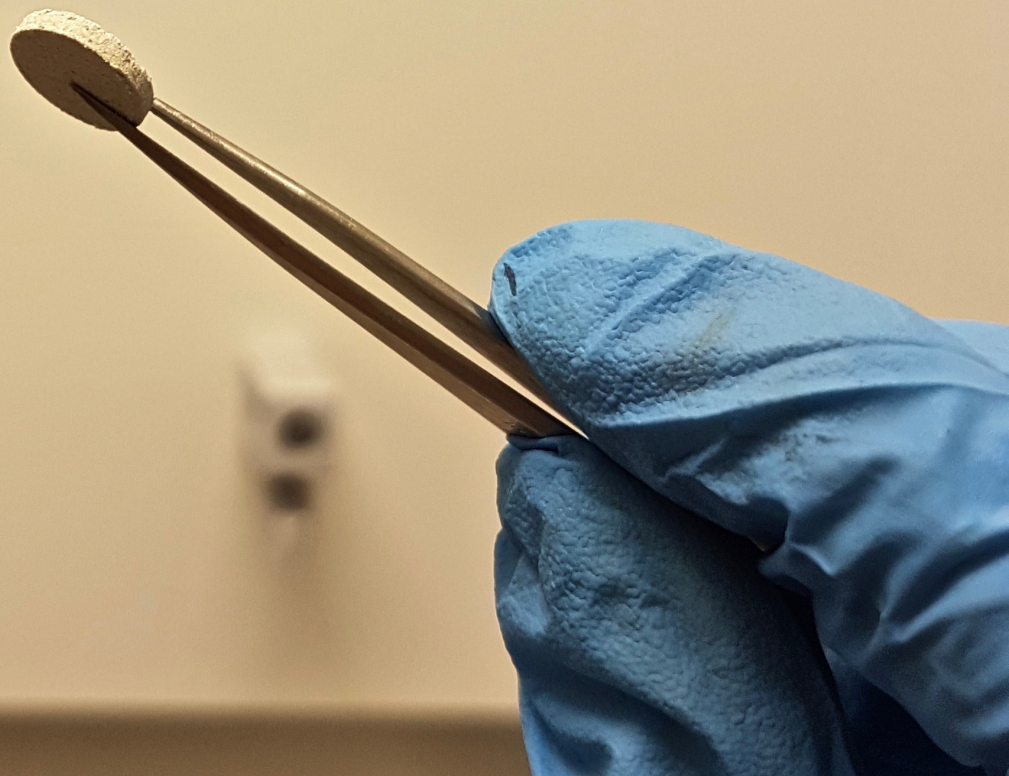


# Study on the effects of Doping Argyrodite with LiCl and LiF in a Solid State Lithium Ion Battery

Intan Balqis Binti Faisol

Technische Universiteit Delft





# Study on the effects of Doping Argyrodite with LiCl and LiF

in a Solid State Lithium Ion Battery

by

**Intan Balqis Binti Faisal**

in partial fulfillment of the requirements for the degree of

**Master of Science**  
in Sustainable Energy Technology

at the Delft University of Technology,  
to be defended publicly on Monday August 13, 2018 at 14:00 PM.

Supervisor:	Dr. ir. M. Wagemaker	
Daily Supervisor:	Dr. S. Ganapathy	
Thesis committee:	Dr. Ir. M. Wagemaker,	TU Delft
	Dr. E. Kelder,	TU Delft
	Dr. L. van Eijk,	TU Delft

*This thesis is confidential and cannot be made public until August 6, 2018.*

An electronic version of this thesis is available at <http://repository.tudelft.nl/>.



# Abstract

Solid electrolyte batteries are generally safer than traditional liquid electrolyte batteries. A promising solid electrolyte is  $\text{Li}_6\text{PS}_5\text{Cl}$  argyrodite for a lithium ion battery. However, it has instability in the active material and electrolyte interphase that will lead to an increase in impedance and rapid capacity loss. This thesis will focus on doping stable salts of LiCl and LiF in the argyrodite for a solid state lithium ion batteries to study the effect of stability of the interphase with active material of NCM 622.

The synthesis of pristine and doped argyrodite was carried out. With XRD analysis, it is discovered that side phases and unreacted precursors are present. These include: LiCl,  $\text{Li}_2\text{S}$ ,  $\text{Li}_3\text{PO}_4$ ,  $\text{Li}_2\text{PS}_3$ , and LiOH.  $\text{Li}_3\text{P}$  is produced during battery cycling. Hence, the argyrodite is not as pure as expected. Nevertheless, since all the argyrodites synthesized have side phases, the experiments are carried out.

Electrochemical Impedance Spectroscopy (EIS) is carried out for each synthesized argyrodite to determine the ionic conductivity and give an estimation of which argyrodite will decompose faster. LiCl doped  $\text{Li}_6\text{PS}_5\text{Cl}$  was estimated to decompose slower, but will have lower resistance than of pristine. In contrast, LiF doped  $\text{Li}_6\text{PS}_5\text{Cl}$  will decompose faster but have higher resistance than pristine  $\text{Li}_6\text{PS}_5\text{Cl}$ .

The cell of: **NCM 622,  $\text{Li}_6\text{PS}_5\text{Cl}$ , C /  $\text{Li}_6\text{PS}_5\text{Cl}$  / In** are cycled with constant C-rate, with the doped  $\text{Li}_6\text{PS}_5\text{Cl}$  being used in the cathode mixture. Pristine  $\text{Li}_6\text{PS}_5\text{Cl}$  will always be used as the separator of anode and cathode. From the electrochemical data from the Maccor, it is found that LiCl doped  $\text{Li}_6\text{PS}_5\text{Cl}$  reduces the specific capacity retention despite more mobile ions expected. This could be due to poor interphase contact. This reasoning and the lower rate of reaction from EIS analysis could also explain the lower chemical degradation for the LiCl doped  $\text{Li}_6\text{PS}_5\text{Cl}$  than of pristine  $\text{Li}_6\text{PS}_5\text{Cl}$ .

The lesser amount of LiF doped  $\text{Li}_6\text{PS}_5\text{Cl}$  decreases the specific capacity retention of NCM 622 which reflects on the EIS analysis. The higher amount of LiF doped  $\text{Li}_6\text{PS}_5\text{Cl}$  however improves the specific capacity retention which is comparable to of pristine  $\text{Li}_6\text{PS}_5\text{Cl}$  despite the lower ionic conductivities. This could be due to similar composition or the higher rate of decomposition which affected the electrochemical performance.

Another type of battery is cycled without the cathode active material of NCM 622. In this case, the pristine  $\text{Li}_6\text{PS}_5\text{Cl}$  is shown to have a large increase in specific capacity which indicates electrolyte decomposition. For lesser amount of LiCl doped  $\text{Li}_6\text{PS}_5\text{Cl}$ , the specific capacity is less than pristine  $\text{Li}_6\text{PS}_5\text{Cl}$  which could mean that the decomposition is lower. For the more LiCl doped  $\text{Li}_6\text{PS}_5\text{Cl}$ , decomposition occurs as there is an increase in specific capacity. LiF doped  $\text{Li}_6\text{PS}_5\text{Cl}$  generally have no increase in capacity which suggests that there are little decomposition.

An alternative doping method was carried out and determined that ionic conductivity was lower and degradation rate would be higher. With additional 5% LiCl doping, the cycling performance is worse, which could also be the result of poor interphase or interphase stability. In contrast, with additional 10% LiCl doping, the cycling performance is improved with better specific capacity retained. However, it shows significant chemical degradation even with fewer cycles overall.

Further recommendations to improve the overall outlook of this research, which includes improving on purity of  $\text{Li}_6\text{PS}_5\text{Cl}$  through better synthesis. Additionally, further analysis of TEM, XRD in operando mode, EDS, and EDS with SEM could be carried out. Alternatively, coating with LiCl and LiF as opposed to doping method could be looked into.



# Preface

The aim of doing a masters in Sustainable Energy Technology is to contribute to the environment and society through technology. Towards the end of the first year of masters, I developed an interest in batteries especially after a course of electrical energy storage taught by Marnix Wagemaker which led me to do a thesis in this research group.

I wanted to do Solid State batteries as it is an emerging technology due to it being a safer battery than traditional liquid electrolyte batteries especially after the numerous cases of exploding mobile phones. Marnix has suggested to look into the idea of coating (or doping in this case) of the argyrodite electrolyte with LiCl and LiF. Developing this thesis was extremely testing as there were plenty of literature reviews, experiments (to practice and actual ones), research, and more. Additionally, there were setbacks such as enduring a broken finger, XRD machines being unusable for a month and repeating experiments. Nevertheless, I am satisfied on the development of this thesis and the knowledge gained in regards to the battery technology, chemistry and physics of it all.

The first person I would like to thank for this thesis is Swapna Ganapathy, my daily supervisor for her support and guidance throughout my thesis and help me with doubts; and Marnix Wagemaker, my supervisor for his ideas. Also, I would like to give a shoutout to the SEE group especially Frans Ooms for helping me from answering my questions to showing me experimental methods. On a personal note, I would like to thank the friends I gained here in TU Delft and Giacomo for making my time here enjoyable. Finally, I would like to thank my parents and Iman for their love and forever supporting my endeavors.

*Intan Balqis Binti Faisal  
Delft, August 2018*



# Contents

<b>1</b>	<b>Introduction</b>	<b>1</b>
<b>2</b>	<b>Background Theory</b>	<b>3</b>
2.1	Solid State Lithium Ion Battery	3
2.2	Argyrodite	4
2.3	Doping, Lithium Chloride and Lithium Fluoride	4
2.4	NCM as an Active Material for Cathode	5
2.5	Indium metal	5
2.6	Electrochemical Impedance Spectroscopy	6
2.7	X-ray Diffraction	8
2.7.1	XRD principle	9
2.7.2	Quantification of Crystalline phases in materials	10
<b>3</b>	<b>Experimental Methods</b>	<b>11</b>
3.1	Battery Preparation	11
3.1.1	Argyrodite Synthesis	11
3.1.2	Catholyte & Cathode mixture	12
3.1.3	Battery Assembly	12
3.2	Battery Analysis	12
3.2.1	Electrochemical Impedance Spectroscopy Measurement	12
3.2.2	Maccor	12
3.2.3	X-ray Diffraction (XRD)	13
<b>4</b>	<b>Material Analysis</b>	<b>15</b>
4.1	Electrochemical Impedance Spectroscopy (EIS) testing	15
4.2	XRD Analysis of reactants	16
4.2.1	NCM 622	16
4.2.2	$\text{Li}_6\text{PS}_5\text{Cl}$	16
4.2.3	Catholyte mixture	17
<b>5</b>	<b>Cycling Of Batteries</b>	<b>19</b>
5.1	Catholyte: NCM 622, pristine/doped $\text{Li}_6\text{PS}_5\text{Cl}$ & Carbon Black	19
5.2	Cathode: Pristine/doped $\text{Li}_6\text{PS}_5\text{Cl}$ & Carbon Black	21
<b>6</b>	<b>Ex-situ XRD Analysis</b>	<b>25</b>
6.1	Cathode: NCM622, pristine/doped $\text{Li}_6\text{PS}_5\text{Cl}$ and Carbon Black	25
6.1.1	with LiCl doped $\text{Li}_6\text{PS}_5\text{Cl}$	25
6.1.2	with LiF doped $\text{Li}_6\text{PS}_5\text{Cl}$	26
6.2	Cathode: Pristine/doped $\text{Li}_6\text{PS}_5\text{Cl}$ and Carbon Black	27
6.2.1	with LiCl doped $\text{Li}_6\text{PS}_5\text{Cl}$	28
6.2.2	with LiF doped $\text{Li}_6\text{PS}_5\text{Cl}$	29
<b>7</b>	<b>Alternative Doping Method</b>	<b>31</b>
7.1	Material Analysis	31
7.1.1	EIS	31
7.1.2	XRD	32
7.2	Cycling Analysis	33
7.2.1	Catholyte: NCM 622, pristine/ball milled LiCl doped $\text{Li}_6\text{PS}_5\text{Cl}$ , Carbon Black	33
7.2.2	Cathode: Pristine/Ball milled $\text{Li}_6\text{PS}_5\text{Cl}$ and Carbon black	35

---

7.3	Ex-situ XRD Analysis . . . . .	36
7.3.1	Cathode: NCM 622, ball milled LiCl doped $\text{Li}_6\text{PS}_5\text{Cl}$ , and Carbon Black . .	36
7.3.2	Cathode: ball milled LiCl doped $\text{Li}_6\text{PS}_5\text{Cl}$ , and Carbon Black. . . . .	36
<b>8</b>	<b>Conclusions &amp; Further Recommendations</b>	<b>39</b>
<b>A</b>	<b>Appendix</b>	<b>41</b>
	<b>Bibliography</b>	<b>61</b>

# 1

## Introduction

Lithium ion batteries are a form of energy storage used for a wide range of applications such as renewable energy storage, mobile phones and electric vehicles. As most renewable energy sources are intermittent, thus the energy supply might not necessarily match with the demand at any time. Energy storage, especially batteries may be among the solution of the main problem of renewable energy. Lithium ion batteries have advanced rapidly in the last two decades with long cyclic stability and increased energy density. These are ideal for applications stated.

Solid state batteries, unlike the traditional liquid electrolyte batteries have the advantage of being generally safer. An increasingly popular electrolyte, Argryrodite are generally unstable as it degrades electrochemically during cycling. Lithium Chloride (LiCl) which is a precursor to the chloride argyrodite is a chemically stable salt. Lithium Fluoride, LiF is even more stable salt compared to LiCl. Therefore, in theory it is possible to coat argyrodite with these salts to prevent direct contact with the active material to slow down decomposition of the argyrodite. However, to simplify the addition of LiCl or LiF salts, doping method is used.

This research will focus on the interphase of the half cell battery of Lithium Nickel Cobalt Manganese Oxide ( $Li(Ni_{0.6}Co_{0.2}Mn_{0.2})O_2$  or NCM 622) and doped chloride argyrodite ( $Li_6PS_5Cl$ ). As this argyrodite is unstable during cycling, it will also focus on using the argyrodite with carbon black as a cathode mixture.

This thesis will begin with the theoretical background to understand the methods or concepts used. The main part of experimental analysis and discussion will be separated into three main parts. First, in preparation for the battery assembly, the argyrodite synthesised and NCM622 will be analysed. Second, is of the actual cycling of the battery, where electrochemical data is analysed. Third, focuses on post cycling of the battery where an Ex-situ analysis is carried out.

The research questions for this thesis will include the following:

- What is the method used and how to determine the quality of the synthesised  $Li_6PS_5Cl$ ?
- What is the effect of the addition of LiCl or LiF in terms of cycling of battery performance? Why is the performance of addition of LiCl or LiF different as opposed to of using pristine argyrodite.
- Will LiCl or LiF affect the side reactions of the degradation of the argyrodite during cycling or synthesis? Is it better to neglect the active material of NCM622 to further understand the effect?
- Will changing the method of LiCl or LiF addition affect the synthesis composition or the cycling performance?



# 2

## Background Theory

This chapter will explain and summarize and review the literature used to develop this thesis. First, it briefly describes solid state batteries in general along with the properties of the materials used which are: argyrodites (with more focus on  $\text{Li}_6\text{PS}_5\text{Cl}$ ),  $\text{LiCl}$ ,  $\text{LiF}$  and  $\text{NCM622}$ , and Indium. In addition to that, this chapter will explain the theory and principles of the measurement instruments used of X-ray Diffraction (XRD) and Electrochemical Impedance Spectroscopy (EIS).

### 2.1. Solid State Lithium Ion Battery

As of today, Lithium ion rechargeable batteries have been successfully commercialized and has become a reliable power source. In Li ion rechargeable batteries, the cathodes that store lithium ions through electrochemical intercalation must contain suitable lattice sites to charge and discharge working ions reversibly. Hence, robust crystal structures with sufficiently strong storing sites are crucial to produce a material with stable cyclability and high specific capacity. Additionally, a cathode with high electrochemical intercalation potential would result in a high energy density with a given anode. This is due to the energy density of the device is the product of the specific capacity of the electrode materials and the working voltage which is the differential electrochemical potentials between the cathode and anode.[1]

The energy and power density of a battery are two essential parameters to evaluate its practical performance. Previous studies on various nanostructured cathode and anode materials with a large surface area and short solid state transport distance shows enhanced power density and better cyclic stability. Also, the energy storage performance has been improved with addition of thin (typically in nanometers scale) and porous carbon materials such as film, nanotubes and graphene on nanostructured cathode or anode materials. These carbon materials can act as electrically conductive additives, structural stabilizers, reactive precursors, or catalysts for storage performance. However, these enhancements are limited by the lithium ion storage capacity and the cell potential. The storage capacity is determined by the amount of Li ions that can be inserted and extracted reversibly under operating conditions of the battery. [1]

For Li-ion batteries, the main type of degradation are capacity fade and power fade. There are several factors of the declination of capacity such as formation and/or growth of the SEI layer on the graphite anode/electrolyte interphase, loss of active materials due to instability of structure and chemistry, and Li plating at low temperature or over-charge conditions. Overall, these processes lead to a consumption of lithium inventory which results in decrease of cell capacity. Another degradation of power fade is mainly associated with the rise of internal impedance. The factors of cell impedance increase includes the formation/growth of the SEI layer on the anode/electrolyte interphase, the formation/growth of passivation layers at cathode/electrolyte interphase, loss of contact between cell components, the reduction of conductivity of the composite binder, and the reduction of electrolyte conductivity due to electrolyte decomposition. [2]

The traditional Li ion Batteries with organic liquid electrolytes have safety issues because of the po-

tential electrolyte leakage and thus flammability. Unlike liquid electrolytes, solid electrolytes provides a safer alternative as it is non-flammable and has a better gravimetric and volumetric energy density due to its reduced packaging demands. It is important to note however that generally, solid electrolyte in a solid state batteries has a lower ionic conductivity than of conventional organic liquid electrolyte. [3]

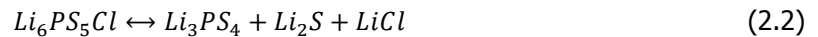
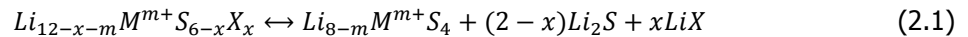
In order to achieve good performance, the solid electrolyte needs to have a high ionic conductivity with a low electronic conductivity which mitigates the electron transport. This prevents self discharge of batteries. A stable interphase between the electrodes and electrolytes are also preferred. [4]

## 2.2. Argyrodite

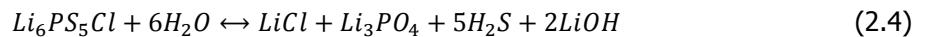
Argyrodites, which are named after the mineral  $\text{Ag}_8\text{GeS}_6$  has a general formula of  $\text{A}^{m+}_{12-m-x}(\text{M}^{n+}\text{Y}^{2-})_4\text{Y}^{2-}_x\text{X}^-_x$  where  $\text{A}^+ = \text{Li}^+, \text{Cu}^+, \text{Ag}^+$ ;  $\text{M}^{m+} = \text{Si}^{4+}, \text{Ge}^{4+}, \text{Sn}^{4+}, \text{P}^{5+}, \text{As}^{5+}$ ;  $\text{Y}^{2-} = \text{O}^{2-}, \text{S}^{2-}, \text{Se}^{2-}, \text{Te}^{2-}$ ;  $\text{X}^- = \text{Cl}^-, \text{Br}^-, \text{I}^-$ ;  $0 \leq x \leq 2$ . As first reported by Deiseroth group, lithium argyrodites are a promising candidate for solid electrolytes. [4]

Argyrodites with the general formula of  $\text{Li}_{7-x}\text{PS}_{6-x}\text{X}_x$  ( $0 \leq x \leq 1$ ;  $\text{X} = \text{Cl}, \text{Br}, \text{or I}$ ) have high Lithium ions ( $\text{Li}^+$ ) conductivity which is an ideal characteristic for an electrolyte.  $\text{Li}_6\text{PS}_5\text{Cl}$  argyrodite especially has a high conductivity ( $\sigma = 1.33 \times 10^{-3} \text{ S cm}^{-1}$  at  $25^\circ\text{C}$ ) and has a lower cost than sulfur based solid electrolyte consisting of germanium (Ge) which makes it a promising electrolyte in a solid state battery.[5]

However, it is generally observed that argyrodite undergoes a rapid capacity loss due to a suspected active material and electrolyte interface instability which leads to an impedance increase[5]. It is found that argyrodites share the same critical decomposition as expressed as Equation 2.1[4]. Applying this reaction for  $\text{Li}_6\text{PS}_5\text{Cl}$ , the expression is related to equation 2.2.



In addition to that, it is found that lithium argyrodites decompose in moisture as it has negative dissociation energies. Phosphorus and silicon argyrodites are highly sensitive to moisture. Also, the vulnerability of hydrolysis only slightly decrease with the increase of the size of the halogen atom. The critical reaction for this case expressed in equations 2.3 and 2.4.[4]



## 2.3. Doping, Lithium Chloride and Lithium Fluoride

Doping is a widely used method to change certain physical and/or chemical properties by small addition (typically less than 1%) of one or more compounds or elements. The position of the dopant (the doping agent) is not necessarily known. [6] [7]

In this thesis, Lithium Chloride ( $\text{LiCl}$ ) is chosen as a dopant for the argyrodite as it is the most stable among the  $\text{Li}_6\text{PS}_5\text{Cl}$  precursors. Lithium Fluoride ( $\text{LiF}$ ) is also researched on as a doping material due to its similar crystal structure and chemical properties to  $\text{LiCl}$ .

Chlorine (Cl) And Fluorine (F) belong to Group 7, which is also known as halogens in the periodic table as shown in 2.1. Halogens are a high electronegative group, which means it is very stable once it accepts an additional electron to form an anion ( $\text{X}^-$ ). Lithium metal (in Group 1) in contrast, has a low electronegativity and will likely to donate an electron ( $\text{Li}^+$ ). In the formation of  $\text{LiCl}$  and  $\text{LiF}$ , F and Cl will accept an electron from a lithium metal. This type of bonding is known as ionic bonding. [8]

As fluorine is positioned the highest of the group 7 in the periodic table, it has the least electrons rings, and thus the least shielding, which makes it very stable due to forces from the nucleus. Chlorine has an additional shielding from an additional electron ring, which makes it less stable than fluorine.  $\text{Cl}^-$  is more polarizable than  $\text{F}^-$ , which means that it has greater ease in electron density distortion towards the cations. Thus,  $\text{F}^-$  has greater ionic character than  $\text{Cl}^-$ . Thus, LiF salt has stronger ionic bonds than of LiCl, and thus when reacted with reactants, LiCl will react with reactants to form  $\text{Li}_6\text{PS}_5\text{Cl}$  as opposed to  $\text{Li}_6\text{PS}_5\text{F}$ . [8]

Group 7: Halogens

H																			He
Li	Be										B	C	N	O	F	Ne			
Na	Mg										Al	Si	P	S	Cl	Ar			
K	Ca	Sc	Ti	V	Cr	Mn	Fe	Co	Ni	Cu	Zn	Ga	Ge	As	Se	Br	Kr		
Rb	Sr	Y	Zr	Nb	Mo	Tc	Ru	Rh	Pd	Ag	Cd	In	Sn	Sb	Te	I	Xe		
Cs	Ba		Hf	Ta	W	Re	Os	Ir	Pt	Au	Hg	Tl	Pb	Bi	Po	At	Rn		
Fr	Ra																		

© Pass My Exams

Figure 2.1: Periodic table with Group 7 highlighted [9]

It is worth noting that in the first intuition is that the argyrodite of  $\text{Li}_6\text{PS}_5\text{F}$  is formed if the reactant of LiF is used instead of LiCl from Reaction 3.1. However, it is nearly impossible to have a fluoride argyrodite due to the strong stability and ionic bonding of LiF. Furthermore, there are no papers which mentions formation of fluoride argyrodites.

## 2.4. NCM as an Active Material for Cathode

Transitional metal oxides as a cathode material have many advantages as their variable valence states facilitate more electron-storing sites [10]. This includes  $\text{Li}(\text{Ni}_x\text{Co}_y\text{Mn}_z)\text{O}_2$  (where  $x+y+z=1$ ) also known as NCM which is a promising cathode material. This is mainly due to NCM generally have higher specific capacity than a well used cathode active material, Lithium Cobalt Oxide (LCO). NCM also have a lower cost due to less cobalt content is required in LCO.  $\text{Li}(\text{Ni}_{0.33}\text{Co}_{0.33}\text{Mn}_{0.33})\text{O}_2$  (or NCM 333) is typically used in the battery market. Recent studies show that NCM showed reversible specific capacity as high as 234 mAh/g and good cycle stability even at 50°C [11]. The bulk material for a nickel-rich layered oxide  $\text{Li}(\text{Ni}_{0.8}\text{Co}_{0.1}\text{Mn}_{0.1})\text{O}_2$  has a higher energy density as higher nickel content allows for higher lithium extraction without structure deterioration. [12]

In several literature, the degradation of NCM is well documented. Its' capacity fade is mainly due to the loss of lithium inventory caused by SEI layer formation/growth at the anode, and loss of the active material at the cathode. In the case of NCM 622 (or NMC 622) is illustrated in Figure 2.2 from a literature that confirms both power fade and capacity fade occurs. Figure 2.2(a) shows the CV curve shifts to the left with increasing number of cycles which confirms the power fade, and Figure 2.2(b) shows that it does not retain its capacity with increasing number of cycles which proves that capacity fade occurs at much later cycles. [2]

In this thesis,  $\text{Li}(\text{Ni}_{0.6}\text{Co}_{0.2}\text{Mn}_{0.2})\text{O}_2$  also known as NCM 622 is used.

## 2.5. Indium metal

Indium metal is used in this thesis as the counter anode. Indium metal is uniform and self-healing. The chemical composition of Indium generally remains the same while being physically intact. Hence it is a stable counter electrode. [13]

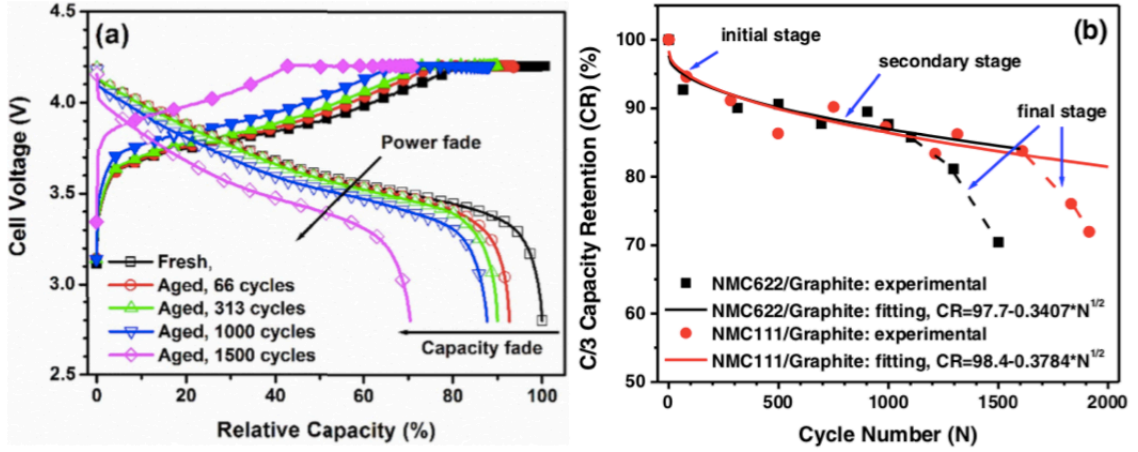


Figure 2.2: (a) 1C and C/3 discharge curves; (b) C/3 capacity retention at room temperature as a function of cycle number for NCM622/graphite cells with NCM111/graphite cells for comparison [2]

## 2.6. Electrochemical Impedance Spectroscopy

According to Ohm's law, resistance is the ratio of Voltage,  $E$  to current,  $I$  as expressed in equation 2.5. This expression is too simplified because in realistic situations, circuit elements have a more complex behaviour. Thus impedance is used in the place of resistance. A typical method to measure Electrochemical Impedance is to apply an AC potential to an electrochemical cell and measuring the current passing through it. Assuming that sinusoidal potential excitation is applied, the response to this potential is an AC current signal which can be analyzed as a sum of sinusoidal functions (Fourier series). [14]

$$R = \frac{E}{I} \quad (2.5)$$

For the cell's response to be pseudo-linear, the electrochemical impedance is normally measured using a small excitation signal. In this case, the current response will be a sinusoid at the same frequency but with the phase shifted as seen in Figure 2.3 [14].

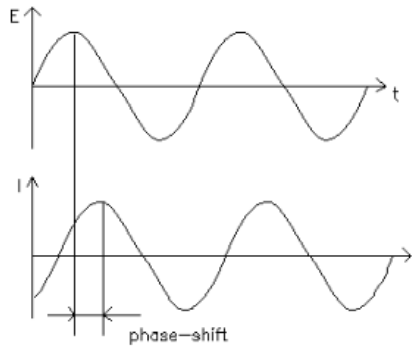


Figure 2.3: Sinusoidal Current Response in a linear system [14]

The excitation signal is thus expressed as:

$$E_t = E_o \sin \omega t \quad (2.6)$$

where  $E_t$  is the potential at time  $t$ ,  $E_o$  is the amplitude of the signal, and  $\omega$  is the radial frequency ( $\omega = 2\pi f$ ). For a linear system, the response signal,  $I_t$  is shifted by phase ( $\phi$ ) and has different amplitude than of  $I_o$  which is then expressed as: [14]

$$I_t = I_o \sin \omega t + \phi \quad (2.7)$$

To calculate impedance of the system, which is similar to Equation 2.5 and by combining Equations 2.6 and 2.7 is determined by: [14]

$$Z = \frac{E_t}{I_t} = \frac{E_o \sin \omega t}{I_o \sin \omega t + \phi} = Z_o \frac{\sin \omega t}{\sin \omega t + \phi} \quad (2.8)$$

The impedance is thus expressed in terms of magnitude  $Z_o$  and phase shift  $\phi$ . Plotting  $E(t)$  against  $I(t)$  as shown in Figure 2.4 will result in an Lissajous (a method of impedance measurement) figure which is circled. [14].

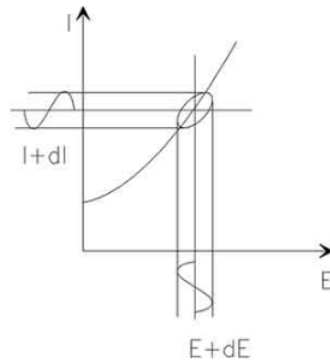


Figure 2.4: Origin of Lissajous figure [15]

With Euler's relationship (as expressed in Equation 2.9, impedance may be expressed as a complex function from the potential (Equation 2.10) and current response (Equation 2.11) as expressed in Equation 2.12 [14].

$$\exp(j\phi) = \cos \phi + j \sin \phi \quad (2.9)$$

$$E_t = E_o \exp(j\omega t) \quad (2.10)$$

$$I_t = I_o \exp(j\omega t - \phi) \quad (2.11)$$

$$Z(\omega) = \frac{E}{I} = Z_o \exp(j\phi) = Z_o (\cos \phi + j \sin \phi) \quad (2.12)$$

For the impedance of an electrochemical cell, the electrolyte resistance is often a significant factor. The resistance depends on type of ions, concentration of ions, temperature, and geometry of the electrolyte. The resistance is then reflected as Equation 2.13, where  $R_b$  is the bulk resistance of a material where  $\kappa$  is the ionic conductivity of a material,  $A$  is the area of the composite films, and  $l$  is the thickness of the composite films. The unit of conductivity,  $\kappa$  is usually Siemens per meter (S/m).

[14]

$$R_b = \frac{1}{\kappa} \frac{A}{l} \rightarrow \kappa = \frac{l}{RA} \quad (2.13)$$

Nyquist impedance plot ( $Z'-Z''$ ) plot can determine the appropriate equivalent circuit and to estimate the circuit parameters values which reflect the carrier transport properties. From Figure 2.5, it is observed that there is a compressed semicircle in the high frequency range, and then a straight inclined line in the low frequency range. Typically in real scenarios, the Nyquist plot deviate from an ideal impedance spectrum which is a perfect semicircle and a straight line to a deformed semicircle and a nearly straight line. This may be due to irregular thickness and morphology of the electrolyte film, and the electrolyte surface roughness[.]. There are two methods to get the value of  $R_b$  from the Nyquist plot. The first, is the intersection point of the semicircle (in high frequencies) and the inclined line (in low frequencies). The other, is by fitting the Nyquist plot using a standard software with predefined parameters[16].

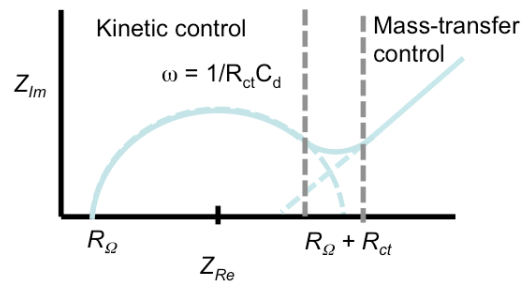


Figure 2.5: Ideal Nyquist plot

Referring to Figure 2.5, if  $R_{ct}$  is large and hence the Nyquist plot mostly consist of the semi-circle, the system is kinetically slow and mass transfer is significant. In contrast, if  $R_{ct}$  is low, and hence the Nyquist plot mostly consist of the straight inclined line, mass transfer always play a role and the system is kinetically simple. [17] [18]

A method to evaluate the data quality of EIS is to use Kramers-Kronig (KK) relations. This relation shows that the plane spectral data shows dependence between magnitude and phase. The integration of the imaginary part determines the real part of the spectrum and vice versa. In this instace, KK analysis is done by fitting the model to experimental EIS data.If the model is a good fit, than it is concluded to be KK compliant [19][20]. Usually, a KK test is necessary although not a sufficient condition for requirements. [21]

## 2.7. X-ray Diffraction

The properties of materials are defined by its chemical composition and microstructure. A key step in determining the structure, properties and applications of a given material is through the quantification of crystalline phases. Typically, the distribution of phases or microstructure is affected by maunfacturing techniques, raw materials used, sintering process, equilibrium reactions, kinetics and phase changes.[22]

This report will use X-ray diffraction analysis due to its ability to characterize: Index of crystalline phases, refinements of unit cell, quantitative analysis of phases, determination of crystal structures, and refinements of crystal structures. Additionally, XRD is suitable for quantitative analysis of phases.

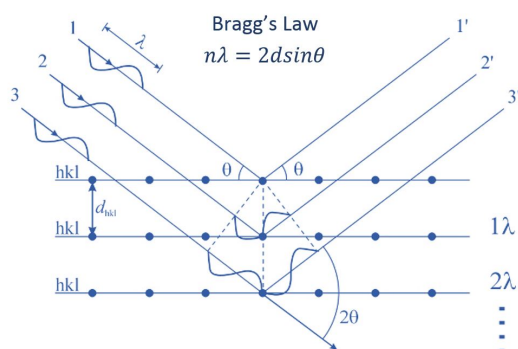


Figure 2.6: Schematic of Bragg's law principle [23]

### 2.7.1. XRD principle

XRD relates to the phenomenon of interactions between the incident X-ray beam and the electrons of the atoms of a material component from coherent scattering. This technique involves incidence of radiation on a sample and in the detection of the diffraction photons (also known as diffracted beam).[22]

Referring to Figure 2.6, at a certain frequency, the x-ray beam that focuses on a beam behaves as a scattering centre and vibrates at the same frequency as the incident beam, spreading in all direction. When the atoms are arranged in a lattice, this incident beam will go through a constructive interference in certain directions, and destructive in others. Likewise when the path difference of successive planes scattered beam is equal to an integer number of wavelength, The constructive interference of scattered radiation occurs. Bragg's law, which is a geometric interpretation from the figure is expressed as Equation 2.14 where  $n$  is the integer number of wavelength,  $d$  is the interplanar distance of the successive crystal planes,  $\theta$  is the angle measured between the incident beam and determined crystal planes [22].

$$n\lambda = 2d \sin \theta \quad (2.14)$$

The diffracted beam is usually expressed through peaks that stand out from the background (in intensity per second) versus the angle  $2\theta$  or  $d$ . Each crystalline compound has a characteristic diffraction pattern which allows phase identification through the angular positions and relative intensities of diffracted peaks. To identify crystalline phases, the XRD with the diffraction patterns of individual phases provided by ICDD (*International Center for Diffraction Data*) are compared. It is also possible to quantify ratio of phases from the XRD peak intensities [22].

The analysis of diffraction pattern can give many information of the structure of the material. These include:

- Angular position of diffraction lines is affected by the geometry of the crystal lattice,
- Intensity of the diffraction line is affected by the type of atoms, its arrangement on the crystal lattice and the crystallographic orientation
- shape of diffraction lines which is affected by instrumental broadening, particle size, and deformation. [22]

However, there are also other factors from the instrument which can affect the diffraction pattern of a sample. These include: displacement of the sample, geometry of the X-ray source, transparency of the sample, misalignment of the diffractometer, and more [22]. Other factors from the sample include the flatness of the sample shape, transparency of the sample, particle size, and more.

### 2.7.2. Quantification of Crystalline phases in materials

In the context of this research, refinement refers to the process of adjusting the model of parameters included in the calculation of a diffraction pattern, to the closest observed of the XRD measurement. Typically, simultaneous refinement includes but not limited to: unit cell and crystal structure, microstructure analysis, quantitative analysis of phases and determination of preferred orientation [22].

The *General Structure Analysis System* (GSAS) program has a great flexibility for single crystal data, neutron diffraction, and powder diffraction which has been widely used in the scientific community. The main parameters that can be adjusted simultaneously for refinement (especially in GSAS) are as follows:

- **Scale factor:** Relates to the amount of phase;
- **Background:** (Also known as baseline) Correction from data collected in the same XRD pattern and interpolation between these points.
- **Peak profile:** The width and position of the peaks are depends on the characteristics of crystallite size and cell respectively;
- **Cell parameters:** Interplanar distance of successive planes of the crystal fitted by Bragg's law;
- **Factor of structure:** Variable parameters that includes atomic positions, the isotropic and anisotropic temperature factors, and the occupation number;
- **Offset:** Parameters of displacement corrections due to external factors
- **Preferential orientation:** Problems generated in the sample preparation correlation [22]

There are many ways to evaluate the output file and refinement data. Hugo Rietveld has suggested the weight fraction as expressed in Equation 2.15, where  $S_j$  is the refined scale factor of component  $i$  in a mixture of  $j$  phases,  $Z$  is the number of formula units in the unit cell of  $i$ ,  $M$  is the mass of formula unit (in atomic mass unit), and  $V$  is the volume of unit cell (in  $\text{\AA}^3$ ). Hence the term  $ZMV$  is the product of  $Z$ ,  $M$ , and  $V$  [24].

$$W_i = \frac{S_i(ZMV)_i}{\sum_j S_j(ZMV)_j} \quad (2.15)$$

The refinement can be assessed from verification of the structural parameters and the profile obtained, the comparison of results with those obtained for single crystals and the observation of plot of calculated and observed patterns and residuals obtained. To verify the quality of refinement, GSAS uses *R-profile* ( $R_p$ ) and *R-Profile Adjust* ( $R_{wp}$ ) as expressed in Equations 2.16 and 2.17 respectively. For good results the value of  $R_{wp}$  should be 2-10%. [22]

$$R_p = \frac{\sum |y_{i,obs} - y_{i,calc}|}{\sum y_{i,obs}} \quad (2.16)$$

$$R_{wp} = \left[ \frac{\sum w_i (y_{i,obs} - y_{i,calc})^2}{\sum w_i (y_{i,obs}^2)} \right]^{0.5} \quad (2.17)$$

# 3

## Experimental Methods

### 3.1. Battery Preparation

The half-cell battery is assembled as shown in Diagram 3.1 with NCM 622 as the active material, Super P Carbon Black as the electron conductors, and  $\text{Li}_6\text{PS}_5\text{Cl}$  as the electrolyte. Indium metal is used as an anode

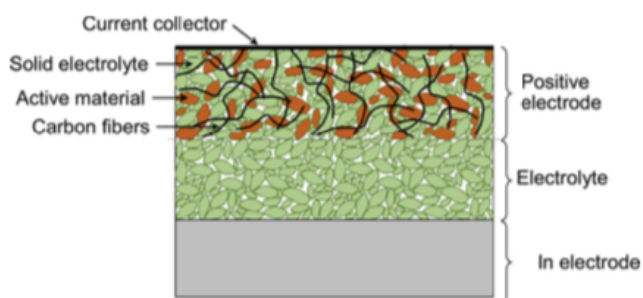


Figure 3.1: Schematic view of the cross section of the battery applied in this research [5]

#### 3.1.1. Argyrodite Synthesis

Lithium Sulfide ( $\text{Li}_2\text{S}$ ), Phosphorus Pentasulfide ( $\text{P}_2\text{S}_5$ ), and Lithium Chloride ( $\text{LiCl}$ ) are precursors of the chloride argyrodite ( $\text{Li}_6\text{PS}_5\text{Cl}$ ). These precursors are weighed in exact molar composition (see Equation 3.1) and always in the Argon glovebox. These reactants are then agate ball milled at 110 RPM for 1 hour to form a homogeneous mixture. These precursors are then enclosed in a glass tube under Argon gas to allow it to be transferred to an oven to be annealed at  $550^\circ\text{C}$  for 10 hours with a heating rate of  $100^\circ\text{C}/\text{hour}$ . The sample in the tube is then transferred back into the argon glovebox in order to break it open and hand grind the sample to a fine powder. This is considered a pristine argyrodite.



To synthesize doped argyrodite, 5 and 10% of  $\text{LiCl}$  mass required is calculated. With this value,  $\text{LiCl}$  is added to the reactants before the ball milling process. This process is repeated with  $\text{LiF}$  in the place of additional  $\text{LiCl}$  added. From this point onwards, **the argyrodites with additional 5% and 10%  $\text{LiCl}$  added will be referred to " $\text{Li}_6\text{PS}_5\text{Cl CL5}$ " and " $\text{Li}_6\text{PS}_5\text{Cl CL10}$ " respectively. Also, with the same weight percentage as the additional  $\text{LiCl}$ ,  $\text{LiF}$  is used instead and will be referred to as " $\text{Li}_6\text{PS}_5\text{Cl F5}$ " and " $\text{Li}_6\text{PS}_5\text{Cl F10}$ " respectively.**

### 3.1.2. Catholyte & Cathode mixture

Catholyte, which in definition is a mixture of cathode active material and electrolyte. For this thesis, the catholyte in solid state battery consists of the active material of NCM 622 (coated, 5 microns (0.1  $\mu$ m)), argyrodite synthesized from section 3.1.1, and super P carbon black. In this experiment, the catholyte mixture is fixed at a ratio of 45.5:45.5:5 by mass for NCM 622, argyrodite, and carbon black respectively. In the argon glovebox, these reactants are hand grind with a agate pestle and mortar until a homogeneous mixture is formed. For each argyrodite synthesized, different cathodes are prepared.

Another type of cathode mixture is prepared using argyrodite and carbon black with the weight ratio of 7:3 respectively. Cathodes mixtures are used for each type of argyrodite synthesised.

### 3.1.3. Battery Assembly

The solid state battery is assembled in the Argon Glovebox with a 10 mm diameter of the Aluminium Oxide Ring, and thus, 10mm of pellet of the active battery.

Approximately 100mg of pristine  $\text{Li}_6\text{PS}_5\text{Cl}$  is poured into the aluminium oxide ring with an electrode underneath. A cylinder which fits in the ring is inserted in the ring. The ring is then inverted and the electrode is removed. The spatula is then used to ensure a smooth and even distribution of the electrolyte in the ring. Then approximately 15mg of cathode mixture is poured above the electrolyte and the spatula is used to distribute a smooth layer that ensures it covers the surface of the electrolyte. Great care is to ensure that the electrolyte and the cathode mixture do not mix together. An electrode was put back into ring and inverted. The pellet press was put under the pressure of 4.5 tons with steps of 0.5 tons with release. This is followed by removing the pellet press and 8mm diameter of Indium (Anode) and stainless steel (for easy cleaning) was inserted and the last electrode was put in. The whole battery was pressed under the pressure of tons and then screwed tightly. It is also important to note that 10mm diameter of O-rings with thickness of 1mm was used to ensure airtightness of the battery.

## 3.2. Battery Analysis

### 3.2.1. Electrochemical Impedance Spectroscopy Measurement

Each argyrodite synthesized are tested separately. Approximately 200g of argyrodite is pressed into a pellet into a solid state battery in the argon glovebox. This battery is then connected to *Nova Autolab*. All impedance measurements were carried out at 10Hz to 1M hz with applied voltage of 0.05V at room temperature. Additionally, with a built-in function of Nova Autolab, Kronig-Kramers (KK) test is carried out. Post impedance testing, the battery is disassembled and the pellet is removed to measure the thickness ( $l$ ) with a thickness gauge meter. ( $l$ )

### 3.2.2. Maccor

After the battery is assembled from subsection 3.1.3, the battery is connected to Maccor Instrument which charges and discharges the battery at a constant C-rate while measuring the voltage, current, capacity with time and cycle. The cycling settings for battery with catholytes are summarized as follows:

- Resting period: 3 hours before start of first cycle and 30 mins in between cycles
- Cut-off Voltage: 3.58V (charging) & 1.88V (discharging)
- Constant C-rate: 0.05C (178mAh per g of NCM 622 used)

Additionally, the cycling setting for the cathode mixture of argyrodite and carbon black are as follows:

- Resting period: 1 hour before the start of the first cycle and 30 mins in between cycles
- Cut-off Voltage: 3.68V (charging) & 0V (discharging)
- Constant C-rate: 0.05C (0.00010205Ah)

### 3.2.3. X-ray Diffraction (XRD)

Every Argyrodite synthesised were measured in the XRD machine for 1 hour. NCM 622 and the cathode mixture with NCM622 were also measured in the XRD using the monochromator for approximately 3 hours. Finally, after cycling, the pellet (electrolyte and cathode) were removed the battery to be analysed using batch mode which has 6 scans at least to test the efficiency of the vacuum sample holder. For every material measured that contains argyrodite, a vacuum sample holder is used as it is air-sensitive.

Each XRD measurement is refined using GSAS EXPGUI. *Pearson Crystal Data* software was used to find information for each phases which includes cell parameters. During refinement, the values of  $R_{wp}$  and  $R_p$  are noted and should be decreasing. Once that value is increasing, then refinement needs to stop and reopen the previous refinements to redo. Refinement is considered satisfied once  $R_{wp}$  and  $R_p$  values cannot get any lower and all the peaks are fitted.



# 4

## Material Analysis

$\text{Li}_6\text{PS}_5\text{Cl}$  argyrodites are synthesized as mentioned in section 3.1.1 prior to be used in the solid state batteries. This chapter analyses the quality of the argyrodite synthesized with Electrochemical Impedance Spectroscopy (EIS) to determine its ionic conductivity. X-ray Diffraction (XRD) is also used to analyze the purity of the argyrodite synthesized and potential side products formed. Additionally, XRD is also used to analyze the quality of NCM 622, and each cathode mixture with NCM 622.

### 4.1. Electrochemical Impedance Spectroscopy (EIS) testing

In this section, each of the synthesised  $\text{Li}_6\text{PS}_5\text{Cl}$  is tested with EIS. The data obtained from EIS is used to determine the ionic conductivity of each argyrodite synthesized.

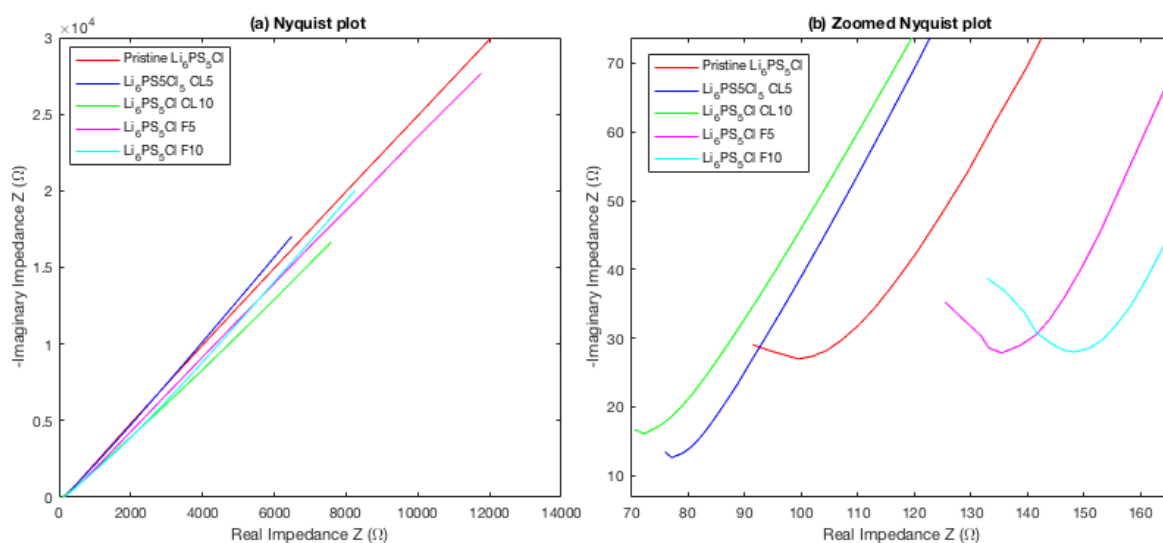


Figure 4.1: Nyquist plot at room temperature: (a) Overall and (b) zoomed at low impedances (also at high frequencies)

The Nyquist plot of each argyrodite synthesized is shown in Figure 4.1. In this figure (a), the inclined straight line dominates which indicates that mass transfer control dominates over the kinetic control. This means that the ionic transport (most likely  $\text{Li}^+$  ions) migrates and/or diffuses across under current.

If the Nyquist plot is zoomed at high frequencies (or at low Real Impedance) as shown in Figure 4.1(b), partial semi-circles which relates to the kinetic control are observed. Thus, chemical reactions such as decomposition will occur. If the impedance instrument is able to measure at higher frequencies, than it may be possible to observe full semicircles of the Nyquist plot. However, due to the limitation

of the Autolab instrument, the maximum frequency it is able to measure is 1 MHz. From the figure, it is expected that LiCl doped  $\text{Li}_6\text{PS}_5\text{Cl}$  have the lowest rate of reaction. Pristine  $\text{Li}_6\text{PS}_5\text{Cl}$  and LiF doped  $\text{Li}_6\text{PS}_5\text{Cl}$  also have significant rate of reaction, with  $\text{Li}_6\text{PS}_5\text{Cl}$  F10 expected to be the highest due to its larger 'semi-circle'.

The ionic conductivity is then calculated using Equation 2.13 with the value of  $A$  of  $7.85 \times 10^{-5} \text{ mm}^2$  (from internal battery diameter of 10mm) and values of  $I$  summarized in Table A.1 in Appendix. From the intersection of the semicircle and the straight line, the bulk resistance,  $R_b$  of the electrolyte can be determined (See Figure A.1 in Appendix for values). Thus, for each argyrodite synthesised, the conductivities are summarised in Table 4.1. The conductivity of the pristine  $\text{Li}_6\text{PS}_5\text{Cl}$  synthesised for this thesis has a number of side products which will be further discussed in Section 4.2.2. With the addition of LiCl, the conductivity increases. In contrast, the addition of LiF decreases the conductivity of the argyrodite.

Table 4.1: Ionic conductivity obtained and calculated from Figure 4.1 and Equation 2.13

Argyrodite	Ionic Conductivity [s/cm]
Pristine $\text{Li}_6\text{PS}_5\text{Cl}$	0.0020
$\text{Li}_6\text{PS}_5\text{Cl}$ CL5	0.0027
$\text{Li}_6\text{PS}_5\text{Cl}$ CL10	0.0028
$\text{Li}_6\text{PS}_5\text{Cl}$ F5	0.0016
$\text{Li}_6\text{PS}_5\text{Cl}$ F10	0.0014

Lissajous analysis was carried out as shown in Figure A.3 in Appendix. The quality of the AC and voltage varies between different readings of the synthesised  $\text{Li}_6\text{PS}_5\text{Cl}$ . This is mainly due to different Autolab instrument used. For a perfect supply of AC the Lissajous figure should be perfectly oval shaped. Since some of the imperfect figures do not deviate much from the oval shaped, the reading is accepted.

Next, KK analysis is carried out. (See Figure A.5 in Appendix). From the analysis, the error are quite low in a range of 0 to 2%. Thus, it is determined that the EIS data is reliable.

## 4.2. XRD Analysis of reactants

The purpose of the analysis of the XRD measurement with refinements is to determine the quality of the  $\text{Li}_6\text{PS}_5\text{Cl}$  synthesised and NCM 622 to be used in assembling the battery later on. With GSAS refinements, the following data can be determined: side products and the scale factor of each phases (products).

### 4.2.1. NCM 622

From the refined XRD measurement as shown in Figure 4.2, the quality of the industrial grade NCM 622 is highly pristine or pure. This is reflected in the XRD analysis where the refinement closely matches the measurement with low  $R_p$  and  $R_{wp}$  values and minimal background.

### 4.2.2. $\text{Li}_6\text{PS}_5\text{Cl}$

The XRD measurement and refinements of each argyrodites are plotted in Figures A.12(a), A.13(a), A.14(a), A.15(a), and A.16(a) in the Appendix. From the refinements, it is discovered that the synthesised  $\text{Li}_6\text{PS}_5\text{Cl}$  contains precursors of lithium chloride ( $\text{LiCl}$ ) and lithium sulfide ( $\text{Li}_2\text{S}$ ); and the side products of: lithium phosphate ( $\text{Li}_3\text{PO}_4$ ) and  $\text{Li}_2\text{PS}_3$ . The most significant side product, which is  $\text{Li}_3\text{PO}_4$  indicates that it has been reacted with air or moisture as stated previously in the literature, despite the synthesis process has taken great care to avoid this from happening. The other side products noted may be due to the insufficient annealing or ball-milling power or duration. Pristine  $\text{Li}_6\text{PS}_5\text{Cl}$  synthesised has the least amount of side reactants and amount of LiCl. As pristine  $\text{Li}_6\text{PS}_5\text{Cl}$  may not have been so pure, nevertheless, it is a good constant in regards to argyrodites with additions of LiCl and LiF.

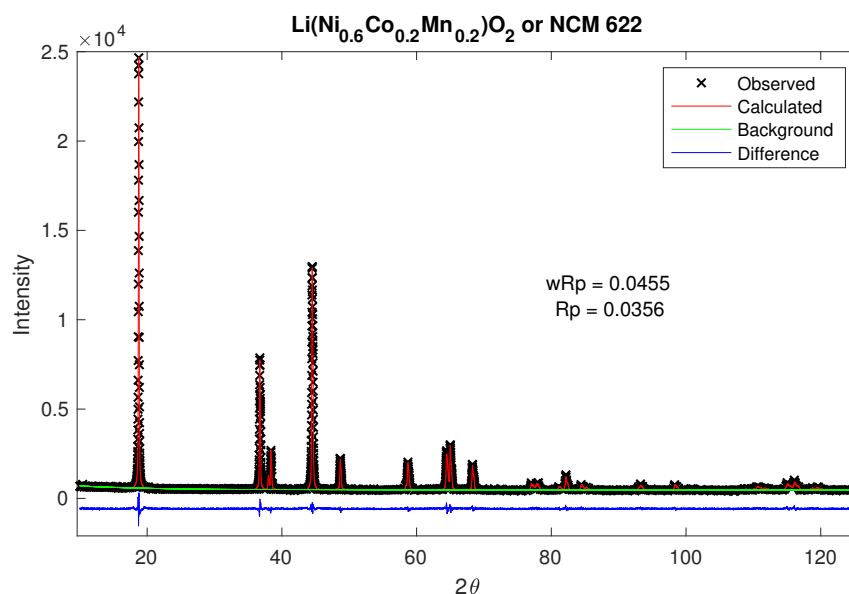


Figure 4.2: XRD measurement and refinement of NCM 622

From the phase fractions refined, the weight fraction is calculated using Equation 2.15. In regards to weight fraction, it is expected that pristine  $\text{Li}_6\text{PS}_5\text{Cl}$  contains the highest amount of  $\text{Li}_6\text{PS}_5\text{Cl}$  with the lowest amount of  $\text{LiCl}$ .  $\text{Li}_6\text{PS}_5\text{Cl}$  CL5 and CL10 have highest weight fraction of  $\text{LiCl}$ . This is indeed reflected in Figure 4.3.

For  $\text{LiF}$  doped argyrodite in the same figure, there are small amounts of  $\text{LiCl}$  that was likely from the unreacted precursors. It could be possible that the very stable  $\text{LiF}$  salts inhibited the reactants to synthesize properly during annealing due to reduction of contact of the precursors. This is proven as  $\text{LiF}$  has the the highest number of impurities. What could be done was the ball milling and annealing of the precursors should be longer.  $\text{LiF}$  present in  $\text{Li}_6\text{PS}_5\text{Cl}$  F5 seems to be more than of  $\text{Li}_6\text{PS}_5\text{Cl}$  F10. However in reality, the percentage could be offset by the larger amount of  $\text{Li}_3\text{PO}_4$  present in  $\text{Li}_6\text{PS}_5\text{Cl}$  F10 than of  $\text{Li}_6\text{PS}_5\text{Cl}$  F5.

### 4.2.3. Catholyte mixture

As mentioned in Section 3.1.2, the cathode mixture consists of the Argyrodite (Pristine or doped), NCM622, and carbon black with the mass ratio of (42.5:42.5:5). XRD of NCM622,  $\text{Li}_6\text{PS}_5\text{Cl}$ , and other phases will give the XRD of the catholyte mixture. Please refer to Figures A.7(a), A.8(a), A.9(a), A.10(a), and A.11(a) in Appendix to see each XRD measurement and refinements of the catholyte mixtures.

Using the Rietveld weight fraction analysis as expressed in Equation 2.15, the graph of weight fraction of different phases in the catholyte mixture is shown in Figure 4.4. From this figure, the mass fraction of NCM 622 and  $\text{Li}_6\text{PS}_5\text{Cl}$  are nearly the same for all the argyrodites synthesised.  $\text{Li}_3\text{PO}_4$  is clearly significant with different quantities. This will definitely affect the results during cycling as  $\text{Li}_3\text{PO}_4$  has its own conductivity and specific capacity which could affect the overall argyrodite. Also,  $\text{Li}_6\text{PS}_5\text{Cl}$  CL10 also has a significant amount of  $\text{Li}_2\text{S}$  while other argyrodites has a small amount of it. The overall result may affect the EIS reading, as other phases are more pronounced than  $\text{LiCl}$  or  $\text{LiF}$ . Thus, it is difficult to determine if  $\text{LiCl}$  or  $\text{LiF}$  addition affects the EIS reading. It is important to note that the Rietveld method to quantify phases may not be accurate. This is due to the fact that the weight of NCM 622 and argyrodite should be equal which is not reflected in the figure. Nevertheless, the ratio of NCM 622 to Argyrodite and its side phases remains nearly constant throughout the catholyte mixture and thus the method is not completely wrong.

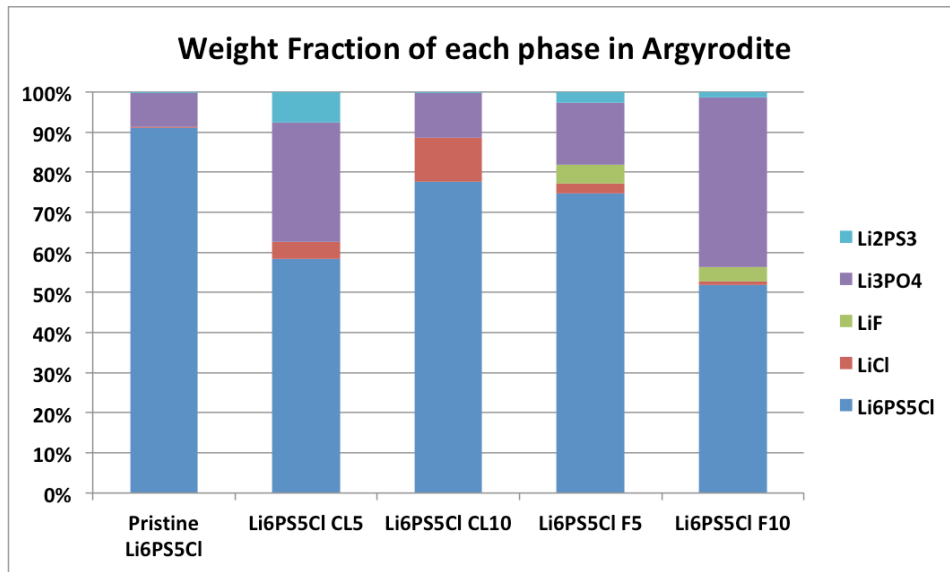


Figure 4.3: Weight Fraction of phases present in Argyrodite synthesised

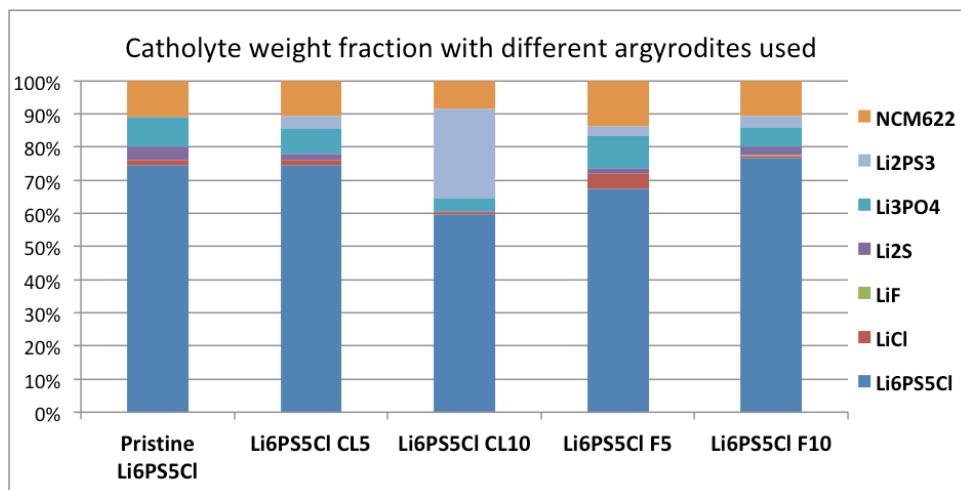


Figure 4.4: Weight fraction of cathode material with different argyrodites used

# 5

## Cycling Of Batteries

After the cathode mixtures are synthesized, the batteries are finally assembled and cycled as detailed in Section 3.1.3 and 3.2.2. This section will analyze the results obtained from the Maccor.

### 5.1. Catholyte: NCM 622, pristine/doped $\text{Li}_6\text{PS}_5\text{Cl}$ & Carbon Black

Overall, there is a significant specific capacity drop after the first cycle followed by a more stable horizontal curve as shown Figures 5.1 and 5.2. This was expected as mentioned in Section 2.4 which indicates that NCM cathodes and the argyrodites degrades after the first cycle (this point will be further discussed in Chapter 6). However, in literature (Section 2.4), NCM degrades significantly after approximately 70 cycles and thus the degradation and decomposition of NCM 622 may be assumed to be negligible.

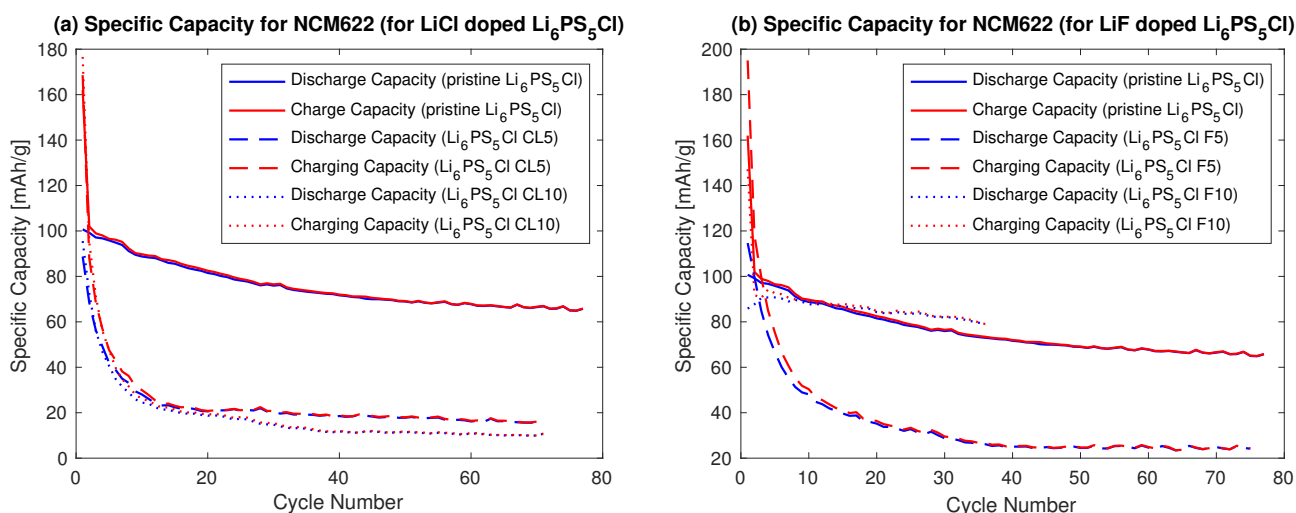


Figure 5.1: Specific capacity of NCM 622 with each cycle with (a) LiCl doped  $\text{Li}_6\text{PS}_5\text{Cl}$ , and (b) LiF doped  $\text{Li}_6\text{PS}_5\text{Cl}$  in comparison with pristine  $\text{Li}_6\text{PS}_5\text{Cl}$

From Figure 5.1, it is observed that using pristine  $\text{Li}_6\text{PS}_5\text{Cl}$  in the catholyte generally gives a larger specific capacity retention for NCM 622 in comparison to of doped  $\text{Li}_6\text{PS}_5\text{Cl}$ . For the LiCl doped  $\text{Li}_6\text{PS}_5\text{Cl}$  in Figure 5.1(a), the LiCl addition appears to reduce the specific capacity retention of NCM 622. Thus, it creates an impression that  $\text{Li}_6\text{PS}_5\text{Cl}$  CL5 and CL10 have lower ionic conductivities than of pristine  $\text{Li}_6\text{PS}_5\text{Cl}$  due to less mobile ions in the cathode region. This is despite the higher ionic conductivities for  $\text{Li}_6\text{PS}_5\text{Cl}$  CL5 and CL10 from the EIS analysis (see Table 4.1). It is possible that this cathode

has poor interphase contact between the active material and the LiCl doped  $\text{Li}_6\text{PS}_5\text{Cl}$  and therefore have higher resistance in the interphase that results in the poor overall specific capacity.

For LiF doped  $\text{Li}_6\text{PS}_5\text{Cl}$  as shown in Figure 5.1(b),  $\text{Li}_6\text{PS}_5\text{Cl}$  F5 is shown to have lower specific capacity retention than of pristine  $\text{Li}_6\text{PS}_5\text{Cl}$ . Thus, the ionic conductivity is lower for  $\text{Li}_6\text{PS}_5\text{Cl}$  F5 than of pristine as  $\text{Li}_6\text{PS}_5\text{Cl}$  F5 has lower lithium ion mobility in the cathode which lowers the specific capacity retention. This correlates to the ionic conductivity values from EIS analysis (Table 4.1). However,  $\text{Li}_6\text{PS}_5\text{Cl}$  F10, appears to have better retention specific capacity of NCM 622 than for pristine  $\text{Li}_6\text{PS}_5\text{Cl}$  despite having the lower ionic conductivity from EIS analysis. This could be due to the composition of the catholyte having similar composition from the XRD analysis (see Figure 4.4) rather than  $\text{Li}_6\text{PS}_5\text{Cl}$  F5.

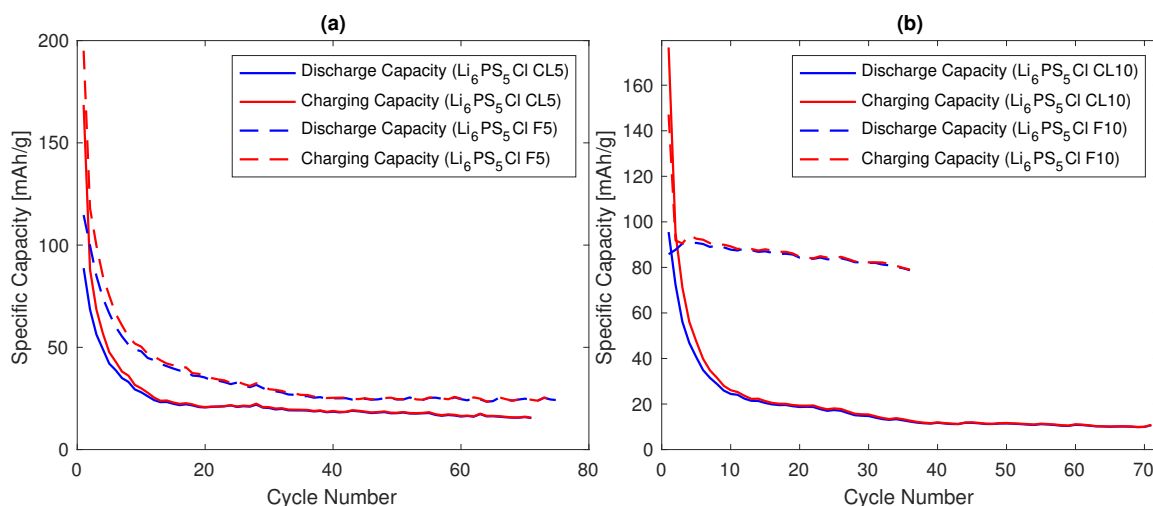


Figure 5.2: Specific capacity of NCM 622 against cycle with LiCl and LiF doped  $\text{Li}_6\text{PS}_5\text{Cl}$  in the cathode mixture of (a) 5% in excess and (b) 10% in excess

As seen from Figure 5.2, which compares the specific capacity of NCM 622 with the same weight fraction excess of LiCl or LiF, LiF doped  $\text{Li}_6\text{PS}_5\text{Cl}$  gives a better performance than LiCl doped as NCM 622 as it is observed to retain higher specific capacity than of LiCl doped  $\text{Li}_6\text{PS}_5\text{Cl}$ . Thus, LiF doping appears to have higher ionic mobility and less ionic resistance. This finding completely contradicts the EIS analysis the LiCl doped  $\text{Li}_6\text{PS}_5\text{Cl}$  has larger ionic conductivities than LiF doped  $\text{Li}_6\text{PS}_5\text{Cl}$ .

The cyclic voltage as shown in Figure 5.3, is observed to be smooth and uniform. In general, as the cycling of the battery progresses, the curve moves inwards as indicated by the black arrows. For LiCl doped  $\text{Li}_6\text{PS}_5\text{Cl}$  as shown in Figure 5.3(a), it is observed that the (light and dark blue) curves are more spread apart than of pristine  $\text{Li}_6\text{PS}_5\text{Cl}$  (green curves).

NCM 622 with:	Charging Overpotential (V)	Discharging Overpotential (V)
$\text{Li}_6\text{PS}_5\text{Cl}$ CL5	0.025	0.058
$\text{Li}_6\text{PS}_5\text{Cl}$ CL10	0.020	0.074
$\text{Li}_6\text{PS}_5\text{Cl}$ F5	0.01	0.019
$\text{Li}_6\text{PS}_5\text{Cl}$ F10	0	0.023

Table 5.1: Overpotentials of NCM 622 with doped Argyrodites at normalized capacity of 0.5 in relation to pristine Argyrodite

The second cycle with the normalized capacity is shown in Figure 5.4. From this figure, the overpotentials of the LiCl and LiF doped are determined with pristine  $\text{Li}_6\text{PS}_5\text{Cl}$  as the reference voltage and summarized in Table 5.1 for the normalized capacity of 0.5. In Figure 5.4(a) and Table 5.1, it is observed that the LiCl doped argyrodites have lower charging overpotentials compared to discharging overpotentials. For the case of LiF doped argyrodite as shown in Figure 5.4(b), it is observed that the

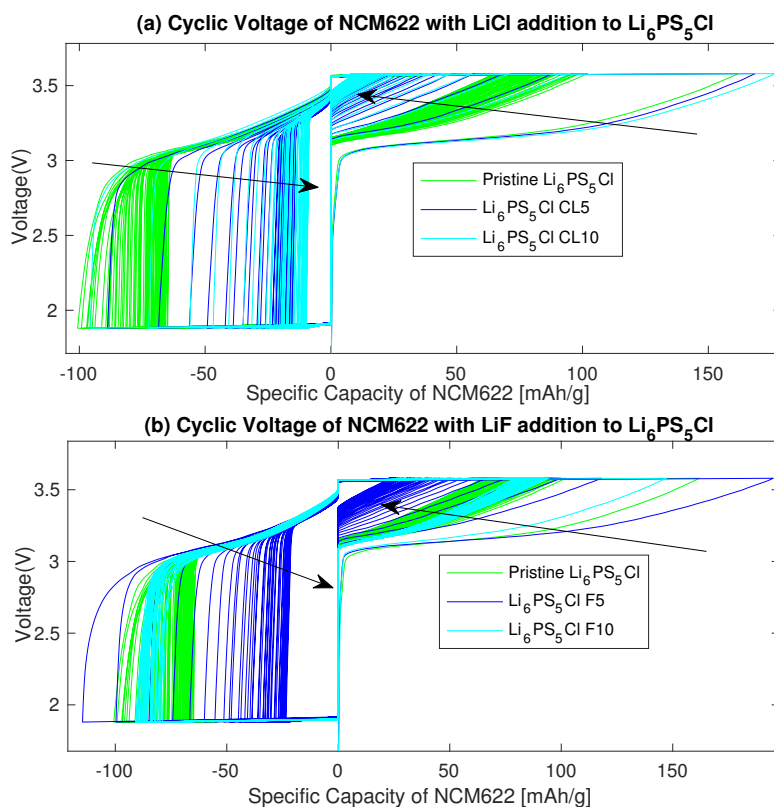


Figure 5.3: Cyclic voltage for the battery with argyrodite doped with (a) LiCl and (b) LiF in the cathode

argyrodite has negligible charging overpotential. However, the addition of LiF will result in overpotentials in relation to pristine  $\text{Li}_6\text{PS}_5\text{Cl}$ . Referring to the values of Table 5.4, LiF doped argyrodites will result in lower charging and discharging overpotentials in comparison to LiCl doped argyrodite.

In this context, higher overpotentials means that more potential is required than of pristine argyrodite. Potential difference, which is proportional to resistance, indicates that LiCl and LiF doped  $\text{Li}_6\text{PS}_5\text{Cl}$  have higher overall resistance than pristine  $\text{Li}_6\text{PS}_5\text{Cl}$ .

## 5.2. Cathode: Pristine/doped $\text{Li}_6\text{PS}_5\text{Cl}$ & Carbon Black

This section will look into the cycling of the battery with the cathode mixture of argyrodite (pristine and doped) and carbon black. The capacity curve for each cycle is shown in Figure 5.5. The specific capacity of the argyrodites are significantly lower without NCM 622. This is to be expected since there is no active cathode material present. Any capacity observed could be a consequence of the decomposition of the electrolyte in the first cycle to  $\text{Li}_2\text{S}$ , which then acts as a cathode cycling reversibly over subsequent cycles. Furthermore, it is observed that pristine  $\text{Li}_6\text{PS}_5\text{Cl}$  is relatively stable up to 21<sup>st</sup> cycle where it then increases in a rapid rate. This indicates that a large scale decomposition of the electrolyte in contact with carbon is occurring leading to the capacity observed. From the Figure 5.5 the performance of the battery is not ideal since the electrolyte is not expected to be electrochemically active in the given voltage window and the increase in capacity on cycling indicates its progressive decomposition on cycling.

For LiCl doped  $\text{Li}_6\text{PS}_5\text{Cl}$  as seen in Figure 5.5(a),  $\text{Li}_6\text{PS}_5\text{Cl}$  CL5 generally has less specific capacity than pristine  $\text{Li}_6\text{PS}_5\text{Cl}$  and CL10.  $\text{Li}_6\text{PS}_5\text{Cl}$  CL10 has generally the largest specific capacity. This could indicate that  $\text{Li}_6\text{PS}_5\text{Cl}$  CL5 is successful in preventing the progressive decomposition of the electrolyte. The  $\text{Li}_6\text{PS}_5\text{Cl}$  CL10 electrolyte by virtue of its higher capacity and irregular behavior indicates more electrolyte decomposition.

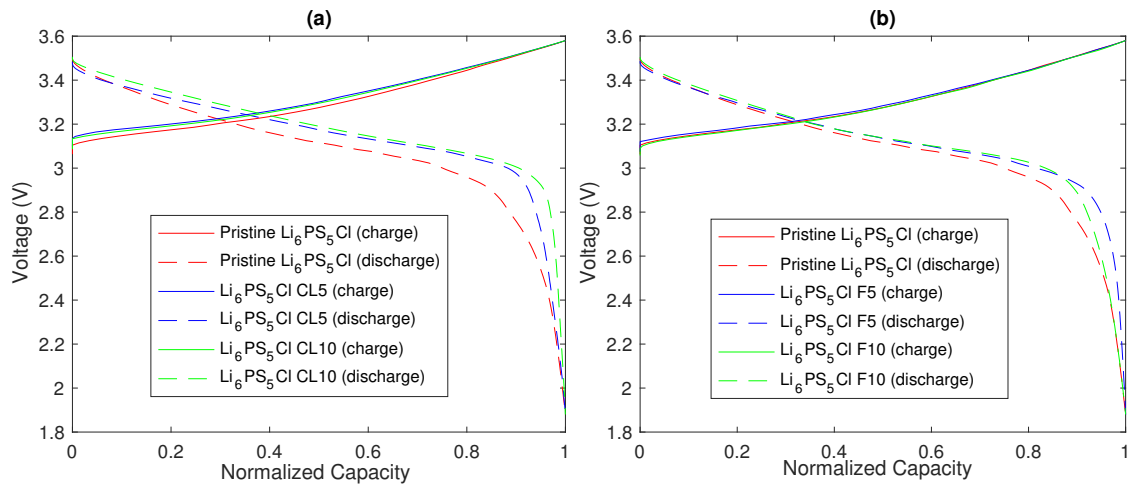


Figure 5.4: Voltage for the second cycle against the normalized specific capacity of NCM 622 for (a) LiCl doped argyrodites and (b) LiF doped argyrodites

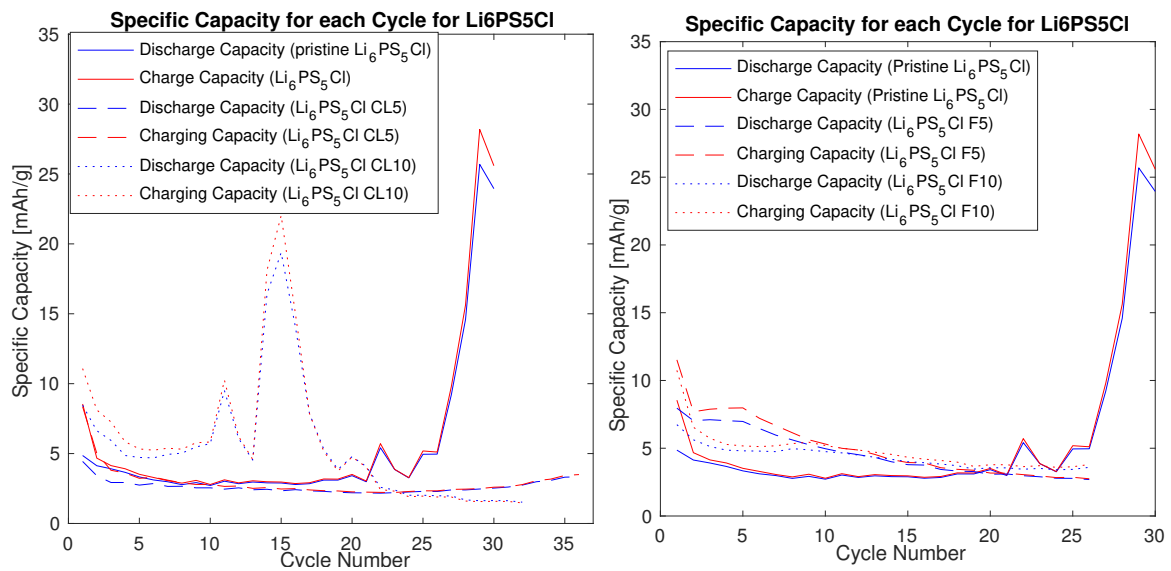


Figure 5.5: Graph of specific capacity per cycle of  $\text{Li}_6\text{PS}_5\text{Cl}$  for doped and pristine argyrodites as cathodes

The cathodes with LiF dopants, has shown to generally have a higher specific capacity than pristine  $\text{Li}_6\text{PS}_5\text{Cl}$  in Figure 5.5(b). Though both  $\text{Li}_6\text{PS}_5\text{Cl}$  F5 and F10 show a higher initial specific capacity, there is no increase in capacity over cycling, which suggest a formation of a stable solid electrolyte interphase between decomposition products formed on the first cycle and the solid electrolyte which prevents its progressive deterioration.

From the figures, it is difficult to determine the overpotential of the figure, as there are no stable values to take into consideration. The cyclic voltage as shown in Figure 7.8 has a more disarray pattern in comparison to of the cyclic voltage when NCM622 is used (as seen in Figure 5.3).

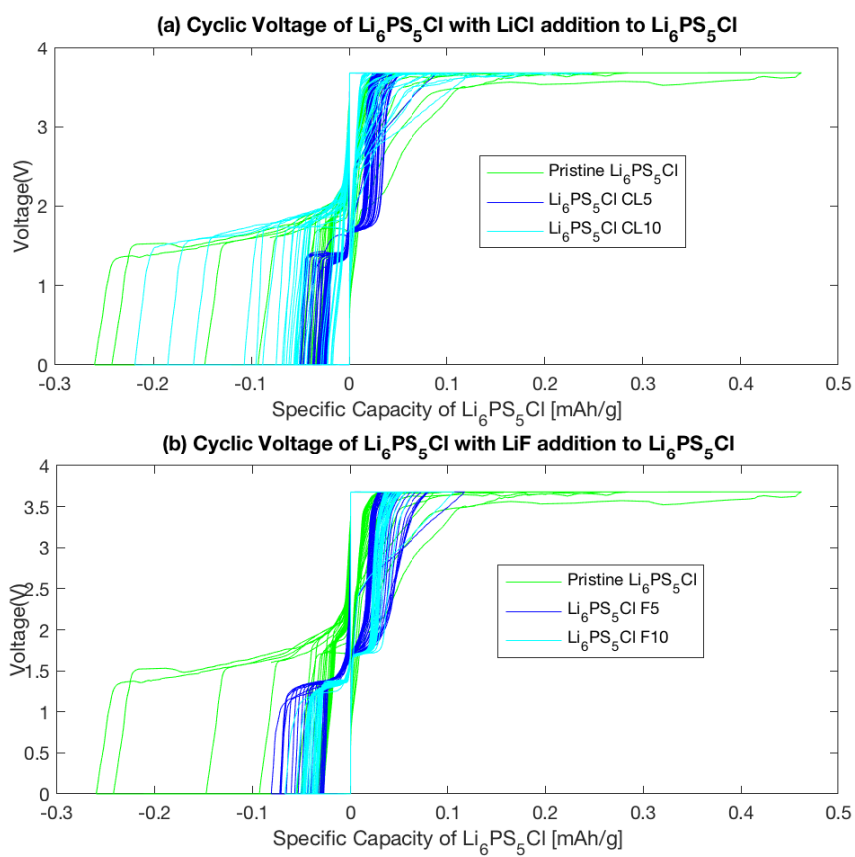


Figure 5.6: Cyclic voltage for battery with cathode mixture of Argyrodite and carbon black with (a) LiCl addition and (b) LiF addition



# 6

## Ex-situ XRD Analysis

In this section, ex-situ analysis is carried out by XRD measurement of the cathode side of the cycled solid state lithium ion battery. Refinements of the XRD measurement is carried out to identify and quantify phases present of the post-cycled battery.

While it is possible to identify all of the peaks, however the GSAS software operates significantly slower as more phases are included in the refinement. As this research requires a lot of refinement with a number of phases, only the significant phases identified are included in the refinements.

### 6.1. Cathode: NCM622, pristine/doped $\text{Li}_6\text{PS}_5\text{Cl}$ and Carbon Black

Potentially, side reactions may occur or existing side products are intensified during cycling. NCM 622 in general degrades minimally, and during GSAS refinement, the phase fraction of NCM 622 is kept constant while others are allowed to be refined. As shown in the refinements of the XRD measurement in the Appendix, the NCM622 peaks remains nearly the same after cycling. Please refer to Figures A.7, A.8, A.9, A.10, and A.11 in Appendix to see the XRD measurement and refinements for these batteries.

#### 6.1.1. with LiCl doped $\text{Li}_6\text{PS}_5\text{Cl}$

Firstly, looking into LiCl doped  $\text{Li}_6\text{PS}_5\text{Cl}$  in the catholyte is analysed as shown in Figure 6.1, where the pristine  $\text{Li}_6\text{PS}_5\text{Cl}$  is compared as well. LiCl is already present in the LiCl doped argyrodites as expected, although undesired for pristine argyrodite. After cycling, pristine  $\text{Li}_6\text{PS}_5\text{Cl}$  is shown to have a large increase in the amount of LiCl, while  $\text{Li}_6\text{PS}_5\text{Cl}$  CL5 has it's LiCl reduced.  $\text{Li}_6\text{PS}_5\text{Cl}$  CL10 in contrast, has a significant increase in the phase fraction of LiCl.

An existing side product,  $\text{Li}_2\text{S}$  has generally shown to be decreasing in amount with the exception of  $\text{Li}_6\text{PS}_5\text{Cl}$  CL5 although the differences between before and post-cycling are small. It may be possible that it had reversible side reactions to form  $\text{Li}_2\text{PS}_3$ . From the graph, it correlates that the change of  $\text{Li}_2\text{S}$  is inversely proportional to the change of  $\text{Li}_2\text{PS}_3$ . It is important to note that the highest peak positions of the XRD measurement of  $\text{Li}_2\text{S}$  and  $\text{Li}_2\text{PS}_3$  are near each other even to merges to form one peak. Thus, it also relies on other smaller peaks to fit the respective phases.

Another existing precursor,  $\text{Li}_3\text{PO}_4$ , is shown to be intensified after cycling for the LiCl doped  $\text{Li}_6\text{PS}_5\text{Cl}$ . However this is likely due to reaction with air and moisture. Thus, the efficiency of the o-rings in the solid state battery may not be so effective to let external air or moisture to enter the active battery. Hence,  $\text{Li}_3\text{PO}_4$  will be neglected in terms of looking into degradation as ideal conditions assume that the battery is airtight enough.

In each case of the NCM catholytes,  $\text{Li}_3\text{P}$  is formed during cycling. It is observed that with increase of LiCl addition inhibits the formation of  $\text{Li}_3\text{P}$ .

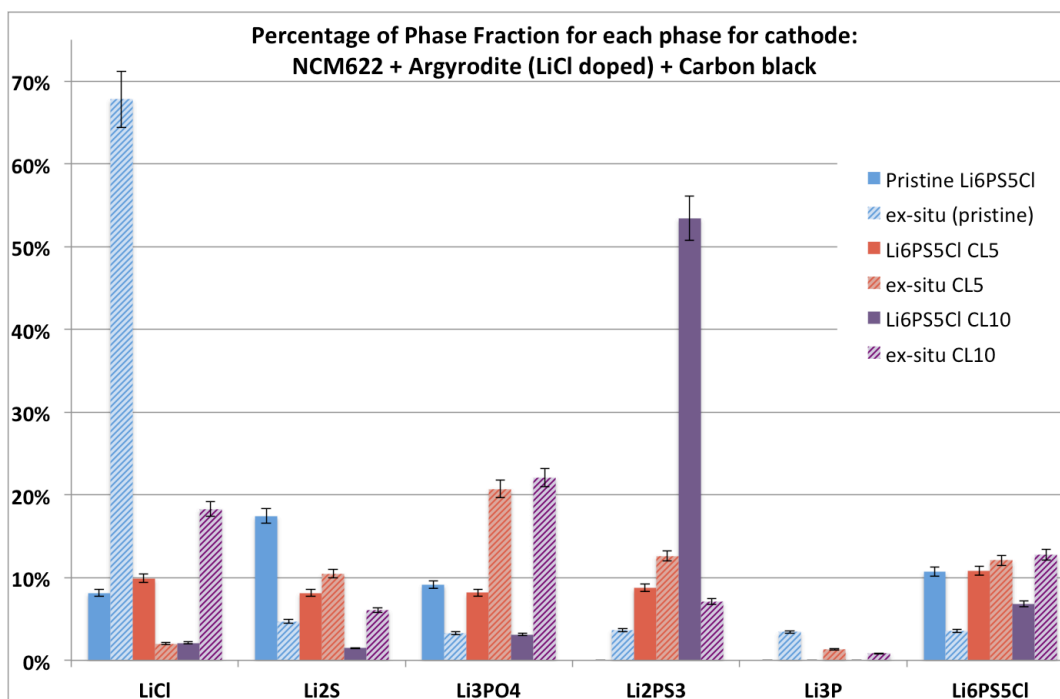


Figure 6.1: Graph of percentage of XRD phase fractions of the catholytes pre-cycling and post-cycling for LiCl doped  $\text{Li}_6\text{PS}_5\text{Cl}$  with 5% error

Overall, the catholyte with pristine  $\text{Li}_6\text{PS}_5\text{Cl}$  decomposes significantly to  $\text{LiCl}$ ,  $\text{Li}_2\text{PS}_3$ , and  $\text{Li}_3\text{P}$ . Taking account of the errors,  $\text{Li}_6\text{PS}_5\text{Cl}$  CL5 degrades slightly to  $\text{Li}_2\text{S}$ ,  $\text{Li}_2\text{PS}_3$ , and  $\text{Li}_3\text{P}$ .  $\text{Li}_6\text{PS}_5\text{Cl}$  CL10 results may be off due to high value of  $\text{Li}_2\text{PS}_3$  phase before cycling. This is mainly due to increased value of  $\text{LiCl}$ ,  $\text{Li}_3\text{PO}_4$ ,  $\text{Li}_2\text{PS}_3$ , and  $\text{Li}_3\text{P}$ .  $\text{Li}_6\text{PS}_5\text{Cl}$  CL10 is shown to be intensified after cycling which is completely wrong. This could be due to the wrong value of  $\text{Li}_2\text{PS}_3$  phase before cycling as it is also unlikely for the phase to be greatly reduced after cycling.

Looking previously at the Nyquist plot in Figure 4.1(b), the kinetic control (the semi-circle part of the Nyquist plot) of the  $\text{Li}_6\text{PS}_5\text{Cl}$  CL5 and CL10 is smaller than of pristine. Kinetic control relates to the rate of reaction. Hence the Nyquist plot corroborates the fact that LiCl doped  $\text{Li}_6\text{PS}_5\text{Cl}$  will react less than of pristine  $\text{Li}_6\text{PS}_5\text{Cl}$ . However, it is difficult to determine if  $\text{Li}_6\text{PS}_5\text{Cl}$  CL5 degrades more than  $\text{Li}_6\text{PS}_5\text{Cl}$  CL10 due to errors of the refinement of the  $\text{Li}_6\text{PS}_5\text{Cl}$  CL10. From the cycling analysis, it is shown that LiCl doped  $\text{Li}_6\text{PS}_5\text{Cl}$  retains less specific capacity than of pristine. As theorized previously that it has poor interphase contact, hence the chemical reaction could be slower for the same reason.

### 6.1.2. with LiF doped $\text{Li}_6\text{PS}_5\text{Cl}$

The change of percentage of phase fractions for of LiF doped  $\text{Li}_6\text{PS}_5\text{Cl}$  together with pristine  $\text{Li}_6\text{PS}_5\text{Cl}$  is shown in Figure 6.2.

Unlike LiCl doped argyrodite, LiCl phase is not expected in LiF doped argyrodites. However LiCl is indeed present as explained in Section 4.2.2. Like the LiCl doped argyrodites as mentioned previously, the percentage of phase fraction of LiCl is reduced slightly after cycling. In the case of  $\text{Li}_6\text{PS}_5\text{Cl}$  F10, the changes may be negligible if errors are taken account of.

Reiterating what was mentioned previously,  $\text{Li}_2\text{S}$  change is inversely proportional to  $\text{Li}_2\text{PS}_3$  change. For LiF doped argyrodite in contrast, the change in percentage of phase fractions of  $\text{Li}_2\text{S}$  are seemingly proportional to  $\text{Li}_2\text{PS}_3$ .

An existing side product of  $\text{Li}_3\text{PO}_4$  is intensified after cycling with  $\text{Li}_6\text{PS}_5\text{Cl}$  F5, but was reduced

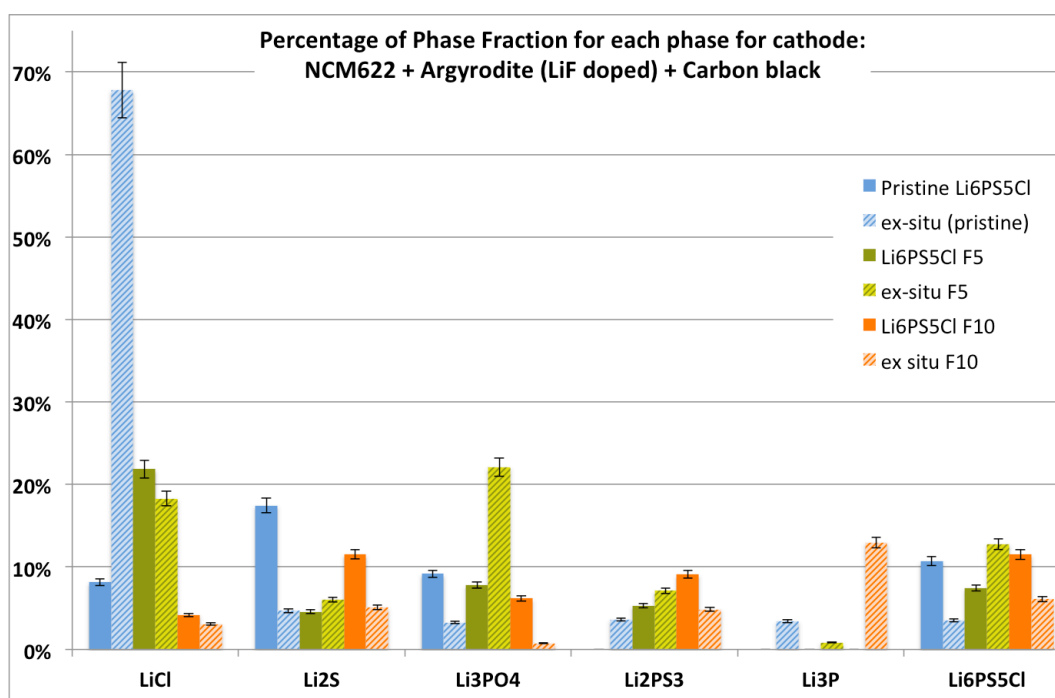


Figure 6.2: Graph of percentage of XRD phase fraction of the catholytes pre-cycling and post-cycling for LiF doped  $\text{Li}_6\text{PS}_5\text{Cl}$  with 5% error

significantly with  $\text{Li}_6\text{PS}_5\text{Cl}$  F10. This is most likely due the efficiency of the o-rings to seal the solid state battery. With pristine  $\text{Li}_6\text{PS}_5\text{Cl}$  and  $\text{Li}_6\text{PS}_5\text{Cl}$  F10, the phase fraction is reduced (or probably remains the same).

$\text{Li}_3\text{P}$  which is formed after cycling also exists with LiF doped  $\text{Li}_6\text{PS}_5\text{Cl}$ . Although  $\text{Li}_6\text{PS}_5\text{Cl}$  F5 gives a very minimal reaction to this,  $\text{Li}_6\text{PS}_5\text{Cl}$  F10 produces  $\text{Li}_3\text{P}$  even higher than of pristine  $\text{Li}_6\text{PS}_5\text{Cl}$ .

In terms of  $\text{Li}_6\text{PS}_5\text{Cl}$  phase,  $\text{Li}_6\text{PS}_5\text{Cl}$  F5 has higher percentage of phase fraction of  $\text{Li}_6\text{PS}_5\text{Cl}$  after cycling.  $\text{Li}_6\text{PS}_5\text{Cl}$  F10 however is shown to have a significant reduction of  $\text{Li}_6\text{PS}_5\text{Cl}$  phase after cycling. This means that pristine  $\text{Li}_6\text{PS}_5\text{Cl}$  and  $\text{Li}_6\text{PS}_5\text{Cl}$  F10 degrades significantly.

In short,  $\text{Li}_6\text{PS}_5\text{Cl}$  F5 forms  $\text{Li}_3\text{P}$  and intensifies it's overall phases with the exception of LiCl. This is difficult to determine if reversible reaction of  $\text{Li}_6\text{PS}_5\text{Cl}$  formation does indeed occur as decomposition definitely occurred.  $\text{Li}_6\text{PS}_5\text{Cl}$  F10 in contrast has all it's phases reduced but has a sharp increase of  $\text{Li}_3\text{P}$ . From the Nyquist plot of Figure 4.1(b) shown previously, the semicircle part (the kinetic control) of the LiF doped  $\text{Li}_6\text{PS}_5\text{Cl}$  is more significant than of pristine  $\text{Li}_6\text{PS}_5\text{Cl}$  and hence the rate of reaction of is higher for the LiF doped  $\text{Li}_6\text{PS}_5\text{Cl}$  than of pristine. However, this finding does not reflect well in this ex-situ analysis as LiF doped  $\text{Li}_6\text{PS}_5\text{Cl}$  is shown to undergo reaction less than pristine  $\text{Li}_6\text{PS}_5\text{Cl}$ . Additionally, the kinetic control of  $\text{Li}_6\text{PS}_5\text{Cl}$  F10 is higher than of  $\text{Li}_6\text{PS}_5\text{Cl}$  F5, which reflects well in this ex-situ analysis due to  $\text{Li}_6\text{PS}_5\text{Cl}$  F10 produces undergoes more chemical reaction than of  $\text{Li}_6\text{PS}_5\text{Cl}$  F5 due to possessing a higher rate of reaction. From the cycling analysis,  $\text{Li}_6\text{PS}_5\text{Cl}$  F5 worsens the specific capacity retention, while  $\text{Li}_6\text{PS}_5\text{Cl}$  F10 improves it. Thus, the high specific capacity could be the result of the decomposition reaction.

## 6.2. Cathode: Pristine/doped $\text{Li}_6\text{PS}_5\text{Cl}$ and Carbon Black

The main limitation of the previous analysis from Section 6.1 is that the phases quantified in terms of phase fraction are in relation to NCM 622 present. While NCM 622 remains somewhat constant however the argyrodite does degrade over time and with cycling and thus, it is difficult to quantify the side products formed in relation to the argyrodite. Thus, the same analysis is carried for the cathode of argyrodite and carbon black in the this subsection. The focus of this subsection is to quantify the

side products of the synthesized  $\text{Li}_6\text{PS}_5\text{Cl}$  in relation to  $\text{Li}_6\text{PS}_5\text{Cl}$  phase. During refinement of the battery with argyrodite as cathodes, the phase fraction of  $\text{Li}_6\text{PS}_5\text{Cl}$  remains constant while the other side products phase fractions are refined. Please refer to Figures A.12, A.13, A.14, A.15 and A.16 to see the XRD measurement and refinement of these batteries.

### 6.2.1. with LiCl doped $\text{Li}_6\text{PS}_5\text{Cl}$

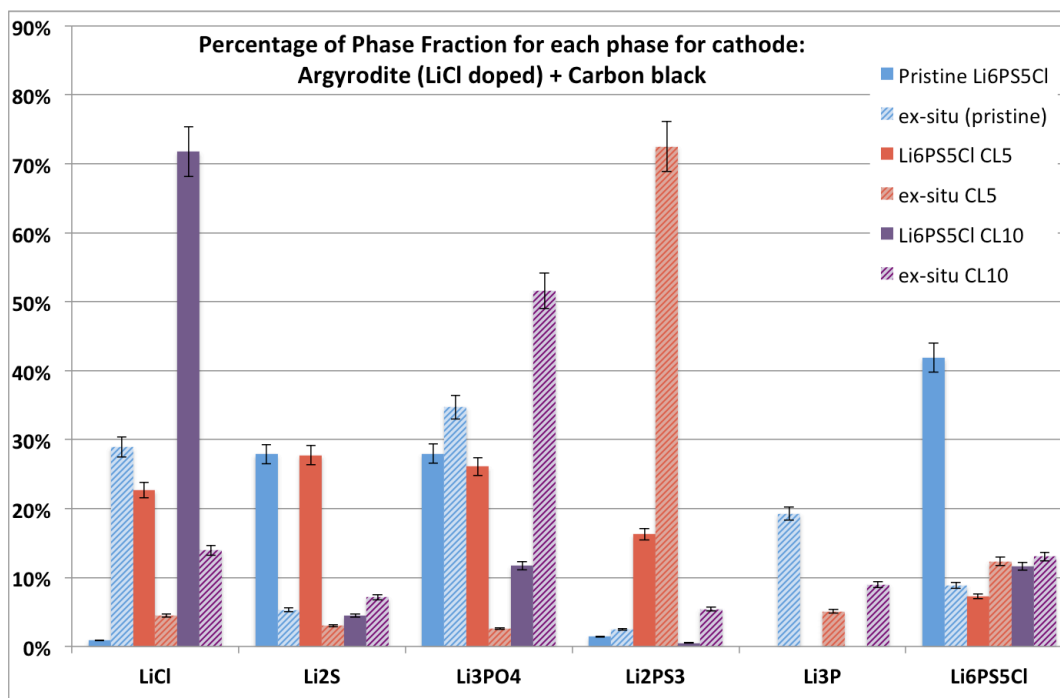


Figure 6.3: Graph of percentage of XRD phase fractions of the Argyrodites as cathodes for pre-cycling and post-cycling for LiCl doped  $\text{Li}_6\text{PS}_5\text{Cl}$  with 5% error

The LiCl doped  $\text{Li}_6\text{PS}_5\text{Cl}$  with carbon black as the cathode has the changes in phases from pre to post-cycling as shown in Figure 6.3 with an error of 5%.

Similar to the LiCl doped catholytes (as seen in Figure 6.1, the percentage of phase fraction for LiCl decreases significantly for the LiCl doped  $\text{Li}_6\text{PS}_5\text{Cl}$  while pristine  $\text{Li}_6\text{PS}_5\text{Cl}$  produces a large amount of LiCl during cycling.

An existing side product of  $\text{Li}_2\text{S}$  has the percentage of phase fraction decreased with the exception of  $\text{Li}_6\text{PS}_5\text{Cl}$  CL10. However, it may not necessarily mean that the amount of  $\text{Li}_2\text{S}$  decreases, and it may mean that it remains the same due to the increase amount of other side products. Additionally from the figure,  $\text{Li}_2\text{S}$  is generally observed to be inversely proportional to  $\text{Li}_2\text{PS}_3$  except for  $\text{Li}_6\text{PS}_5\text{Cl}$  CL10.  $\text{Li}_2\text{PS}_3$  is formed significantly more for LiCl doped than of pristine.

Another existing side product,  $\text{Li}_3\text{PO}_4$  is intensified after cycling with the exception of  $\text{Li}_6\text{PS}_5\text{Cl}$  CL5. While pristine  $\text{Li}_6\text{PS}_5\text{Cl}$  has a slight change,  $\text{Li}_6\text{PS}_5\text{Cl}$  CL10 has a large increase in the phase fraction. As mentioned previously, this side product depends on the presence of air or moisture and hence the airtightness of the battery or air and moisture content 'trapped' in the battery.

Reiterating previously,  $\text{Li}_3\text{P}$  is produced during cycling. Like the NCM 622 catholytes, the addition of LiCl inhibits the reaction of  $\text{Li}_3\text{P}$ . In this case however,  $\text{Li}_6\text{PS}_5\text{Cl}$  CL5 produces less phase fraction of  $\text{Li}_3\text{P}$  than for  $\text{Li}_6\text{PS}_5\text{Cl}$  CL10.

Overall, it can be concluded that pristine  $\text{Li}_6\text{PS}_5\text{Cl}$  has the worst decomposition as it degrades to

$\text{LiCl}$ ,  $\text{Li}_3\text{PO}_4$ ,  $\text{Li}_2\text{PS}_3$ , and  $\text{Li}_3\text{P}$ . Although it is shown that  $\text{Li}_6\text{PS}_5\text{Cl}$  CL5 has the  $\text{Li}_6\text{PS}_5\text{Cl}$  phase intensified, decomposition definitely occurs. What could have affected this data is the offset by phase factors of  $\text{Li}_2\text{S}$ ,  $\text{Li}_3\text{PO}_4$  and/or  $\text{Li}_2\text{PS}_3$ . Nevertheless, it is assumed that  $\text{Li}_6\text{PS}_5\text{Cl}$  CL5 decomposes less severely in comparison to pristine  $\text{Li}_6\text{PS}_5\text{Cl}$  as it only degrades to  $\text{Li}_2\text{PS}_3$ , and  $\text{Li}_3\text{P}$  and reduces unwanted side products of  $\text{Li}_2\text{S}$  and  $\text{Li}_3\text{PO}_4$ . It is important to note that the decomposition to  $\text{Li}_2\text{PS}_3$  is greatly intensified after cycling. For  $\text{Li}_6\text{PS}_5\text{Cl}$  CL10 (considering the error bars), it degrades to  $\text{Li}_3\text{PO}_4$ ,  $\text{Li}_2\text{PS}_3$  and  $\text{Li}_3\text{P}$ . The amount of  $\text{Li}_2\text{S}$  after cycling is a difficult to determine if it is reduced or intensified as the changes are considerably small. Thus, although the side products of  $\text{LiCl}$  doped  $\text{Li}_6\text{PS}_5\text{Cl}$  are smaller than of pristine  $\text{Li}_6\text{PS}_5\text{Cl}$ , it is still significant.

Reiterating previously from the EIS analysis,  $\text{LiCl}$  doped  $\text{Li}_6\text{PS}_5\text{Cl}$  has lower rate of reaction than of pristine  $\text{Li}_6\text{PS}_5\text{Cl}$ ,  $\text{Li}_6\text{PS}_5\text{Cl}$  CL5 and CL10 will react slower than of pristine  $\text{Li}_6\text{PS}_5\text{Cl}$ . This is indeed reflected in the figure as pristine  $\text{Li}_6\text{PS}_5\text{Cl}$  degrades more or produces more side products than of  $\text{LiCl}$  doped  $\text{Li}_6\text{PS}_5\text{Cl}$ . Furthermore, it is difficult to quantify whether  $\text{Li}_6\text{PS}_5\text{Cl}$  CL5 degrades more than  $\text{Li}_6\text{PS}_5\text{Cl}$  CL10 although cycling analysis suggests that decomposition is higher for  $\text{Li}_6\text{PS}_5\text{Cl}$  CL10 than  $\text{Li}_6\text{PS}_5\text{Cl}$  CL5.

### 6.2.2. with $\text{LiF}$ doped $\text{Li}_6\text{PS}_5\text{Cl}$

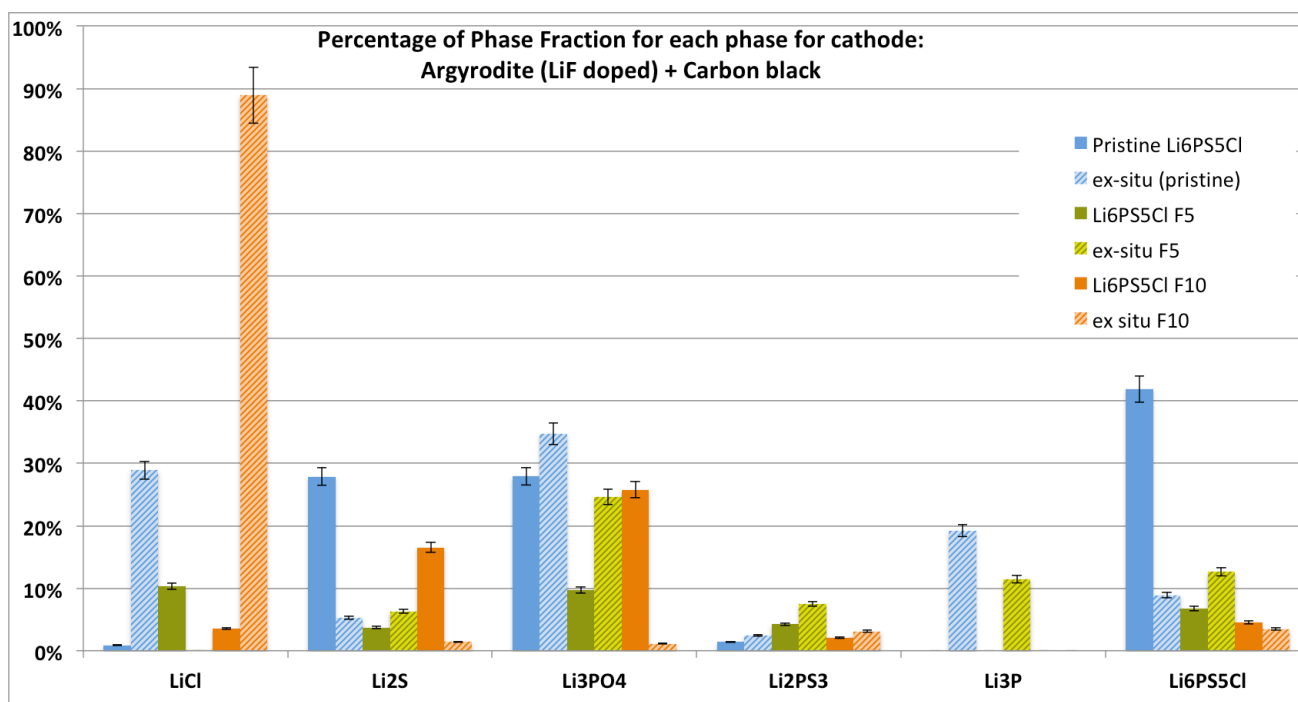


Figure 6.4: Graph of percentage of XRD phase fraction of Argyrodites as cathodes for pre-cycling and post-cycling for  $\text{LiF}$  doped  $\text{Li}_6\text{PS}_5\text{Cl}$  with 5% error

Next, the cathode mixture of  $\text{LiF}$  doped  $\text{Li}_6\text{PS}_5\text{Cl}$  with carbon black are analyzed. The changes in the percentage of phase fractions before and after cycling are shown in Figure 6.4.

As mentioned previously,  $\text{LiCl}$  is an unwanted side product in this case. Pristine  $\text{Li}_6\text{PS}_5\text{Cl}$  shows a great amount of  $\text{LiCl}$  produced after cycling. It seems that the  $\text{LiCl}$  in  $\text{Li}_6\text{PS}_5\text{Cl}$  CL5 is reacted with as after cycling the amount is reduced to a negligible value. However, with  $\text{Li}_6\text{PS}_5\text{Cl}$  F10  $\text{LiCl}$  is greatly intensified after cycling by approximately 75%.

Looking into the unwanted side product of  $\text{Li}_2\text{S}$ , it was reacted under pristine  $\text{Li}_6\text{PS}_5\text{Cl}$  and  $\text{Li}_6\text{PS}_5\text{Cl}$  F10.  $\text{Li}_6\text{PS}_5\text{Cl}$  F5 seems to intensify the percentage of phase fraction slightly. For  $\text{Li}_2\text{PS}_3$ , where in the case of NCM 622 where it seems proportional to the values of  $\text{Li}_2\text{S}$ , the same relationship cannot

be applied here with the exception of  $\text{Li}_6\text{PS}_5\text{Cl}$  F5. However, the changes of the percentage of phase fraction before and after cycling of  $\text{Li}_2\text{PS}_3$  is small especially if the errors are considered, it is possible that no reaction is taking place.

For pristine  $\text{Li}_6\text{PS}_5\text{Cl}$  and  $\text{Li}_6\text{PS}_5\text{Cl}$  F5, the percentage of phase fraction of the  $\text{Li}_3\text{PO}_4$  is intensified considerably which could also mean that the amount has increased as well. However,  $\text{Li}_6\text{PS}_5\text{Cl}$  F10 it seems that  $\text{Li}_3\text{PO}$  is reacted with as after cycling, the percent of phase fractions are very minimal. This could be an error as the negative change is too large. Again, this relies on the air and moisture content of the battery

In the case of  $\text{Li}_3\text{P}$ ,  $\text{Li}_6\text{PS}_5\text{Cl}$  F5 and pristine  $\text{Li}_6\text{PS}_5\text{Cl}$  produces this phase.  $\text{Li}_6\text{PS}_5\text{Cl}$  F10 however does not seem to have  $\text{Li}_3\text{P}$  after cycling as the phase was not able to fit in the XRD measurement during refinement. In contrast, looking previously to the catholytes in Figure 6.2 where  $\text{Li}_6\text{PS}_5\text{Cl}$  F10 produces more  $\text{Li}_3\text{P}$  than pristine  $\text{Li}_6\text{PS}_5\text{Cl}$  and  $\text{Li}_6\text{PS}_5\text{Cl}$  F5.

To summarize this subsection, pristine  $\text{Li}_6\text{PS}_5\text{Cl}$  decomposes significantly to  $\text{LiCl}$ ,  $\text{Li}_3\text{PO}_4$ ,  $\text{Li}_3\text{P}$ , and possibly  $\text{Li}_2\text{PS}_3$ . Although it seems like the phase of  $\text{Li}_6\text{PS}_5\text{Cl}$  in  $\text{Li}_6\text{PS}_5\text{Cl}$  F5 seems to be intensified during cycling (similar to the  $\text{Li}_6\text{PS}_5\text{Cl}$  F5 used in catholyte), it is assumed that decomposition still occur as the side phase fractions of  $\text{Li}_2\text{S}$ ,  $\text{Li}_3\text{PO}_4$ ,  $\text{Li}_2\text{PS}_3$ , and  $\text{Li}_3\text{P}$  is formed or intensified during cycling. Finally,  $\text{Li}_6\text{PS}_5\text{Cl}$  F10 appears to have little decomposition from the  $\text{Li}_6\text{PS}_5\text{Cl}$  phase fraction percentage difference.

Reiterating previously from the EIS findings, LiF doped  $\text{Li}_6\text{PS}_5\text{Cl}$  have significant kinetic control than is comparable to of pristine  $\text{Li}_6\text{PS}_5\text{Cl}$ , which means LiF doped  $\text{Li}_6\text{PS}_5\text{Cl}$  should decompose faster than pristine  $\text{Li}_6\text{PS}_5\text{Cl}$ . This is not reflected at all since the LiF doped  $\text{Li}_6\text{PS}_5\text{Cl}$  reacts less than of pristine. Furthermore from the cycling analysis, it is suggested that the LiF doped  $\text{Li}_6\text{PS}_5\text{Cl}$  undergoes less decomposition than pristine  $\text{Li}_6\text{PS}_5\text{Cl}$ . Additionally, it could also be due to poor interphase as theorised in the cycling analysis.

# 7

## Alternative Doping Method

The whole experiment was repeated with a new methodology on the LiCl doped  $\text{Li}_6\text{PS}_5\text{Cl}$  synthesis. LiCl was first ball milled with Zirconia ball mill jar to get smaller grains, and pristine argyrodite were synthesized separately. Afterwards, 5% and 10% of the ball milled LiCl required were added to the argyrodite and agate ball milled to a homogenous mixture. **These argyrodite with additional 5% and 10% of LiCl will be referred to as  $\text{Li}_6\text{PS}_5\text{Cl}$  5CL-bm and  $\text{Li}_6\text{PS}_5\text{Cl}$  10CL-bm respectively from here onwards**

### 7.1. Material Analysis

Similar to the previous synthesis of Argyrodite, the alternate method of synthesizing the argyrodite, the material analysis is carried out using EIS and XRD. XRD measurement is also carried out for catholyte mixture with NCM 622.

#### 7.1.1. EIS

The Argyrodite undergoes EIS and the results are shown in Figure 7.1. It is observed that the semi-circle part of the Nyquist plot is more significant than the original method used. Thus, the kinetic control is more pronounced in these argyrodites. However, in the overall Nyquist plot as shown in part (a), the straight inclined line still dominates which indicates that mass transfer control is preferred. Conductivity of these argyrodites are summarized in Table 7.1. From these results, the conductivity are shown to be much lower than of  $\text{Li}_6\text{PS}_5\text{Cl}$  CL5 and CL10.  $\text{Li}_6\text{PS}_5\text{Cl}$  CL5-bm has higher conductivity than  $\text{Li}_6\text{PS}_5\text{Cl}$  CL10-bm although the two values of  $\text{Li}_6\text{PS}_5\text{Cl}$  CL5-bm and CL10-bm are close. Considering that the values are very small, accuracy of the values is considered to be low.

Argyrodite	Ionic Conductivity [S/cm]
$\text{Li}_6\text{PS}_5\text{Cl}$ CL5-bm	0.0001238
$\text{Li}_6\text{PS}_5\text{Cl}$ CL10-bm	0.0001036

Table 7.1: Conductivity derived from Equation 2.13 and Figure 7.1

The AC supply for  $\text{Li}_6\text{PS}_5\text{Cl}$  CL5-bm does not have a good quality as seen from the Lissajous Figure in Figure A.4 in Appendix.  $\text{Li}_6\text{PS}_5\text{Cl}$  CL10-bm however shows a good smooth oval in the Lissajous Figure which indicates there is a good reading. Again, this is due to different Autolab instrument used.

With the KK test (see Figure A.6), the errors are relatively low with the values up to 0.4% for real impedance and 1.6% for imaginary impedance. Thus, the values are going to be acceptable

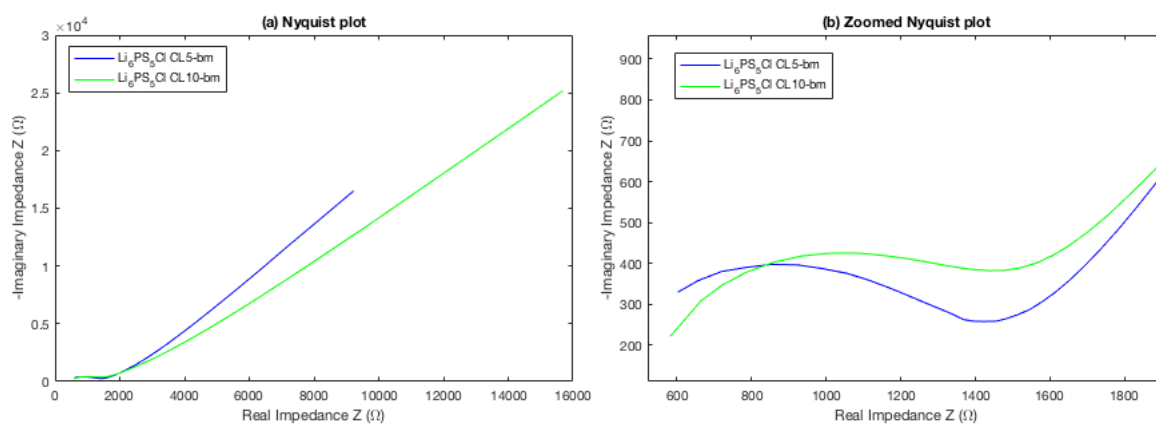


Figure 7.1: Nyquist plot (a) Overall and (b) zoomed at low impedances (high frequencies)

### 7.1.2. XRD

In this subsection, the quality of the argyrodite synthesised and the cathode mixture containing the NCM 622 are analyzed. From the refinements, the phase fractions is converted to weight fraction using Equation 2.15.

For the argyrodite synthesised as shown in Figure 7.2, more than 70% of the synthesis are  $\text{Li}_6\text{PS}_5\text{Cl}$ . The amount of LiCl as expected is larger in  $\text{Li}_6\text{PS}_5\text{Cl}$  CL10-bm than in  $\text{Li}_6\text{PS}_5\text{Cl}$  CL5-bm. There are still side products of  $\text{Li}_3\text{PO}_4$ ,  $\text{Li}_2\text{PS}_3$ ,  $\text{LiOH}$ , and  $\text{Li}_2\text{S}$ . The side products are not consistent with one another as  $\text{Li}_6\text{PS}_5\text{Cl}$  VL5-bm has a significant amount of  $\text{Li}_3\text{PO}_4$ , while  $\text{Li}_6\text{PS}_5\text{Cl}$  CL10-bm has a significant amount of  $\text{Li}_2\text{PS}_3$ . Experimental wise, this is not a good synthesis method in comparing the difference of the LiCl addition due to different purity and side phases present in both argyrodites. Furthermore, comparing the ball milled LiCl addition to that of pristine argyrodite (as previously used in the previous chapters), the side phase of pristine  $\text{Li}_6\text{PS}_5\text{Cl}$  has a significant amount of  $\text{Li}_3\text{PO}_4$  like  $\text{Li}_6\text{PS}_5\text{Cl}$  CL5-bm although not the same ratio of  $\text{Li}_6\text{PS}_5\text{Cl}$  to  $\text{Li}_3\text{PO}_4$ .

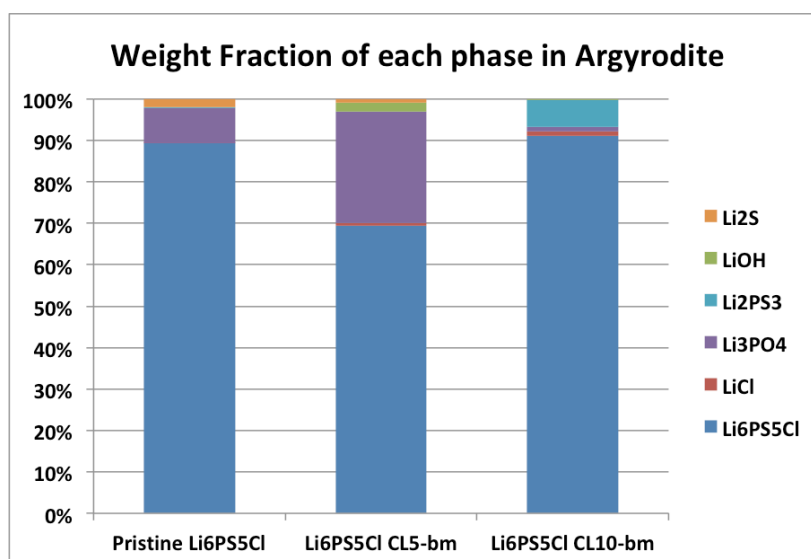


Figure 7.2: Argyrodite weight fraction with addition of ball milled LiCl via ball mill

Next, the catholyte mixture undergoes a XRD analysis with the weight fraction as shown in Figure 7.3. Similar to Section 4.2.3, the values are wrong as the argyrodite and NCM 622 weight fraction should be equal. Nevertheless, the ratio of the NCM622 to the Argyrodite with its side phases remains constant throughout the catholyte mixtures.

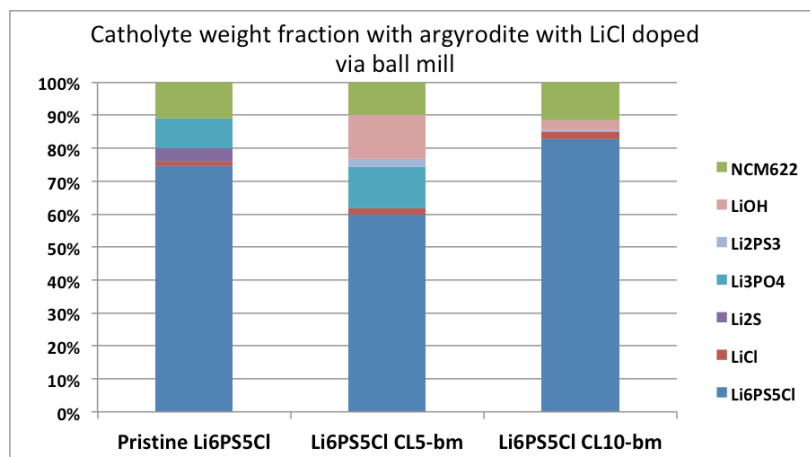


Figure 7.3: weight fraction of catholyte with addition of ball milled LiCl via ball mill

## 7.2. Cycling Analysis

The battery is assembled with the cathode mixture of NCM 622, pristine or ball milled LiCl doped Li<sub>6</sub>PS<sub>5</sub>Cl, and super P carbon Black. It is allowed to cycle for approximately 36 cycles. Another battery is cycled with the cathode mixture of pristine or ball milled LiCl doped Li<sub>6</sub>PS<sub>5</sub>Cl and Carbon Black. The cycling data from the Maccor is analysed in this section.

### 7.2.1. Catholyte: NCM 622, pristine/ball milled LiCl doped Li<sub>6</sub>PS<sub>5</sub>Cl, Carbon Black

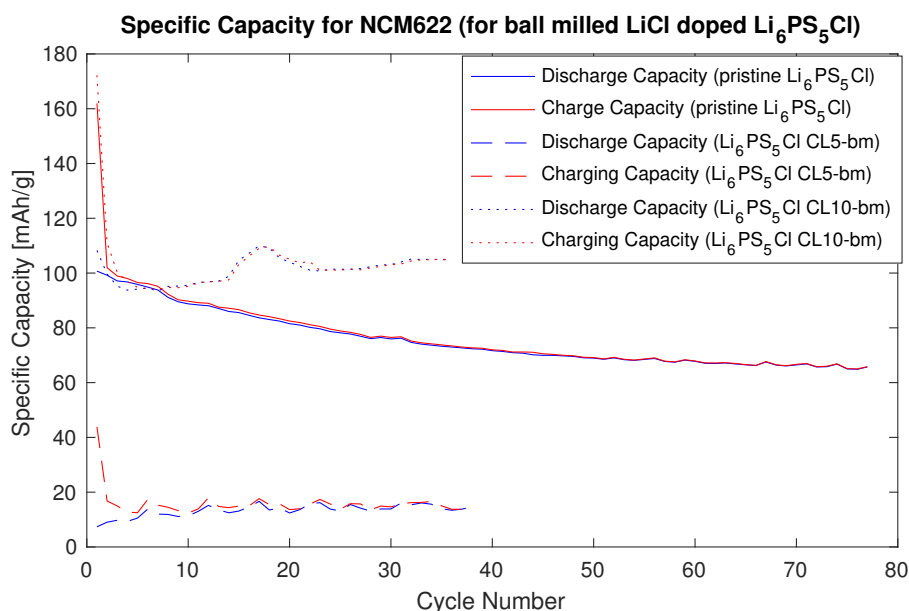


Figure 7.4: Curve of Specific Capacity Cycle of NCM 622 with each cycle

The batteries are assembled and cycled with its specific capacity for each cycle are shown in Figure 7.4. From this figure, the battery with Li<sub>6</sub>PS<sub>5</sub>Cl CL5-bm has the specific capacity retention is largely reduced. This could be either from less mobility of ions or the interphase between NCM 622 and Li<sub>6</sub>PS<sub>5</sub>Cl CL5 is smaller. For Li<sub>6</sub>PS<sub>5</sub>Cl CL10, it is shown to have a better specific capacity retention than of pristine

$\text{Li}_6\text{PS}_5\text{Cl}$ . This could mean that the conductivity of ions are larger for pristine  $\text{Li}_6\text{PS}_5\text{Cl}$  although the EIS testing contradicts this. Additionally, the interphase of the NCM 622 and  $\text{Li}_6\text{PS}_5\text{Cl}$  F10 could be stable as it has less capacity degradation than of pristine  $\text{Li}_6\text{PS}_5\text{Cl}$ .

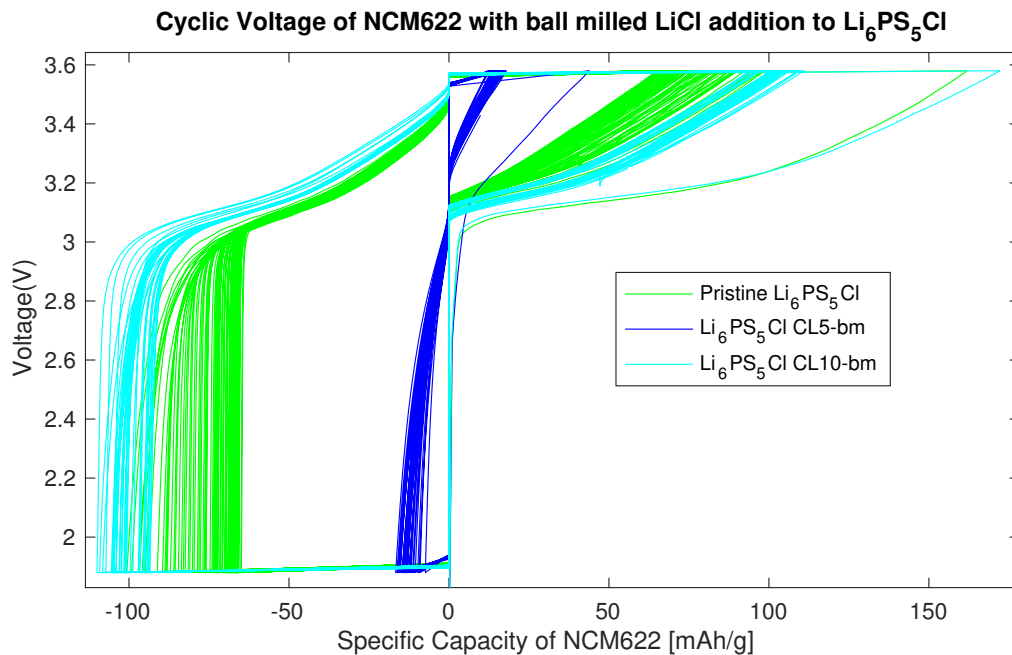


Figure 7.5: Cyclic Voltage of the batteries with cathode of NCM622, pristine/ball milled LiCl doped  $\text{Li}_6\text{PS}_5\text{Cl}$ , and carbon black

Next, the cyclic voltage of the batteries are shown in Figure 7.5. From this figure, curves of the battery with  $\text{Li}_6\text{PS}_5\text{Cl}$  CL5-bm and CL10-bm are more compact than the previous method (in Figure 5.3) where the curves were spread apart. However, it is also noted that the cycling of the catholytes with ball milled LiCl doped  $\text{Li}_6\text{PS}_5\text{Cl}$  were cycled less than the previous method. Like the previous method, the curves are smooth and uniform.

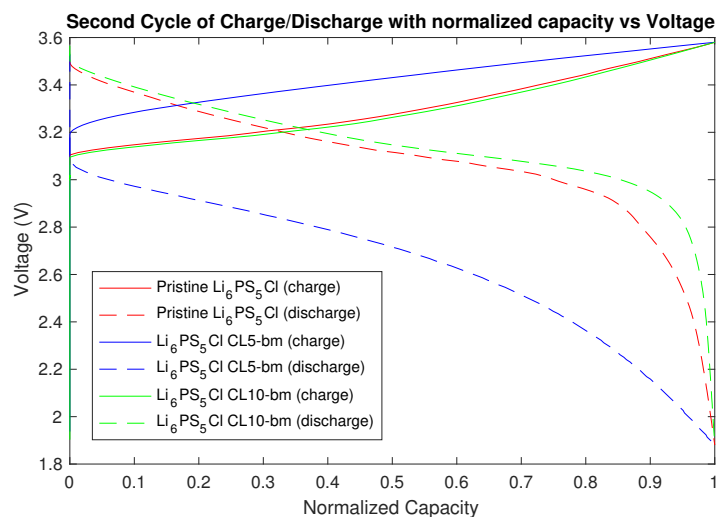


Figure 7.6: Voltage from the second cycle against the normalized capacity of NCM 622 for ball milled LiCl doped  $\text{Li}_6\text{PS}_5\text{Cl}$

From the data used in Figure 7.4, the overpotentials is calculated by composing a graph of Voltage against the normalized capacity for the second cycle. This is shown in Figure 7.6. The overpotentials

values are then summarized in Table 7.2. From the overpotential values,  $\text{Li}_6\text{PS}_5\text{Cl}$  CL5-bm are shown to be more resistive than pristine  $\text{Li}_6\text{PS}_5\text{Cl}$ . However,  $\text{Li}_6\text{PS}_5\text{Cl}$  CL10-bm are shown to be less resistive than pristine  $\text{Li}_6\text{PS}_5\text{Cl}$ .

NCM 622 with:	Charging Overpotential (V)	Discharging Overpotential (V)
$\text{Li}_6\text{PS}_5\text{Cl}$ CL5-bm	0.156	-0.400
$\text{Li}_6\text{PS}_5\text{Cl}$ CL10-bm	-0.012	0.031

Table 7.2: Overpotentials of NCM 622 with doped Argyrodites at normalized capacity of 0.5 in relation to pristine Argyrodite

### 7.2.2. Cathode: Pristine/Ball milled $\text{Li}_6\text{PS}_5\text{Cl}$ and Carbon black

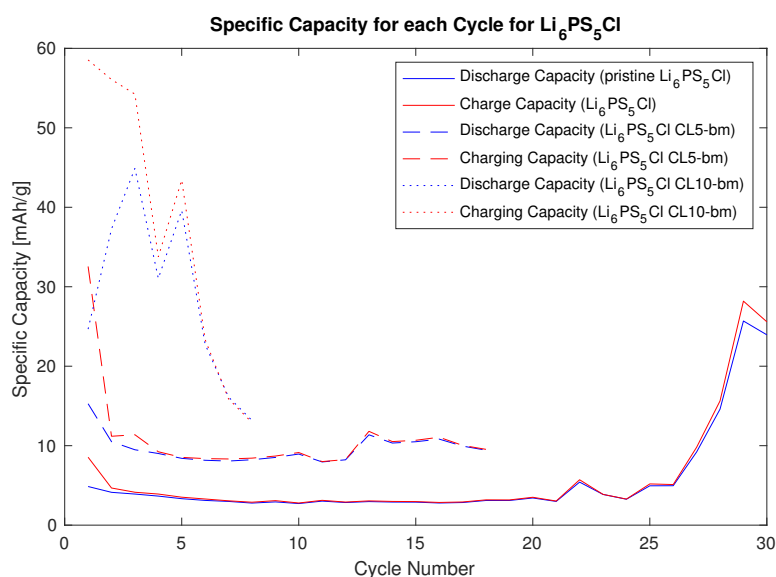


Figure 7.7: Specific Capacity for each cycle for argyrodites as cathodes

Next the batteries with cathode without NCM 622 are cycled and analysed in regards to ball milled  $\text{LiCl}$  doped  $\text{Li}_6\text{PS}_5\text{Cl}$ . The specific capacity for each cycle is shown in Figure 7.7. Overall, it has a much lower specific capacity than with NCM 622 (in Figure 7.4) as expected.  $\text{Li}_6\text{PS}_5\text{Cl}$  CL5-bm and  $\text{Li}_6\text{PS}_5\text{Cl}$  CL10-bm are shown to have higher specific capacity although it is still relatively unstable. This indicates that the ball milled dopants added to the argyrodite electrolyte do not impede its decomposition, though more cycling data is required to make an analysis.

Next, the cyclic voltage of the battery is shown in Figure 7.8. Like Figure 7.8, the curves are messy, rough, and not uniform. More cycling or experiments are necessary to interpret the data.

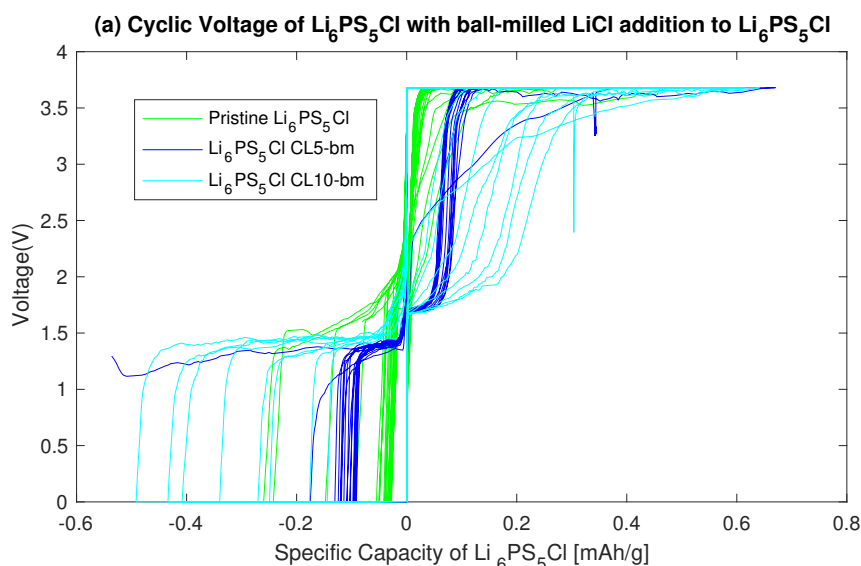


Figure 7.8: Cyclic Voltage of the batteries with Argyrodite as cathodes

### 7.3. Ex-situ XRD Analysis

XRD measurement and refinement are carried out as an ex-situ analysis. For the measurement and refinement of the XRD please refer to Figures A.17, A.18, A.19 and A.20 in the Appendix.

#### 7.3.1. Cathode: NCM 622, ball milled $\text{LiCl}$ doped $\text{Li}_6\text{PS}_5\text{Cl}$ , and Carbon Black

The difference of phase fraction in pre and post cycling are shown in Figure 7.9. To summarize this figure, pristine  $\text{Li}_6\text{PS}_5\text{Cl}$  decomposes mostly to  $\text{LiCl}$  and  $\text{Li}_3\text{P}$ .  $\text{Li}_6\text{PS}_5\text{Cl}$  CL5-bm also decomposes significantly to  $\text{Li}_3\text{P}$  and  $\text{LiOH}$ .  $\text{Li}_6\text{PS}_5\text{Cl}$  CL10-bm degrades to form significant products of  $\text{Li}_2\text{PS}_3$ ,  $\text{Li}_3\text{P}$  and probably  $\text{LiOH}$  (considering the error). From the EIS discussion in Sections 7.1.1 and 4.1,  $\text{Li}_6\text{PS}_5\text{Cl}$  CL5-bm and  $\text{Li}_6\text{PS}_5\text{Cl}$  CL10-bm have a larger kinetic control than of pristine  $\text{Li}_6\text{PS}_5\text{Cl}$ . Thus, the ball milled  $\text{LiCl}$  doped  $\text{Li}_6\text{PS}_5\text{Cl}$  has a higher rate of reaction than of pristine  $\text{Li}_6\text{PS}_5\text{Cl}$ . If the battery with  $\text{Li}_6\text{PS}_5\text{Cl}$  CL5-bm and CL10-bm were allowed to cycle longer, then the side phases might be intensified. Considering the battery with the ball milled  $\text{LiCl}$  doped was cycled half of pristine  $\text{Li}_6\text{PS}_5\text{Cl}$  and still get significant degradation with side products, it is safe to assume that the EIS data corroborates with the ex-situ analysis.

#### 7.3.2. Cathode: ball milled $\text{LiCl}$ doped $\text{Li}_6\text{PS}_5\text{Cl}$ , and Carbon Black

The batteries without the active material of NCM 622 were cycled and the percentage of phase fraction from the XRD analysis is shown in Figure 7.10. In this figure, the Pristine  $\text{Li}_6\text{PS}_5\text{Cl}$  degrades to  $\text{LiCl}$ ,  $\text{Li}_3\text{PO}_4$ ,  $\text{Li}_2\text{PS}_3$  and  $\text{Li}_3\text{P}$ .  $\text{Li}_6\text{PS}_5\text{Cl}$  CL5-bm appears to have no degradation, but from an increase of  $\text{LiCl}$ ,  $\text{Li}_2\text{PS}_3$ , and  $\text{Li}_3\text{P}$  confirms otherwise. It could be that the phase fraction of  $\text{LiOH}$  in the argyrodite is wrong as it very unlikely for the significantly large loss of  $\text{LiOH}$  to occur.  $\text{Li}_6\text{PS}_5\text{Cl}$  CL10-bm degrades to  $\text{Li}_3\text{PO}_4$ ,  $\text{Li}_3\text{P}$ , and  $\text{LiOH}$ . Reiterating previous statement,  $\text{Li}_6\text{PS}_5\text{Cl}$  CL5-bm and CL10-bm have higher rate of reaction than for pristine  $\text{Li}_6\text{PS}_5\text{Cl}$ . However, it is not reflected well in this Figure. This is most likely due to fewer cycles in comparison to pristine  $\text{Li}_6\text{PS}_5\text{Cl}$ .

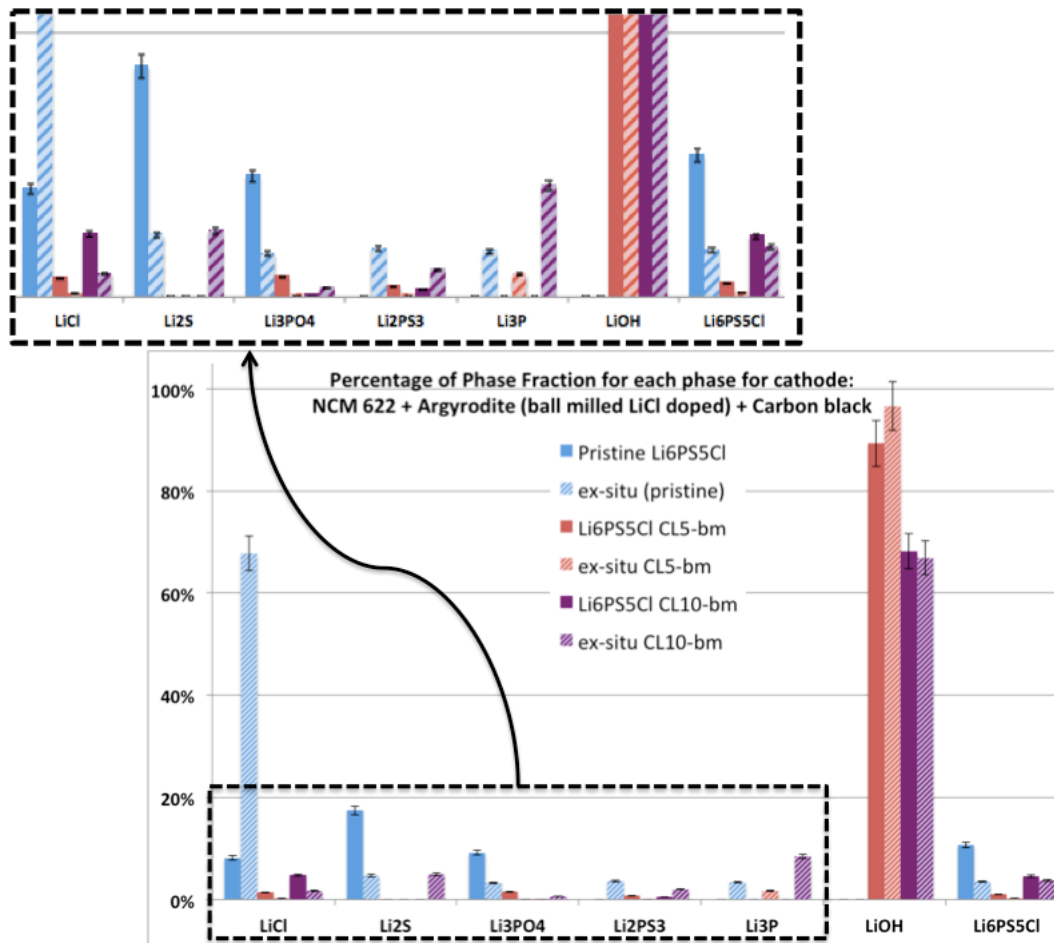


Figure 7.9: Percentage of phase fraction for before and after cycling of cathodes with NCM 622 with 5% error. Zoom at low percentage is also included in the floating box

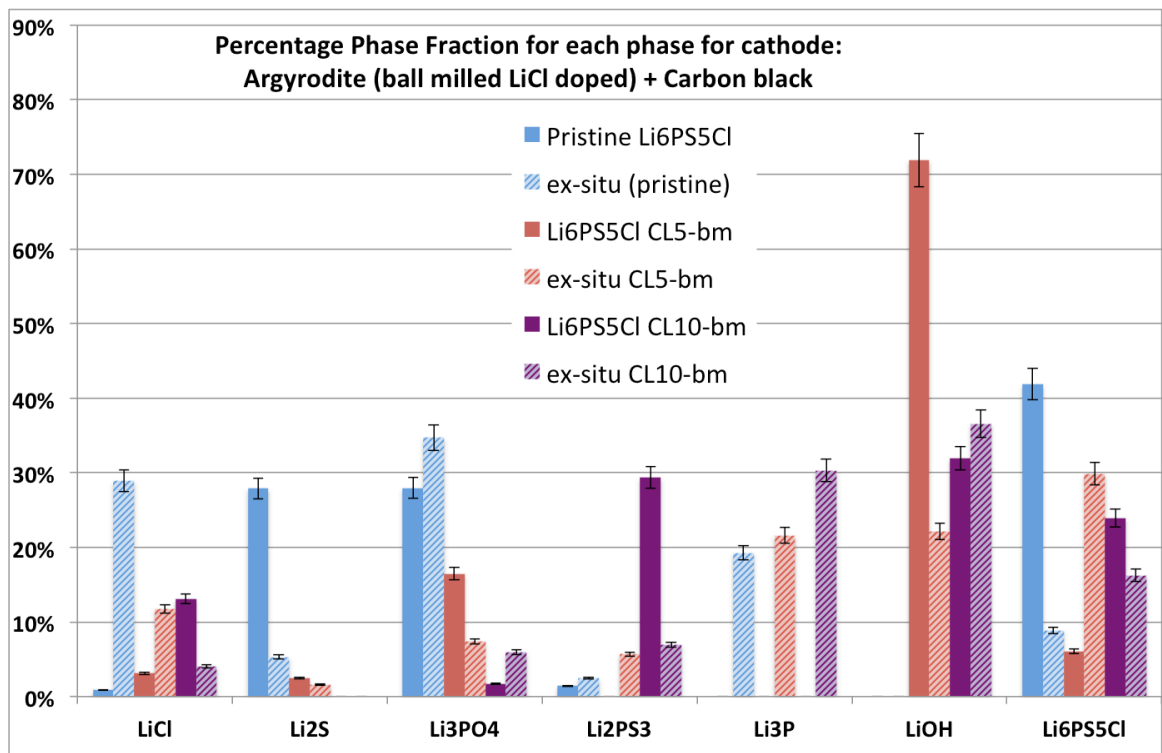


Figure 7.10: Percentage of phase fraction for before and after cycling of cathodes of argyrodite and carbon black with 5% error

# 8

## Conclusions & Further Recommendations

To conclude, doping LiCl into  $\text{Li}_6\text{PS}_5\text{Cl}$  increases the ionic conductivities and decreases the chemical rate of reaction. However, it lowers the specific capacity retention of NCM 622. This could be due to the poor interphase contact between the argyrodite and active material. Additionally, doping LiCl into  $\text{Li}_6\text{PS}_5\text{Cl}$  helps to mitigate decomposition by reducing its kinetic control properties. However, the reasoning of the poor interphase contact also could explain the low decomposition.

Doping LiF to  $\text{Li}_6\text{PS}_5\text{Cl}$  decreases the ionic conductivity but increases the chemical rate of reaction. For the case of  $\text{Li}_6\text{PS}_5\text{Cl}$  F5, it reduces the specific capacity retention which confirms that there are less mobile ions in the cathode region. However for  $\text{Li}_6\text{PS}_5\text{Cl}$  F10, the specific capacity retention of the active material is comparable to of pristine  $\text{Li}_6\text{PS}_5\text{Cl}$  which may be due to catholyte having similar composition. Also it shows that  $\text{Li}_6\text{PS}_5\text{Cl}$  F10 degrades significantly more than pristine  $\text{Li}_6\text{PS}_5\text{Cl}$  and  $\text{Li}_6\text{PS}_5\text{Cl}$  F5. Hence the high specific capacity for  $\text{Li}_6\text{PS}_5\text{Cl}$  F10 may be caused by the high rate of decomposition.

With the alternative doping method of ball milling the ball milled LiCl after  $\text{Li}_6\text{PS}_5\text{Cl}$  synthesis, it is shown to have more resistance and higher rate of degradation from the EIS analysis. During cycling with NCM 622, it is shown that specific capacity retention is better for  $\text{Li}_6\text{PS}_5\text{Cl}$  CL10-bm than pristine and  $\text{Li}_6\text{PS}_5\text{Cl}$  CL5-bm. This could be due to high rate of degradation as side phases are intensified during cycling compared to pristine  $\text{Li}_6\text{PS}_5\text{Cl}$  and  $\text{Li}_6\text{PS}_5\text{Cl}$  CL5-bm. For  $\text{Li}_6\text{PS}_5\text{Cl}$  CL5-bm however specific capacity degradation was the worst among pristine  $\text{Li}_6\text{PS}_5\text{Cl}$  and  $\text{Li}_6\text{PS}_5\text{Cl}$  CL10-bm. This was expected due to lower conductivity and thus less mobile ions. It could also mean that the interphase was bad too. This could also explain why the side phases were intensified less than of others.

To improve the quality of the research, the purity of the  $\text{Li}_6\text{PS}_5\text{Cl}$  needs to be greatly improved due to a significant amount of side phases present before cycling. The side phases likely affected the results of the experiments especially during cycling. The main factor of the impurities formed of the  $\text{Li}_6\text{PS}_5\text{Cl}$  is from the method of synthesis. Also, doping  $\text{Li}_6\text{PS}_5\text{Cl}$  LiF should be longer in terms of ball-milling and annealing as LiF seems to mitigate the synthesis of  $\text{Li}_6\text{PS}_5\text{Cl}$ . Another improvement is to gently heat the cathode mixtures to form a faster equilibrium with all of the mixtures. Additionally, to better understand the effect of LiCl or LiF doping of Argyrodite, the following methods could be carried out:

- **Transmission Electron Microscopy (TEM) analysis** to observe the surface morphology of the LiCl or LiF positions in relation to the argyrodite. It is ideal that the doping is uniformly distributed and it needs to be confirmed.
- **XRD in operando mode** to check the phase changes for each cycle of the battery and thus able to make a better estimation of rate of decomposition
- **Energy Dispersive X-ray Spectrometry (EDS)** for quantifying chemical compositions with more accuracy than XRD. Elemental mapping may also be determined which is identifying phases

across the surface

- **EDS with scanning electron microscope (SEM)** to do line profile analysis in which the relative elemental concentration of each element can be determine in a position along the line of sample

Additionally, an interesting factor to look at is ageing. Since decomposition of the argyrodite will naturally occur even in storage, will LiCl or LiF improve or worsens the ageing process? Alternately, it is better to explore other methods in adding LiCl or LiF salts such as **Wet Chemistry Method** and **Atomic Layer Deposition**. These methods will be defined as coating and not doping. With coating, it is expected for the LiCl or LiF to have a more uniform microscopic structure and distribution as well as forming a 'protective layer' around the argyrodite atomic particles.



## Appendix

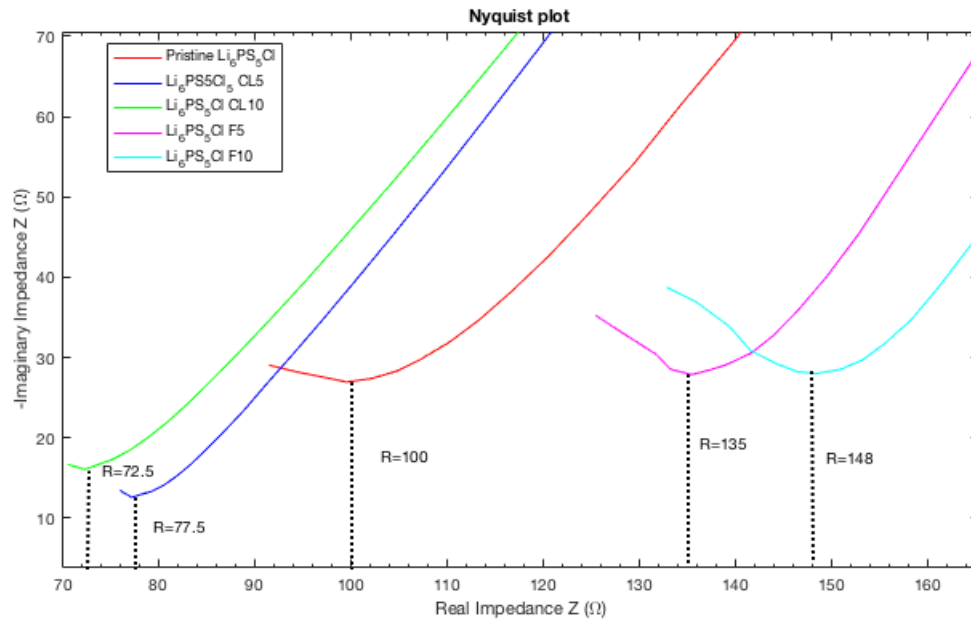


Figure A.1: Intersection of semi circle and straight line to determine Resistance of the bulk,  $R_b$

Table A.1: Thickness of Argyrodite pellet used on EIS testing

Argyrodite	Thickness of the pellet, $l$ [mm]
Pristine $\text{Li}_6\text{PS}_5\text{Cl}$	1.60
$\text{Li}_6\text{PS}_5\text{Cl}$ CL5	1.65
$\text{Li}_6\text{PS}_5\text{Cl}$ CL10	1.60
$\text{Li}_6\text{PS}_5\text{Cl}$ F5	1.65
$\text{Li}_6\text{PS}_5\text{Cl}$ F10	1.65
$\text{Li}_6\text{PS}_5\text{Cl}$ CL5-bm	1.40
$\text{Li}_6\text{PS}_5\text{Cl}$ CL10-bm	1.20

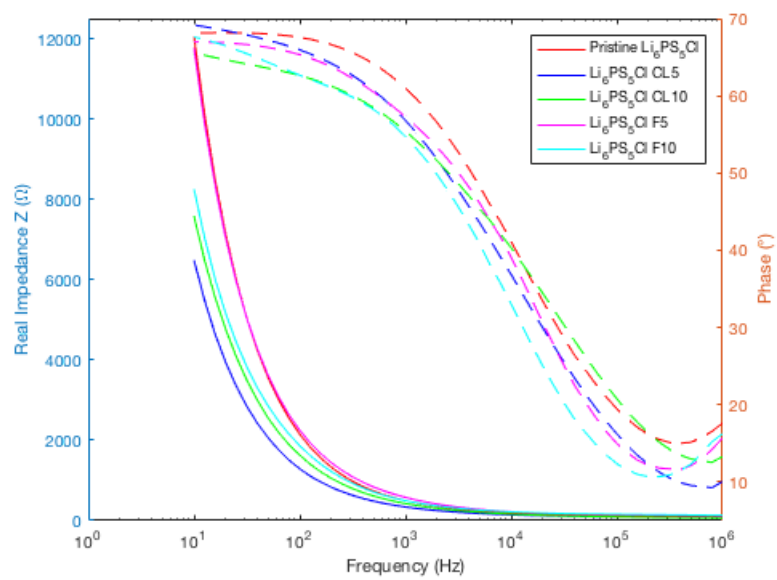


Figure A.2: Relation of Real Impedance  $Z$  and phase against frequency

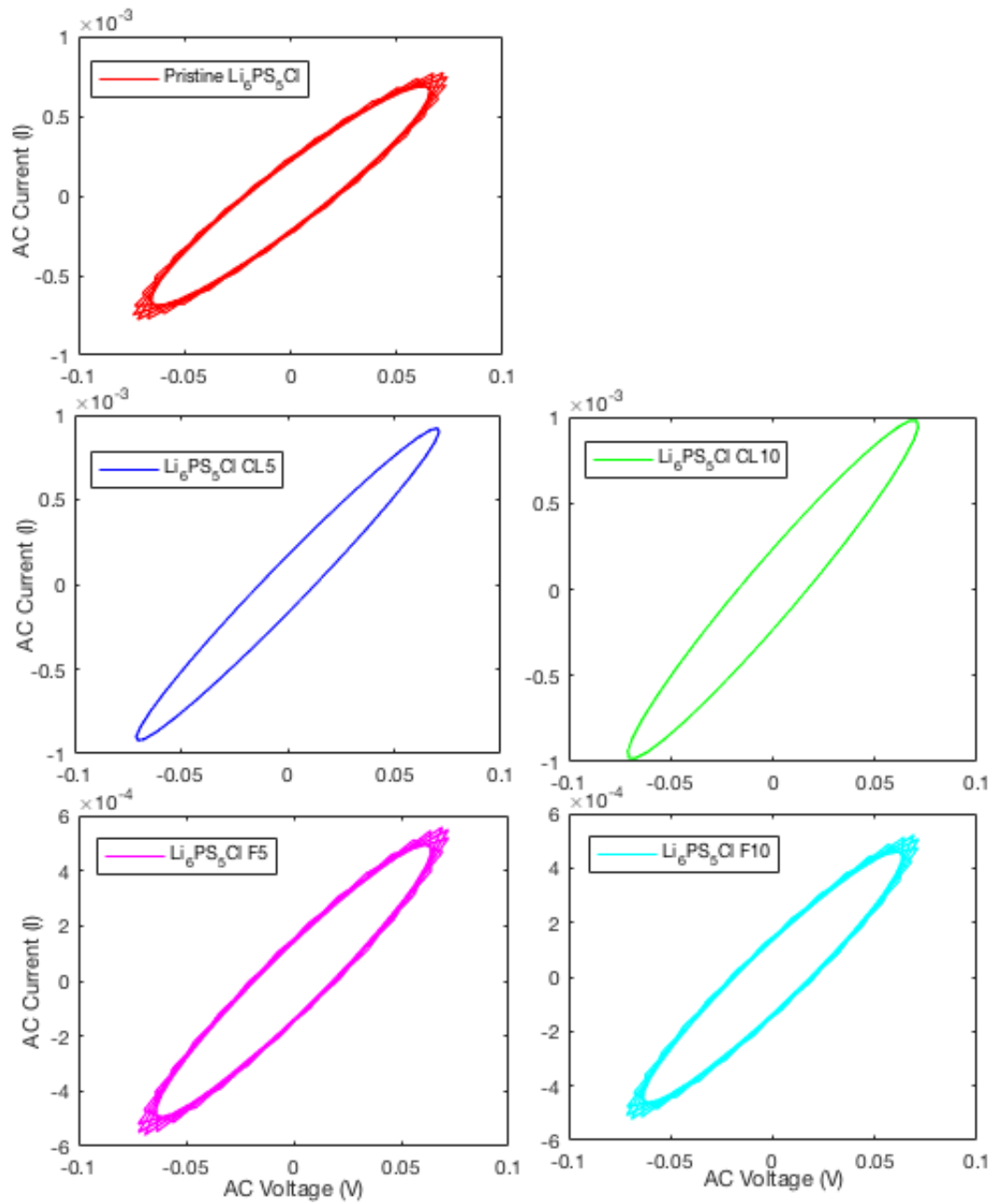


Figure A.3: Lissajous figure from EIS measurement

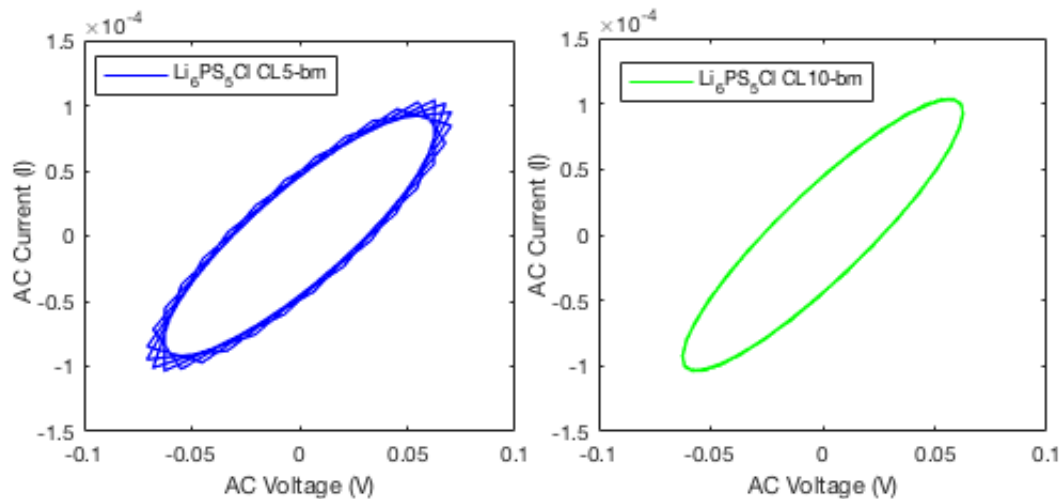


Figure A.4: Lissajous Figure from EIS measurement for alternate method

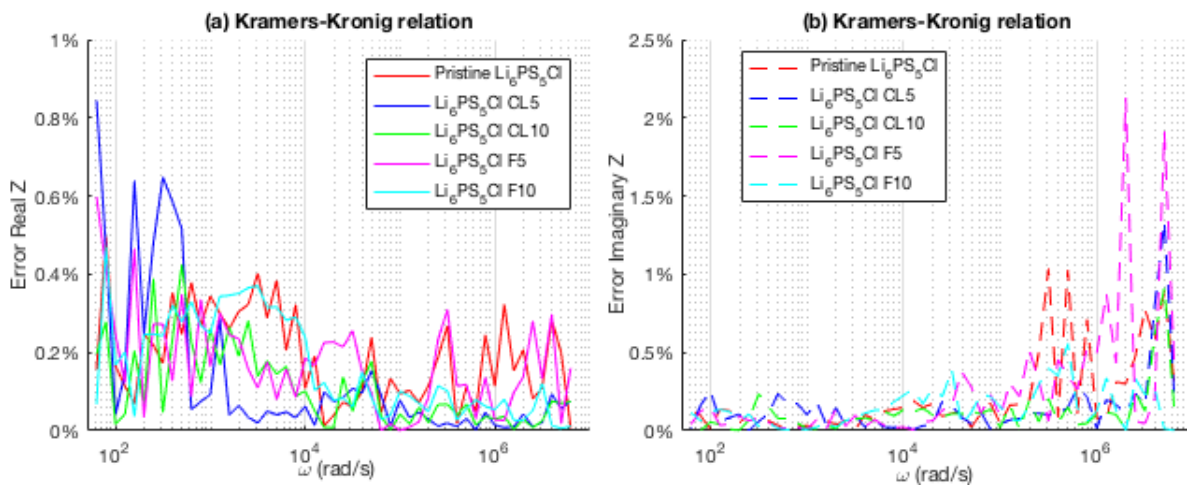


Figure A.5: EIS: Kramers-Kronig relation for (a) real impedance and (b) Imaginary impedance

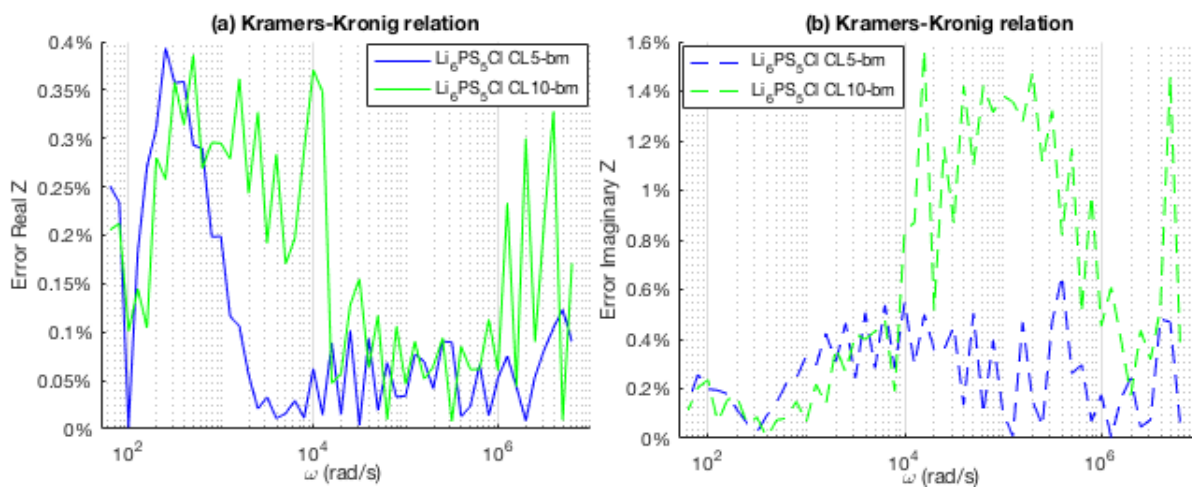


Figure A.6: EIS: Kramers-Kronig relation for (a) real impedance and (b) Imaginary Impedance for alternate method

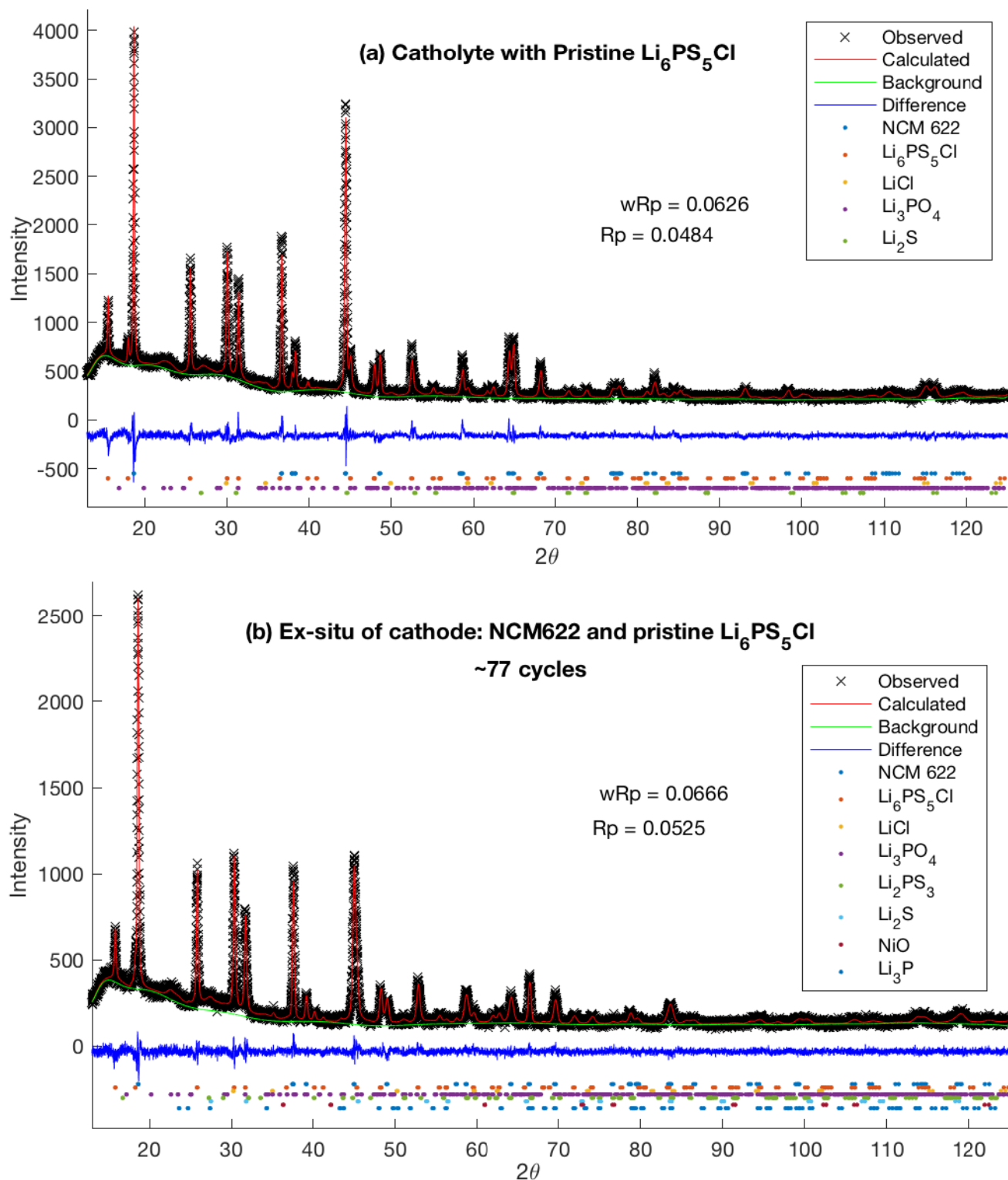


Figure A.7: XRD measurement and refinement with different phases identified for cathode of: NCM622, pristine  $\text{Li}_6\text{PS}_5\text{Cl}$ , Carbon black for (a) before cycling and (b) after 77 cycles

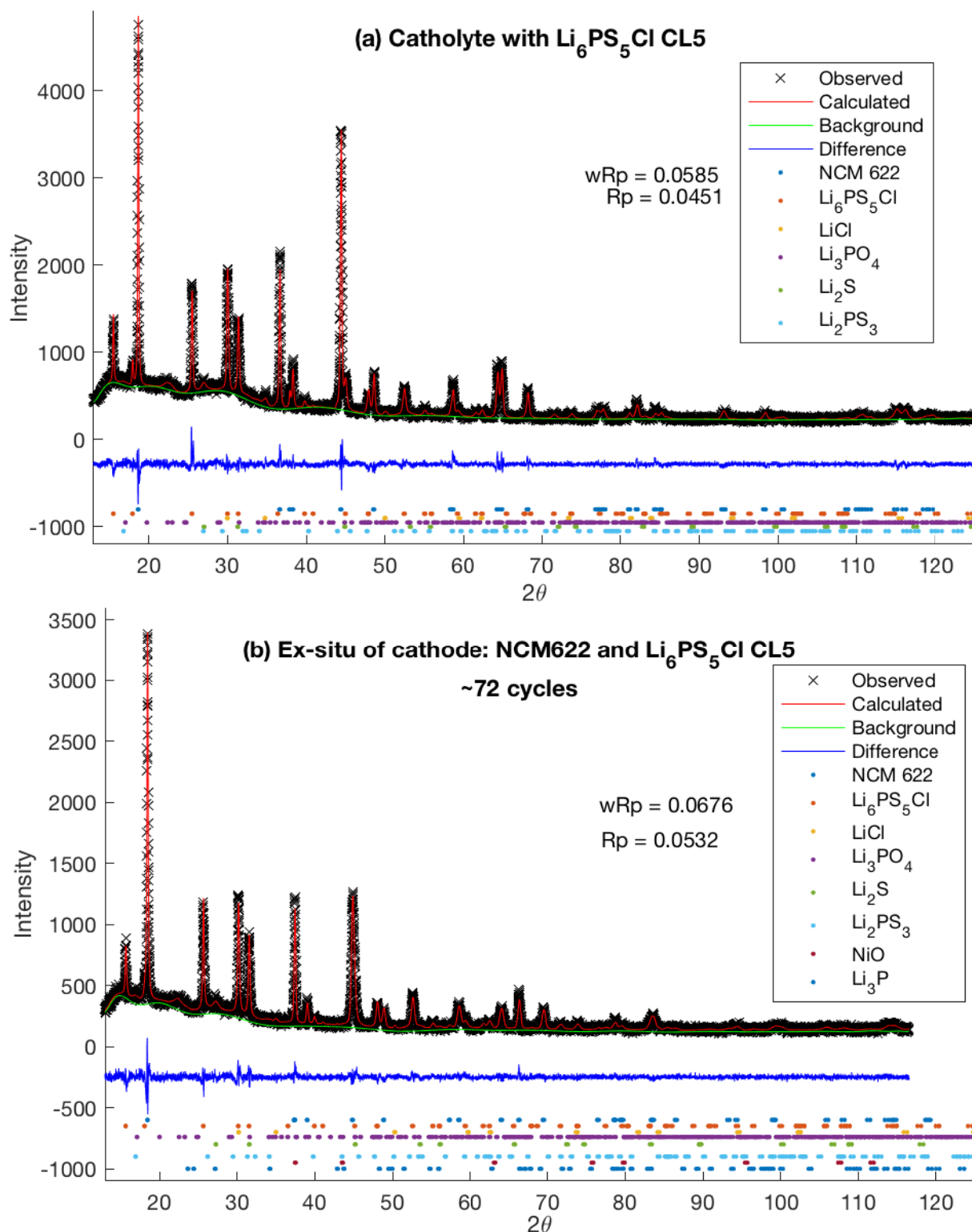


Figure A.8: XRD measurement and refinement with different phases identified for cathode of: NCM622,  $\text{Li}_6\text{PS}_5\text{Cl}$  CL5, Carbon black for (a) before cycling and (b) after 72 cycles

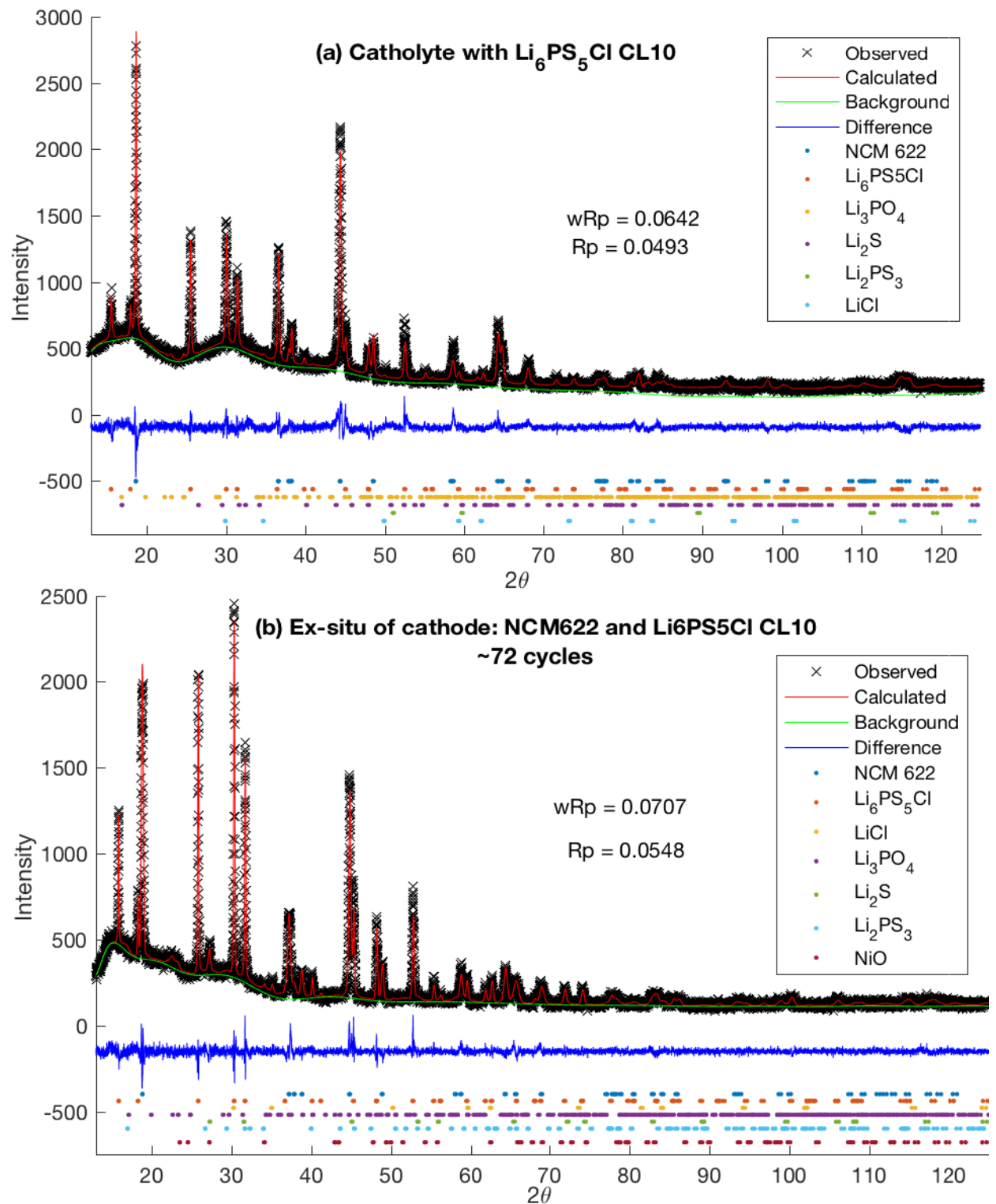


Figure A.9: XRD measurement and refinement with different phases identified for cathode of: NCM622,  $\text{Li}_6\text{PS}_5\text{Cl}$  CL10, Carbon black for (a) before cycling and (b) after 72 cycles

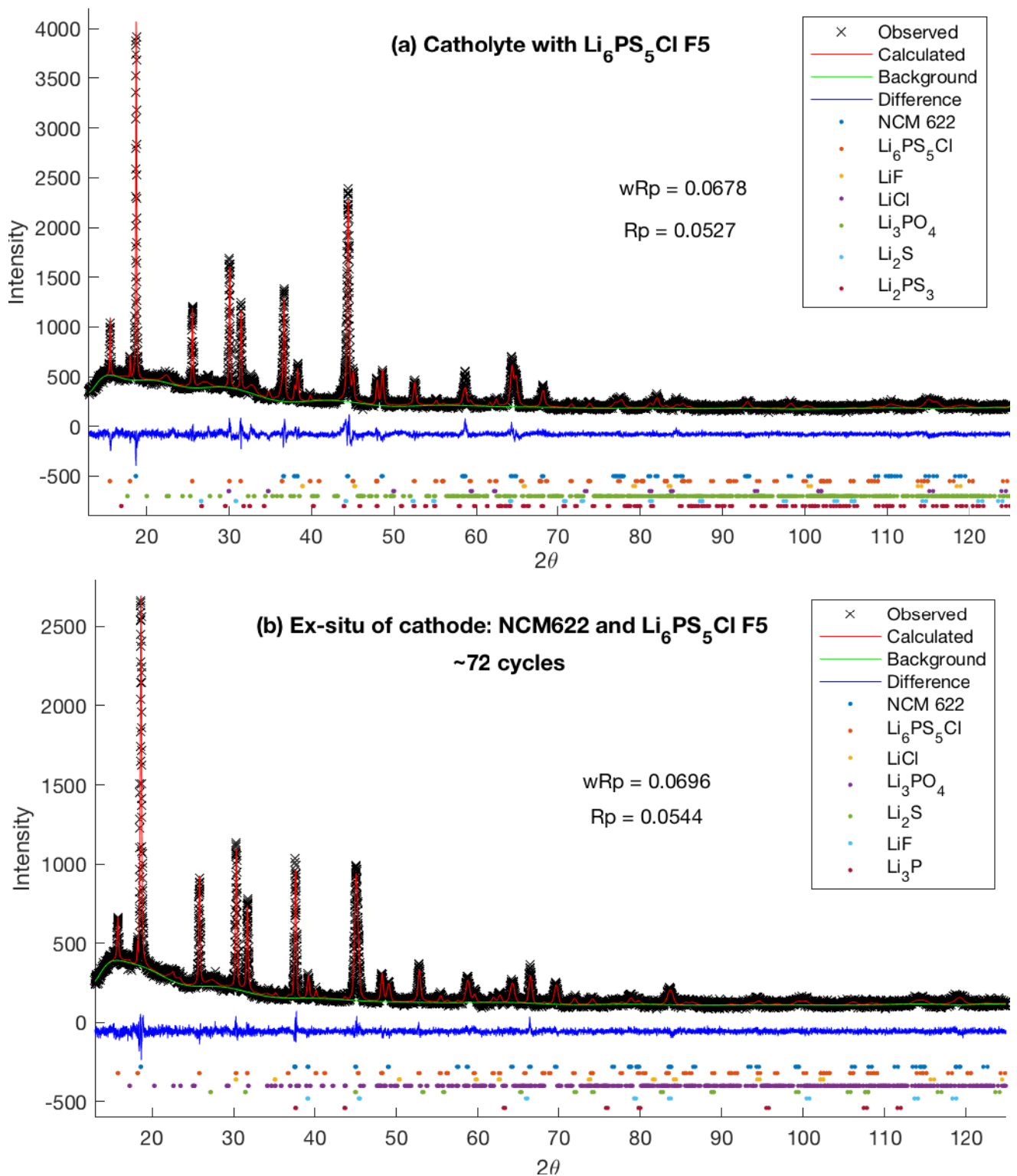


Figure A.10: XRD measurement and refinement with different phases identified for cathode of: NCM622,  $\text{Li}_6\text{PS}_5\text{Cl}$  F5, Carbon black for (a) before cycling and (b) after 72 cycles

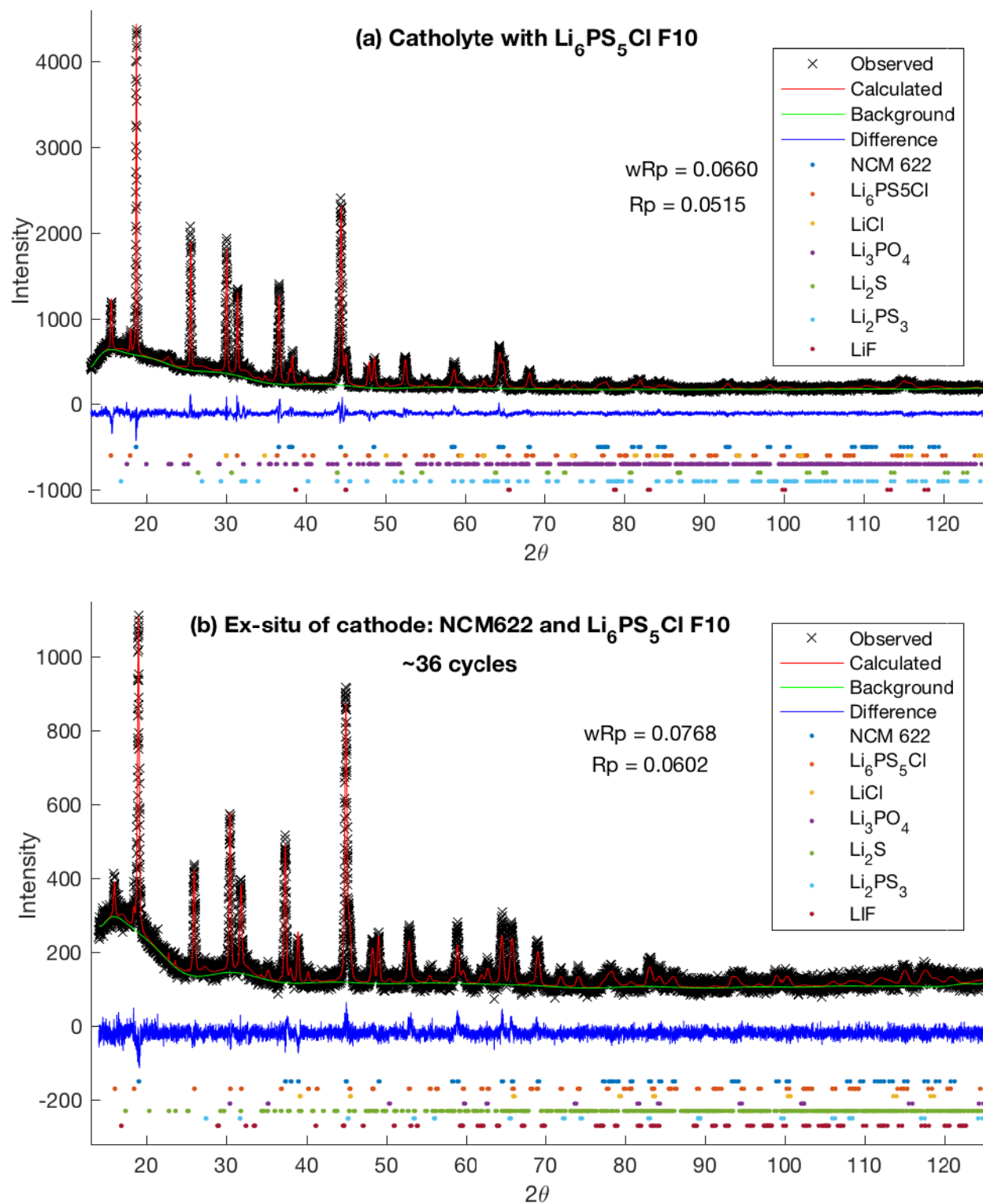


Figure A.11: XRD measurement and refinement with different phases identified for cathode of: NCM622,  $\text{Li}_6\text{PS}_5\text{Cl}$  F10, and Carbon black for (a) before cycling and (b) after 36 cycles

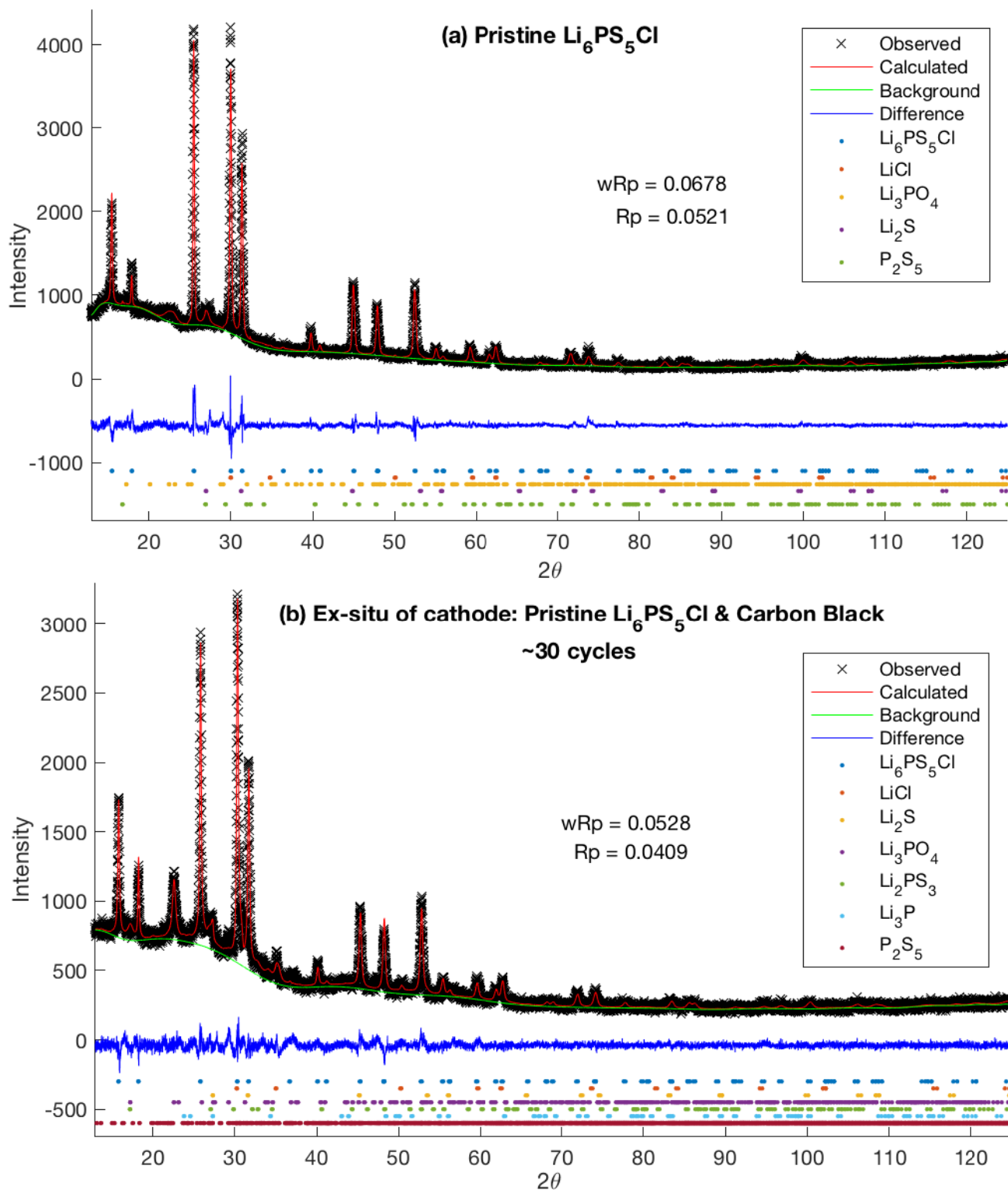


Figure A.12: XRD measurement and refinement with different phases identified for cathode of: pristine  $\text{Li}_6\text{PS}_5\text{Cl}$  and Carbon black for (a) before cycling and (b) after 30 cycles

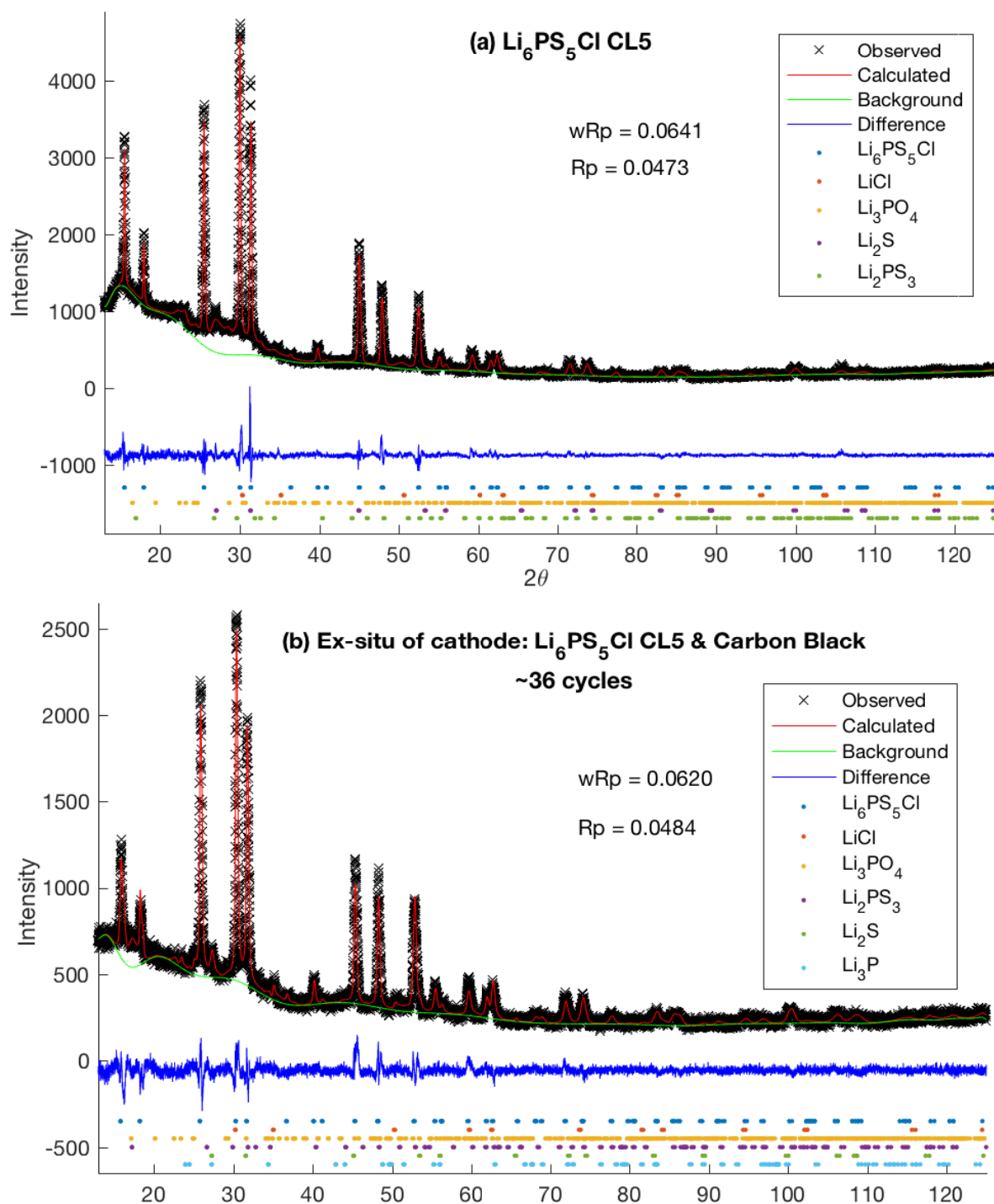


Figure A.13: XRD measurement and refinement with different phases identified for cathode of:  $\text{Li}_6\text{PS}_5\text{Cl}$  CL5 and Carbon black for (a) before cycling and (b) after 36 cycles

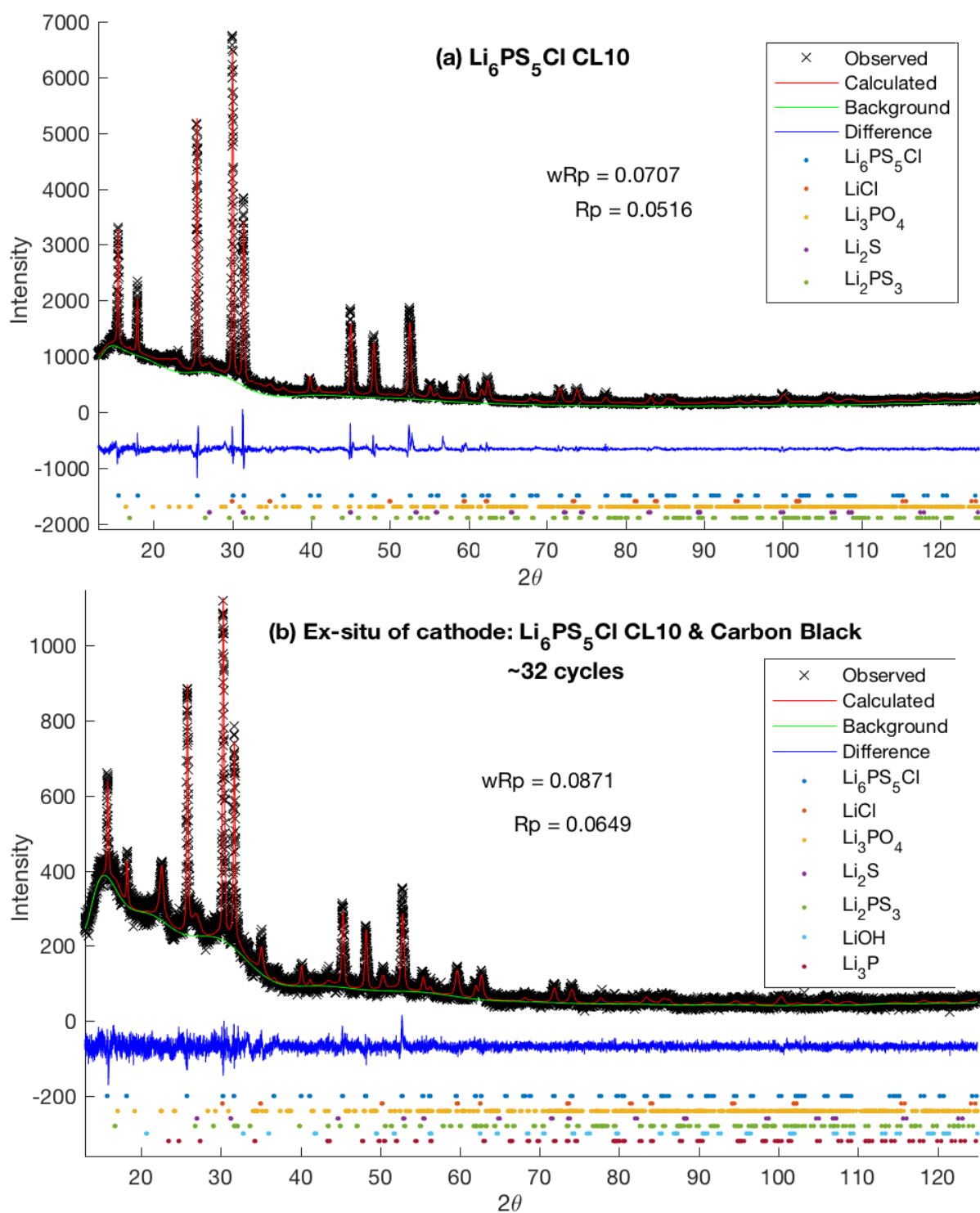


Figure A.14: XRD measurement and refinement with different phases identified for cathode of:  $\text{Li}_6\text{PS}_5\text{Cl}$  CL10 and Carbon black for (a) before cycling and (b) after 32 cycles

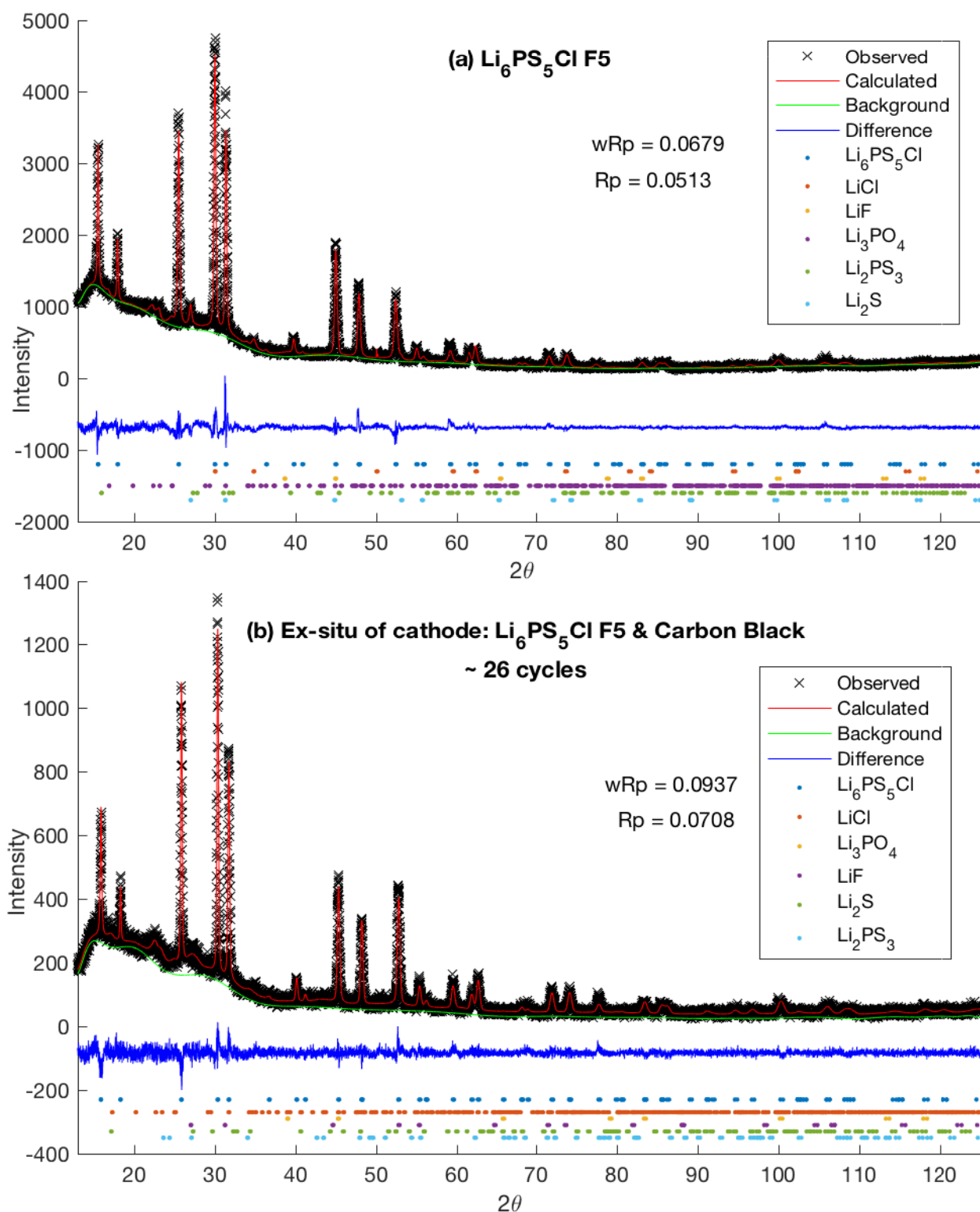


Figure A.15: XRD measurement and refinement with different phases identified for cathode of:  $\text{Li}_6\text{PS}_5\text{Cl}$  F5 and Carbon black for (a) before cycling and (b) after 26 cycles

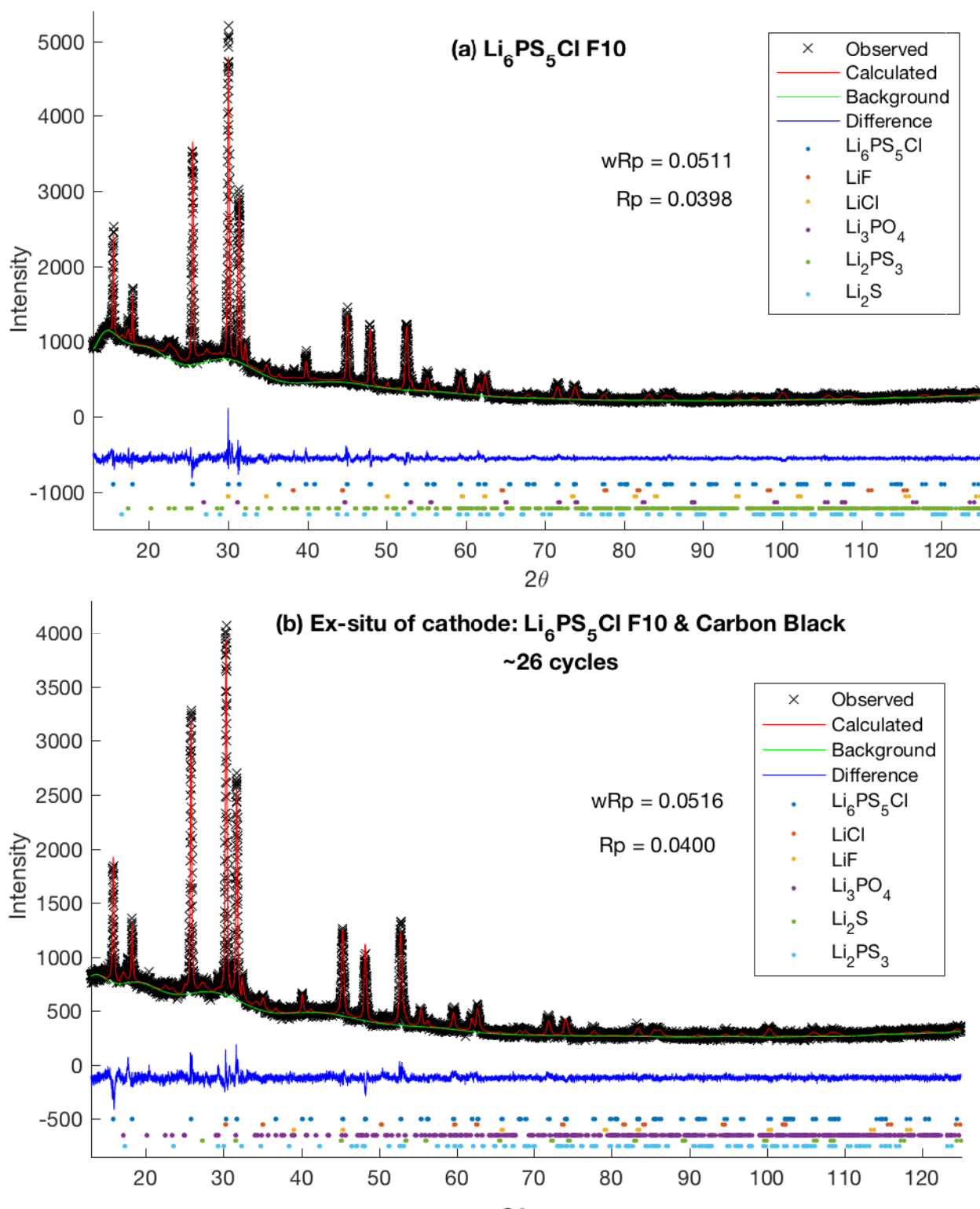


Figure A.16: XRD measurement and refinement with different phases identified for cathode of:  $\text{Li}_6\text{PS}_5\text{Cl}$  F10 and Carbon black for (a) before cycling and (b) after 26 cycles

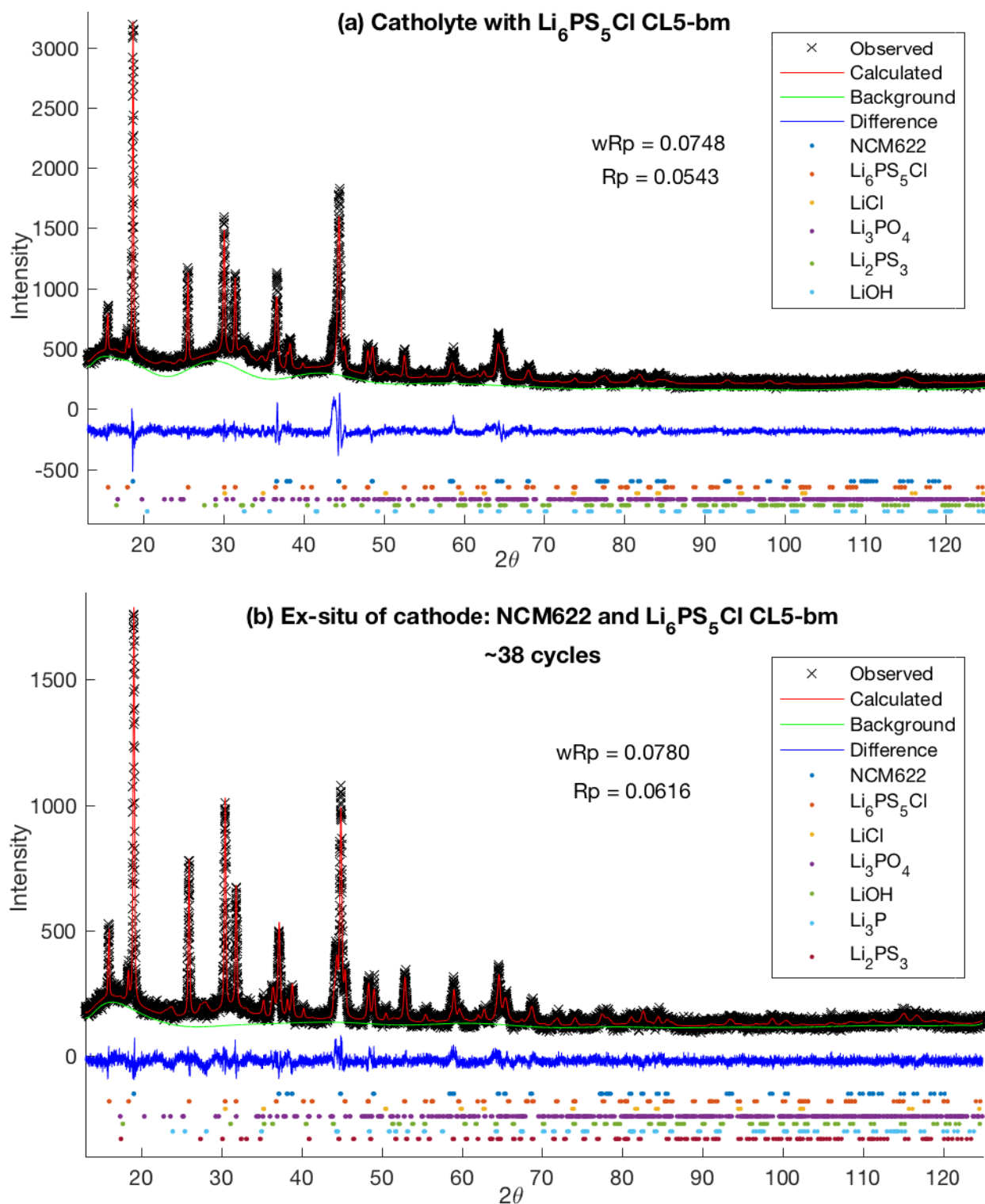


Figure A.17: XRD measurement and refinement with different phases identified for cathode of: NCM622,  $\text{Li}_6\text{PS}_5\text{Cl}$  CL5-bm, Carbon black for (a) before cycling and (b) after 38 cycles

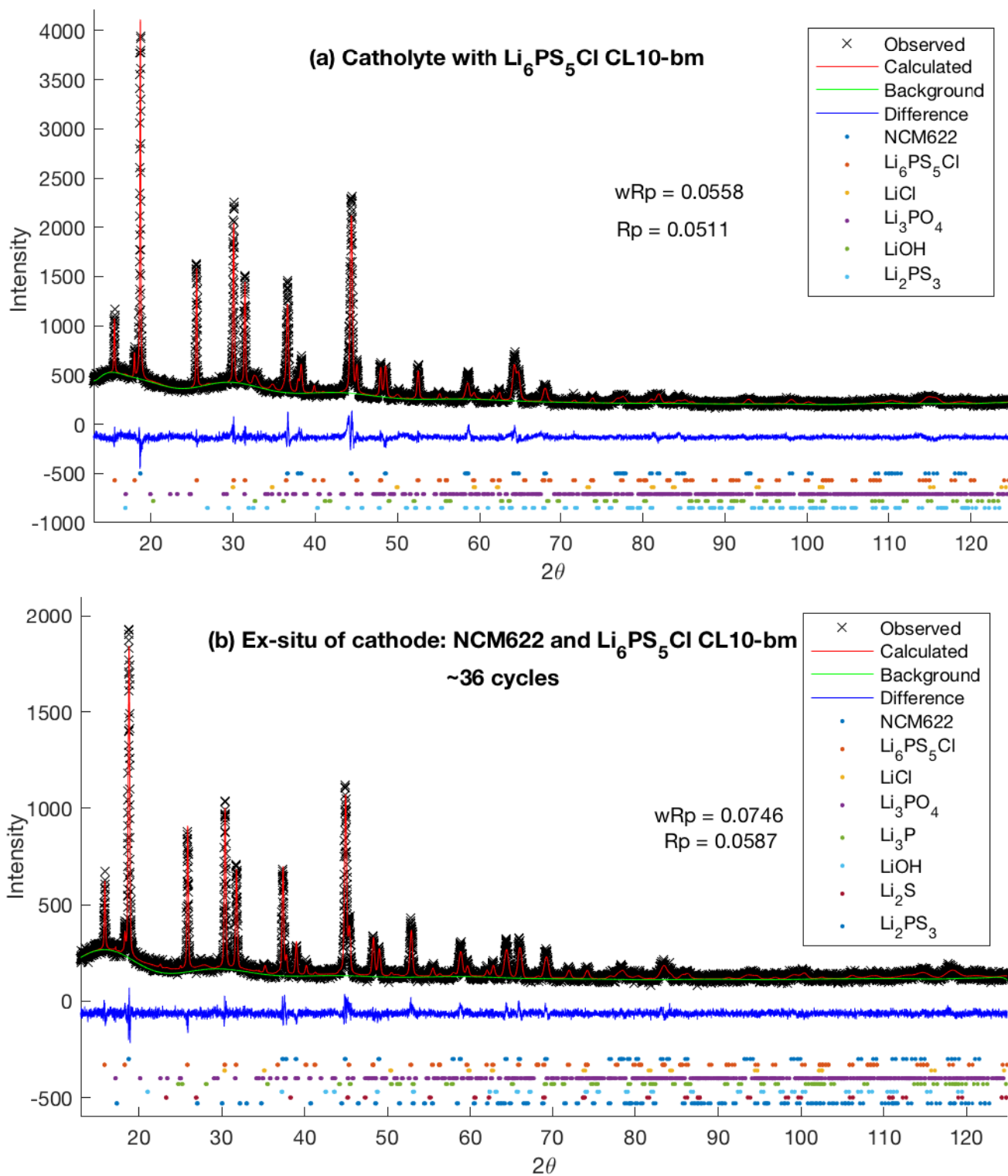


Figure A.18: XRD measurement and refinement with different phases identified for cathode of: NCM622,  $\text{Li}_6\text{PS}_5\text{Cl}$  CL10-bm, Carbon black for (a) before cycling and (b) after 36 cycles

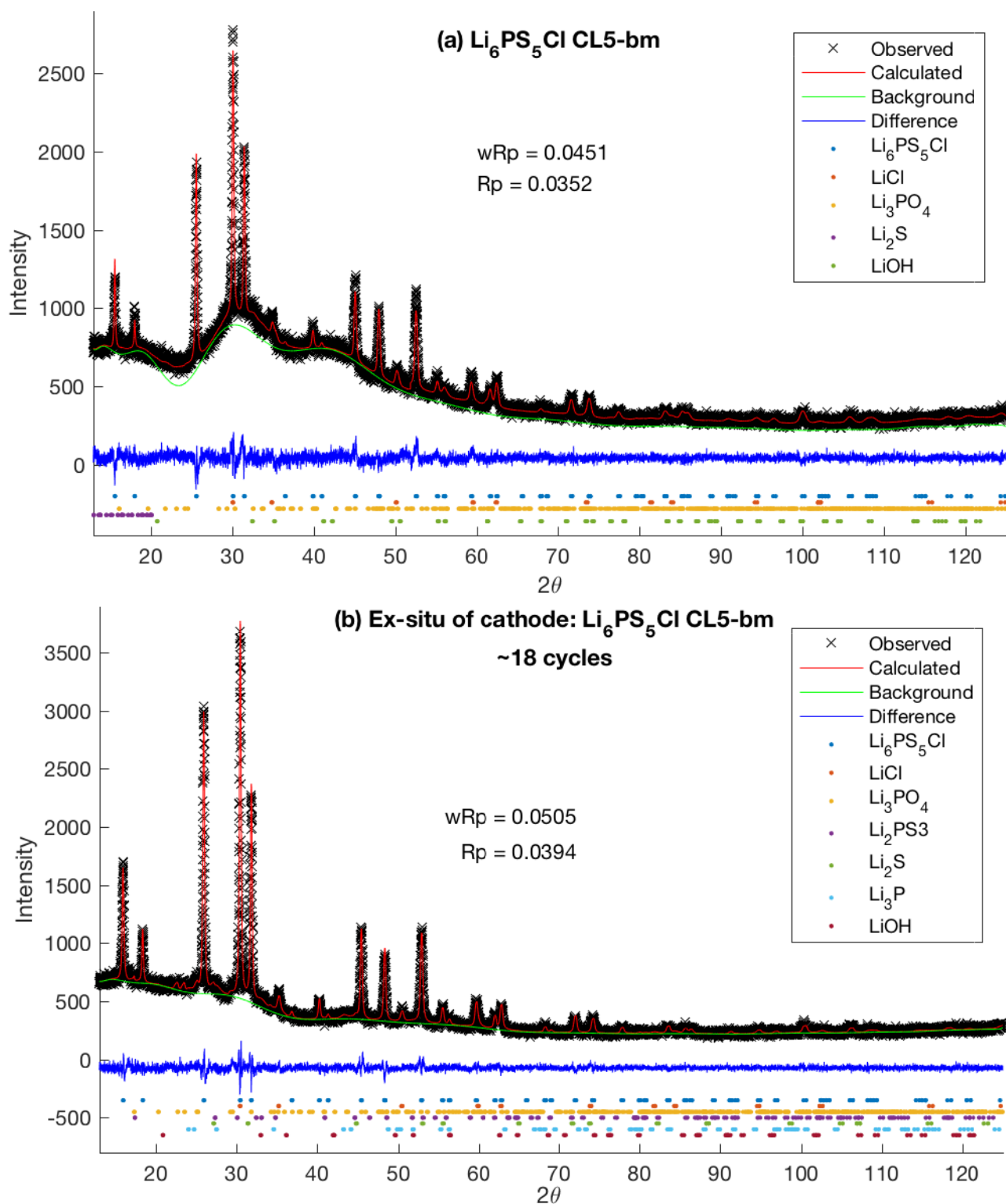


Figure A.19: XRD measurement and refinement with different phases identified for cathode of:  $\text{Li}_6\text{PS}_5\text{Cl}$  CL5-bm, Carbon black for (a) before cycling and (b) after 18 cycles

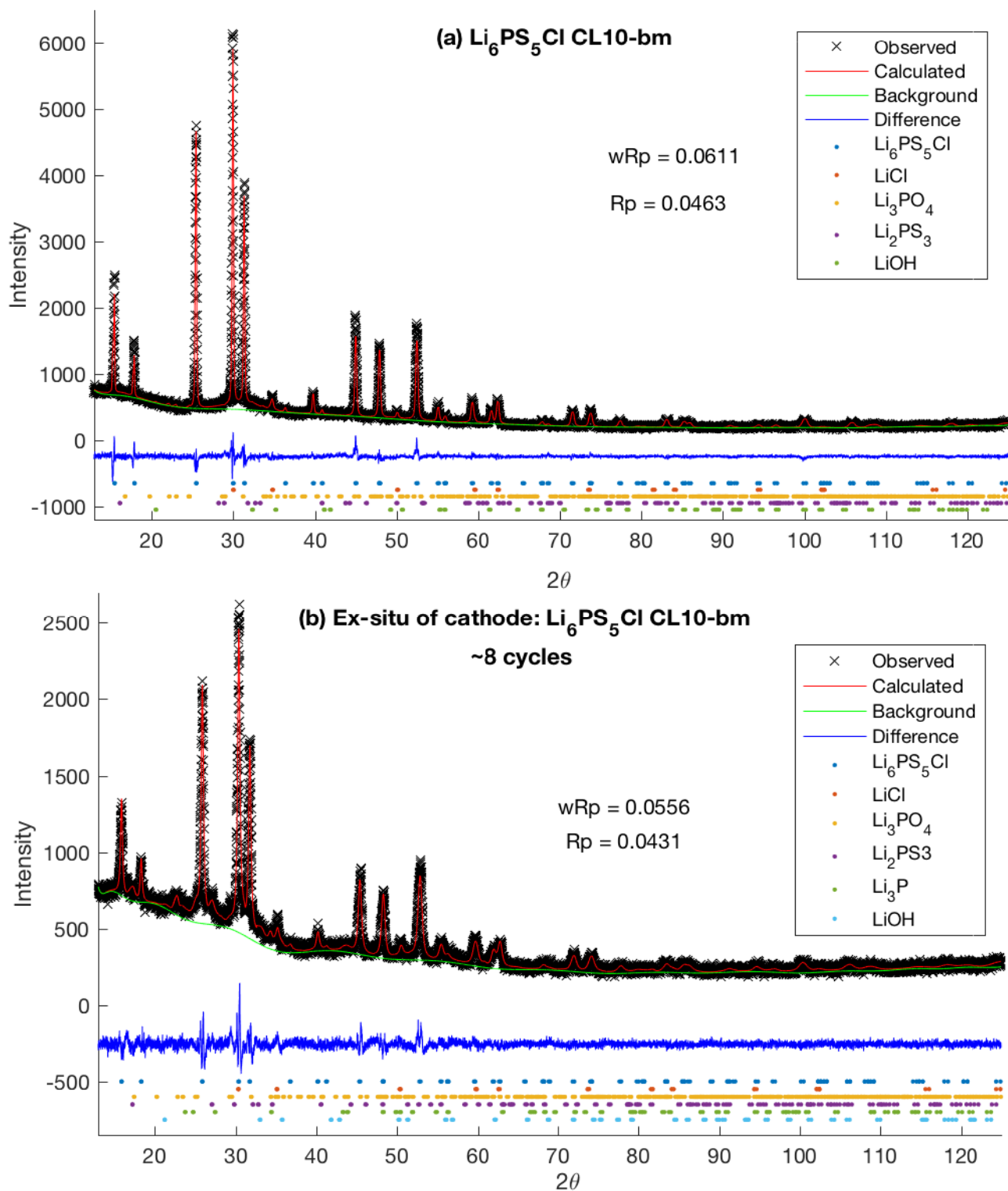


Figure A.20: XRD measurement and refinement with different phases identified for cathode of:  $\text{Li}_6\text{PS}_5\text{Cl}$  CL10-bm, Carbon black for (a) before cycling and (b) after 8 cycles



# Bibliography

- [1] C. Liu, Z. G. Neale, and G. Cao, *Understanding electrochemical potentials of cathode materials in rechargeable batteries*, *Materials Today* **19**, 109 (2016).
- [2] Y. Leng, S. Ge, D. Marple, X.-G. Yang, C. Bauer, P. Lamp, and C.-Y. Wang, *Electrochemical Cycle-Life Characterization of High Energy Lithium-Ion Cells with Thick  $\text{Li}(\text{Ni}_{0.6}\text{Mn}_{0.2}\text{Co}_{0.2})\text{O}_2$  and Graphite Electrodes*, *The Electrochemical Society* **164**, 1037 (2017).
- [3] J. W. Fergus, *Ceramic and polymeric solid electrolytes for lithium-ion batteries*, *Journal of Power Sciences* **195**, 4554 (2010).
- [4] H. M. Chen, M. Chen, and S. Adams, *Stability and ionic mobility in argyrodite-related lithium-ion solid electrolytes*, *Phys. Chem. Chem. Phys* **17**, 1694 (2015).
- [5] G. Auvergniot, A. Cassel, J. B. Ledeuil, V. Viallet, V. Seznec, and R. Dedryvère, *Interface Stability of Argyrodite  $\text{Li}_6\text{PS}_5\text{Cl}$  toward  $\text{LiCoO}_2$ ,  $\text{LiNi}_{1/3}\text{Co}_{1/3}\text{Mn}_{1/3}\text{O}_2$ , and  $\text{LiMn}_2\text{O}_4$  in Bulk All-Solid-State Batteries*, *Chemistry of Materials* **29**, 3883– (2017).
- [6] Q. Zhou, Z. Fang, J. Li, and M. Wang, *Applications of  $\text{TiO}_2$  nanotube arrays in environmental and energy fields: A review*, *Microporous and Mesoporous Materials* **202**, 22 (2015).
- [7] R. Krishnan, *What is the difference between doping and substitution?* (online forum comment), Research Gate (2013).
- [8] M. Clugston and R. Flemming, *Advanced chemistry* (Oxford University Press, 2000).
- [9] *Chemistry: Group 7 - halogens*, Pass My Exams (online).
- [10] B. C. Melot and J.-M. Tarascon, *Design and preparation of materials for advanced electrochemical storage*, *Accounts of Chemical Research* **46**, 1226 (2013).
- [11] K. M. Shaju and P. G. Bruce, *Macroporous  $\text{Li}(\text{Ni}_{1/3}\text{Co}_{1/3}\text{Mn}_{1/3})\text{O}_2$ : A high-power and high-energy cathode for rechargeable lithium batteries*, *Advanced Materials* **18**, 2330 (2006).
- [12] N. Nitta, F. Wu, J. T. Lee, and G. Yushin, *Li-ion battery materials: present and future*, *Materials today* **18**, 252 (2015).
- [13] K. Tanner, *Is indium the way to go for the next wave of efficient battery storage* (online), Trend-intech (2017).
- [14] D. Loveday, P. Peterson, and B. Rodgers, *Evaluation of organic coatings with electrochemical impedance spectroscopy. part 1: Fundamentals of electrochemical impedance spectroscopy*, JCT CoatingsTech (2004).
- [15] M. E. E. Alahi, A. Nag, N. A. Manesh, S. Mukhopadhyay, and J. Roy, *A simple embedded sensor: Excitation and interfacing*, in *Advanced Interfacing Techniques for Sensors* (Springer, 2017) pp. 111–138.
- [16] J. Mohanta, D. K. Padhi, and S. Si, *Li-ion conductivity in *peo*-graphene oxide nanocomposite polymer electrolytes: A study on effect of the counter anion*, *Applied Polymer Science* **135**, 46336 (2018).
- [17] M. Sluyters-Rehbach, *Impedances of electrochemical systems: Terminology, nomenclature and representation-part i: Cells with metal electrodes and liquid solutions (iupac recommendations 1994)*, *Pure and applied chemistry* **66**, 1831 (1994).

- 
- [18] M. E. Orazem and B. Tribollet, *Electrochemical impedance spectroscopy*, Vol. 48 (John Wiley & Sons, 2011).
- [19] P. Agarwal, M. E. Orazem, and L. H. Garcia-Rubio, *Measurement models for electrochemical impedance spectroscopy i. demonstration of applicability*, *Journal of the Electrochemical Society* **139**, 1917 (1992).
- [20] B. A. Boukamp, *A linear kronig-kramers transform test for immittance data validation*, *Journal of the electrochemical society* **142**, 1885 (1995).
- [21] *Electrochemical Impedance Spectroscopy (EIS) Part 6 – Measuring raw signals in EIS*, Metrohm Autolab B.V.
- [22] C. T. Knies, J. C. de Lima, and P. B. Prates, *The Quantification of Crystalline Phases in Materials: Applications of Rietveld Method, Sintering - Methods and Products* (InTech, 2012).
- [23] B. D. Cullity, *Elements of X-ray diffraction*, Addison-Wesley series in metallurgy and materials (Addison-Wesley, 1967).
- [24] S. Danuta and M. Henryk, *Applied Crystallography - Proceedings Of The Xvii International Conference* (World Scientific Publishing Company, 1998).